LOW FREQUENCY NOISE MODELLING OF BIPOLAR JUNCTION TRANSISTORS FOR VLSI CIRCUITS

by

Anthony Ng

B.A.Sc., Simon Fraser University, 1991

A THESIS SUBMITTED IN PARTIAL FULFILLMENT

OF THE REQUIREMENTS FOR THE DEGREE OF

MASTER OF APPLIED SCIENCE

in the School

of

Engineering Science

SIMON FRASER UNIVERSITY

April 1992

ISBN 0-315-83621-0

Approval

Name : Anthony Chi-choi Ng

Degree : Master of Applied Science

Title of Thesis : **Low Frequency Noise Modelling of Bipolar Junction Transistors for VLSI circuits**

Examining Committee :

______________________________ for

Dr. John D. Jones
Associate Professor
School of Engineering Science
Chair

____

Dr. M. J. Deen
Associate Professor, Senior Supervisor
School of Engineering Science

____

Dr. S. R. Morrison
Professor, Committee Member
Department of Physics

____

Dr. Andrew Rawicz
Associate Professor, External Examiner
School of Engineering Science

Date Approved : May 4, 1992

PARTIAL COPYRIGHT LICENSE

Title of Thesis/Project/Extended Essay

"Low Frequency Noise Modelling of Bipolar Junction Transistors"

Author:

(signature)

ANTHONY NG

(name)

8th May 1992

(date)

ABSTRACT

Bipolar junction transistors (BJTs) are widely used in a variety of digital and analog applications, and as an essential component in BiCMOS circuits. As the operating power and device geometry of bipolar junction transistors in VLSI technology are aggressively reduced to sub-micron dimensions, the effect of the device's noise becomes increasingly important to the overall performance of BJT-based circuits, particularly for communication applications.

In this thesis, a low frequency noise model for bipolar junction transistors that can predict their noise power under different operating conditions was developed. This model contains two low frequency noise sources: one due to diffusion noise which arises from mobility fluctuation, and the other due to GR noise which arises from the generation and recombination (GR) of carriers through trapping centers. Together with the current and emitter area dependence determined from the experiments, these two noise sources were combined into a single expression that gave good agreement with a wide range of low frequency noise data in BJTs as a function of frequency, temperature, base current and emitter area. This good agreement indicates that diffusion noise and GR noise are the dominant noise sources in the bipolar transistors studied, and a simple simulation model can be formulated using these two noise sources. A collector current fluctuation model due to fluctuating occupancy of the traps in the depletion region was also developed in this project in order to provide a physical explanation for the current and emitter area dependence observed. Based on this model, a simple way of measuring the trap activation energy from the noise data was discovered and verified.

For the experiments, seven bipolar transistors with emitter areas varying from $1.6\mu m^2$ to $144\mu m^2$ were used, and the noise measurements were performed at ten

temperatures between 283K to 373K with more than five biasing currents at each temperature, and at frequencies from 10Hz to 100kHz. The variation of the current noise power spectra $S_{ib}(f)$ with the base current i_b shows that $\frac{S_{ib}(f)}{i_b{}^{\gamma}}$ is approximately constant with $\gamma \cong 2$. Curve fitting the experimental carrier number fluctuation $\overline{\Delta N^2}$ using the GR noise model showed that $S_{ib}(f)$ is proportional to the square of the collector current, and inversely proportional to the square of the emitter area. This experimental finding has a significant effect on the noise performance of small emitter area BJTs, for example, a reduction in area by results in almost an order of magnitude increase in the current noise power. A Fermi-level calculation indicates that the corresponding trap levels are close to 300 meV below the conduction band. Experimentally deduced relationships between the current noise power variation with emitter size and base current were in good agreement with predictions based on the collector current fluctuation model due to trapping centers in the depletion region developed for bipolar junction transistors in this research. Both the experimental results and theory developed add to present understanding, and to previously published information on low frequency noise in bipolar junction transistors.

In addition to the provision of a noise model that is simple enough to be used for simulation purposes, and detailed enough to describe the variation of flicker noise with frequency, temperature, base current and emitter area, the significance of this thesis work also includes the understanding of the noise characteristics of present and emerging bipolar transistors.

ACKNOWLEDGEMENTS

It is a pleasure to express my deep appreciation to Dr. M.J. Deen for his encouragement, suggestion, patience and constructive criticisms of this work. He has provided valuable advice and guidance throughout this research and has afforded me the opportunity for academic advancement. I wish to thank Dr. Ash Parameswaran (for Dr. John Jones) for chairing my thesis committee, Dr. Andrew Rawicz and Dr. Roy Morrison for being my thesis committee members.

Special thanks are also due to Mr. John Ilowski and Mr. Bob Hadaway of Northern Telecom Electronics Ltd, Ottawa, for providing me with the opportunity to get involved in their research and for the use of their Semiconductor Characterization Laboratory. John's supervision during my work term in Northern Telecom Electronics Limited is greatly appreciated. Thanks are due to Mr. Boris Pokes, Dr. Ping Yan, Dr. Ian Wylie, Dr. Jim Kendall and Mr. Tom Macelwee of Northern Telecom Electronics for their discussion and assistance.

Finally, I express my deep appreciation to my colleagues, the other members of the Semiconductor Device Research Group - Joseph Liang, Xiaotang Lu, Forrest Ma, Arya Raychaudhuri, Zhixin Yan and Yu Zhu for their valuable comments, probing questions, advice and input during my weekly/biweekly research group meetings. I am fortunate to have the opportunity to conduct my research with such a talented and congenial group of students under the supervision of Dr. Deen.

Table of Contents

List of Figures

List of Tables

Chapter 1 INTRODUCTION

Noise is some unpredictable and unwanted fluctuation that, when added to a signal, reduces the information content of that signal. The 'statics' heard in a radio, the 'snowy screen' of a television, and the fluctuation of a d.c. signal around its expected value are all examples of electronic noises. Noise in charge carriers defines the lowest limit of a signal that can be detected. Below this limit the signal would be 'drowned out' by the background noise. Electronics noise therefore directly affects the accuracy of measurements and the minimum power of a signal that can be used in a circuit to transmit information.

Since noise is random in nature, it is represented as a time varying random variable X(t) in noise theory. The mean value, $\overline{X}$, of X(t) and the variance of X(t) about its mean, $\overline{\Delta X^2}$, are two important parameters for characterizing the random variable X(t). Another important characteristic of a random signal is its spectral density function (SDF). The spectrum density function of a signal describes how a signal distributes its power at different frequencies. From definition, SDF represents the time averaged noise power over a one Hertz bandwidth at any given frequency f. A white noise is a particular kind of noise which has a SDF that is constant for all frequencies. Thermal noise generated from a resistor and the shot noise generated in a current are white noises at low frequencies. In this thesis, the term 'noise power spectrum' would be used interchangeably with the term 'spectral density function'.

Noises always exist in electronic signals. A d.c. current I(t) or voltage V(t) is actually the summation of an ideal d.c. component and a fluctuating a.c. component.

The SDFs of a d.c. current I(t) and voltage V(t) are represented by $S_I(f)$ and $S_v(f)$ and abbreviated as their 'noise power spectra'. These noise spectra describe how their noise powers distribute at different frequencies. The noise voltage generator $V_n(t) = \sqrt{S_v(f)}$ and noise current generator $I_n(t) = \sqrt{S_i(f)}$ are defined such that the total noise power of a circuit can be evaluated by applying a.c. circuit theory to these quantities.

1.1 Noise in VLSI Bipolar Transistors

Bipolar transistors are widely used in a wide variety of analog applications and are now being considered as competitive candidates for some digital applications. Miniaturization through very large scale integration (VLSI) is a key method to increase the integrability and speed of these devices, and allows more devices to be packed together into a single circuit. For example, Intel's i486 microprocessor has more than 1.2 million transistors built into a single VLSI circuit with 50 times the performance of the original IBM PC. However, new problems are created in the process of miniaturization, among which the effect of "noisy" carriers is one of the most troublesome problems.

As charge carriers move through the miniaturized circuit, their interaction with objects inside the conduction channel create disruptions to the flow of the carriers similar to the way a rock creates 'rapids' inside a stream. The crystal lattice, space charges, impurities and lattice imperfection inside a conduction channel interact with the charge carriers and create fluctuations in both the number and the mobility of the carriers.

As the device size is being reduced aggressively, larger number of transistors are being packed into a single circuit to increase functionality and speed. The noise generated from these noisy carriers accumulate in the analog signals as these signals propagate through each transistor in the circuit. As more and more transistors are packed together, the accumulated noise power eventually becomes comparable to the signal power and affects the performance of the overall circuit. This is why the noise effect of carriers can no longer be ignored and must be carefully considered in designing 'sensitive' circuits. Since many analog circuits also operate at low frequencies, and since VLSI technology will be used to implement high complexity analog circuits, the low frequency noise of bipolar transistor in VLSI technology must be studied in detail and reduced to a level that is low enough for the proper functioning of the current and future advanced circuits.

1.2 Noise Simulation

Due to the long turn around time and the expensive cost of the actual fabrication of a VLSI circuit, noise simulation becomes a realistic alternative to determine whether the overall noise performance of a circuit would be good enough to allow a circuit function properly. In order to perform accurate noise simulation, a good noise model should be simple enough for large scale simulation and powerful enough to predict the variation of noise for a complete range of operating conditions such as different frequencies, temperatures, d.c. biases and device areas. The noise models currently implemented in HSPICE for bipolar transistor includes those of the flicker noise, shot noise and thermal noise. However, these models, only allows variations in the biasing level and frequency while other important factors like the device area and operating temperature have not been included. Without the ability to simulate the noise performance at different emitter areas and operating temperatures, devices of identical structure but with different device sizes must then be characterized separately for their noise model and each device has to be characterized at a range of operating temperatures. Furthermore, generation-recombination noise, which is a very important type of noise that affects the noise performance of most modern transistors, is not included in these models.

1.3 Goal of the Project

The primary goal of my M.A.Sc project is to investigate how the low frequency noise of some modern bipolar transistors varies with temperature, biasing conditions and their emitter areas, and to provide explanations for the variations observed. During my research, a one dimensional space-charge region carrier trapping model for bipolar transistors was developed to provide a physical explanation for the phenomena observed. This model takes into account the effects of the electrons trapped in the space-charge region on both the modification of the conduction channel resistance and the diffusion current.

Another goal my project is to develop a low frequency noise model for the bipolar transistors investigated. With suitable use of fitting parameters, the proposed model should be simple enough for simulation purposes and accurate enough to predict how the noise power varies at different frequencies, biasing conditions, temperatures and device sizes. Our noise model includes two noise mechanisms. One due to mobility fluctuation (diffusion noise), and the other is due to the generation and recombination of carriers through trapping centers (GR noise). Together with the current and emitter area dependence determined from the experiments, these two noise sources were combined into a single expression that gave good agreement with a wide range of flicker noise data in BJTs as a function of frequency, temperature, base current and emitter area. This good agreement indicates that diffusion and GR noise sources are the dominant ones in the bipolar transistors studied, and a simple simulation model can be formulated using these two noise sources.

For the experiments, seven bipolar transistors with emitter areas varying from 1.6 μm^2 to 144μm^2 were used, and the noise measurements were performed at ten temperatures between 283K to 373K with more than five biasing currents at each temperature, and at frequencies from 10Hz to 100kHz. The variation of the current noise power spectra $S_{ib}(f)$ with base current i_b show that $S_{ib}(f) / i_b^{\gamma}$ is approximately constant with $\gamma \cong 2$. The experimental results also show that the generation-recombination noise peaks at 303K and 355.5K. Curve fitting the experimental carrier number fluctuation $\overline{\Delta N^2}$ using the GR noise model shows that $\overline{\Delta N^2}$ is proportional to the square of the collector current, and is inversely proportional to the square of the emitter area. This experimental finding has a significant effect on the noise performance of small emitter area BJTs. For example, a reduction in area by results in almost an order of magnitude increase in the current noise power.

In summary, the significance of my thesis work is its contribution to the understanding of the noise characteristics of present and emerging bipolar transistors and the proposal of a simple yet accurate simulation model for these modern bipolar transistors.

Chapter 2 Theoretical Background

2.1 Classification of Various Noise Sources in Bipolar Transistors

There are different kinds of noise sources in a bipolar transistor as shown in Figure 2.1. Flicker noise and generation recombination noise (GR noise) are low frequency noise because they have relatively higher noise power than other noise sources at low frequency.

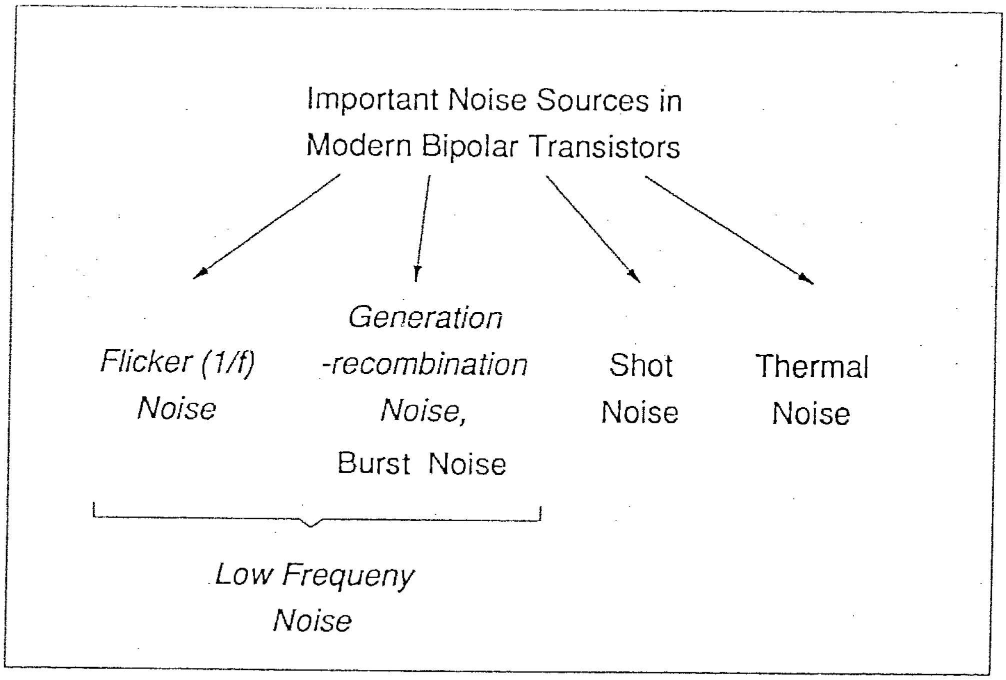

Figure 2.1 - Common noise sources in a bipolar transistor

Flicker noise is characterized by a $\frac{1}{f^{\gamma}}$ spectrum with γ close to unity. This is also why the name 1/f noise is also used to describe this kind of noise. This type of noise can be explained either by mobility fluctuation or number fluctuation. It is believed that mobility fluctuation is caused by the interaction of carriers with slowly fluctuating longitudinal acoustical-phonon populations. Number fluctuation is caused by the fluctuation in the number of carriers across the conduction channel. Flicker noise due to mobility fluctuations is described by the following equation,

$$\frac{S_x(f)}{x^2} = \frac{\alpha}{N\,f} \tag{2.1}$$

where x is the quantity in which flicker noise is measured, α is the Hooge's constant, N is the number of carriers and f is the frequency. The number of carriers can be expressed in other terms including the current, the saturation velocity and the length of the device [43 equation 4]. Since flicker noise is one of the noises being investigated in this project, it will be explained in detail in next section. Shot noise [1] is a result of the passage of discrete charge carriers across a barrier where the carriers pass independently of each other. In a semiconductor material, shot noise is modelled as a current source in parallel with the dynamic impedance of the noise generating barrier. Shot noise in bipolar transistor can be represented by two shot noise sources : one originateing from the collector current that can be represented by

$$\overline{i_1^2} = 2\,q\,I_c\,\Delta f \tag{2.2}$$

and the other originating from both the emitter and base current that is represented by

$$\overline{i_2^2} = 2\,q\,(\,I_E + I_{BE}\,)\,\Delta f \tag{2.3}$$

Thermal noise [2] is caused by the random motion of the current carriers; it produces a fluctuating electromotive force across its terminals. The thermal voltage noise power in a semiconductor material can be represented by [1],

$$S_v(f) = 4\,k\,T\,R \tag{2.4}$$

where R is the resistance of the conduction channel. Generation-recombination (GR) noise is caused by the trapping and detrapping of carriers by traps or dislocations inside a semiconductor material. Due to the random trapping and detrapping of carriers, the total number of carriers fluctuates and this in turn causes the resistance of the conduction channel to fluctuate. Similar to flicker noise, GR noise is the main topic being investigated in this thesis and will be discussed in detail in the next section. Burst noise[1] [3] is also a form of GR noise. It consists of random pulses of variable length and equal height. Sometimes the random pulses seem to be superimposed upon each other. A typical GR noise can be described by the following equation:

$$S_{GR}(f) = 4\,\overline{\Delta N^2}\,\frac{\tau}{1+\omega^2\tau^2} \tag{2.5a}$$

where the trapping time constant $\tau = \tau_0 \exp\frac{q\,(E_t - E_F)}{k\,T}$, (2.5b)

ω is the frequency, $\overline{\Delta N^2}$ is the variance of the fluctuation of the number of carriers. At low frequencies, the power of flicker noise and GR noise are larger than the power of other noises and are critical to the low frequency performance of low frequency analog circuits.

Fundamental Noise and Non-Fundamental noise

Noise source inside a semiconductor material can be classified as fundamental and non-fundamental depending on the nature of the noise source. A noise source is fundamental if it is related to the basic operation of a device and cannot be eliminated as far as the operation of the device is concerned. Non-fundamental noise are noise sources

1 If dislocations are not present at the emitter edge, then the burst noise can be produced at the space charge region of the device if a trap is present.

that can be removed without affecting the operation of a device. In bipolar transistors, GR noise is non-fundamental noise because GR noise originates from 'avoidable' traps and can be reduced by reducing the number of traps or defects through improved fabrication technique. On the other hand, flicker noise originates from the 'unavoidable' crystal scattering and collision during the diffusion of charge carriers which is critical to the operation of a bipolar transistor. It is therefore fundamental to the operation of a bipolar junction transistor.

Van der Ziel explained in [4] that carrier trapping by and detrapping from traps results in non-fundamental noise sources. These traps may be in the device's conduction channel, in the oxide near the conducting channel interface, or in a space charge region, and they cause a Lorentzian or 1/f type noise spectra. They are called non-fundamental because the magnitude of their spectra is proportional to the trap density. Their noise effect can thus be strongly reduced by eliminating most of the traps. On the other hand, there are other noise sources that are fundamental to the operation of the device and must exist as far as the operation of the device is concerned. For example, noise sources due to various scattering mechanisms in collision-dominated devices and the Bremsstrahlung 1/f noise in collision-free devices are unavoidable in the operation of the device. They are therefore called fundamental noise sources.

2.2 Low Frequency Noises in Bipolar Transistors

To date, most researchers agree that among the many types of low frequency noises in bipolar transistor, the dominant ones are diffusion noise and generation-recombination noise [4]. Diffusion noise in bipolar transistor is one kind of flicker noise and is fundamental to the operation of the transistor. Generation-recombination noise, as explained previously, exhibits Lorentzian or $1/f^{\beta}$ type of spectrum and is non-fundamental. Five major low frequency noise sources in a modern bipolar transistor are listed in Table 2.1. In additional to Table 2.1, Table 2.2 lists the two other low frequency noise sources that are inherit in a poly-emitter npn transistor which is the type of bipolar transistor being used in our research and under the measuring conditions used.

Location	Type of Low Frequency Noise	Source
E-B space charge region at the oxide's surface	GR (Number Fluctuation)	Fluctuating occupancy of holes in surface oxide traps [6-8]
E-B space charge region	GR (Number Fluctuation)	Fluctuating occupancy of holes at dislocations in the E-B space charge region [6-8]
E-B hole diffusion	Mobility Fluctuation	hole current injected from the base to the emitter
E-C electron diffusion	Mobility Fluctuation	electron diffuse from the emitter to the collector
base surface near the B-C junction [9]	Recombination noise	holes recombined in the base

Table 2.1 The five major flicker noise sources in a bipolar transistor

Location	Type of Low Frequency Noise	Source
Poly-silicon interface which control the base current [10]	Recombination noise	hole recombination at the poly / monosilicon interface and in the polysilicon itself [11-12]
non-ohmic metal to p-type polysilicon contact in the extrinsic base [13]	Recombination noise	hole recombination at the p-type polysilicon contact

Table 2.2 Two additional noise sources in a poly-emitter transistor

2.3 Noise Theory for our Measurements

As explained previously, our low frequency noise model contains fundamental noise (diffusion noise) and non-fundamental noise (GR noise) and it is formulated as

$$S_{total}(f) = S_d(f) + S_{gr}(f) \qquad (2.6)$$

in which S_d (f) represents spectral density function of the fundamental diffusion noise and S_{gr} (f) represents the SDF of the non-fundamental GR noise. S_d(f) is modelled using both the classical Hooge's model due to Langevin's noise source [14-17,42] and Kleinpenning's mobility fluctuation theory for electron emitter-collector diffusion noise [6, 7]. The non-fundamental flicker noise S_{gr} (f) causes Lorentzian type of flicker noise spectrum and is modelled using McWhorter's model [20]. The origins of the two noise sources used in the model are illustrated in Figure 2.2.

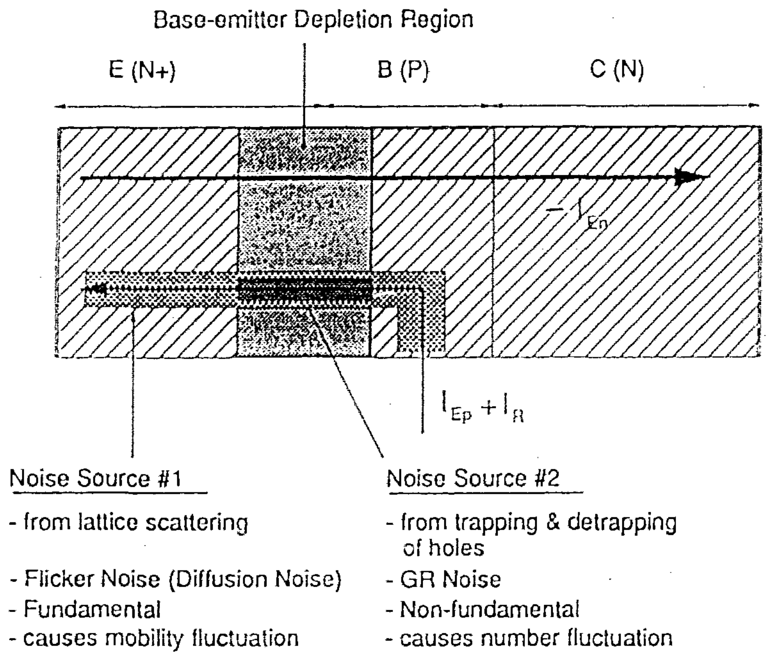

Figure 2.2 Origins of the two noise sources used in the model

2.3.1. Number-Fluctuation and Mobility-fluctuation

According to Van der Ziel [2], a semiconductor channel of length L with N electrons of mobility μ has a channel resistance of

$$R = \frac{L^2}{q\mu N} \tag{2.7a}$$

From the above equation,

$$\frac{\delta R}{R} = -\frac{\delta N}{N} - \frac{\delta \mu}{\mu} \tag{2.7b}$$

From equation (2.7b), both the mobility and the number of carrier fluctuations lead to a fluctuation in the channel resistance and cause a fluctuation in the overall voltage and current. If the fluctuation in mobility and number are independent then

$$\frac{S_R(f)}{\overline{R}^2} = \frac{S_N(f)}{\overline{N}^2} + \frac{S_\mu(f)}{\overline{\mu}^2} \tag{2.8}$$

where $\overline{x}$ denotes the average value of the random variable x. Therefore noise in voltage and current is due to fluctuation in the conduction channel's resistance that originate from both the mobility fluctuation and number fluctuation. In our theory, we assume that the flicker noise (diffusion noise) contributes noise through mobility fluctuation while the non-fundamental GR noise contributes noise through number fluctuation. Besides the mobility and number fluctuations, there are other noise mechanisms that contribute to the total low frequency noise :

$$S_f(f) = \frac{S_\mu(f)}{\mu^2} + \frac{S_N(f)}{N^2} + \frac{S_c(f)}{c^2} + \frac{S_{cn}(f)}{cn^2} + \text{less significant terms} \tag{2.9}$$

in which $\frac{S_\mu(f)}{\mu^2}$ is the mobility fluctuation which originates from the diffusion fluctuation through the Einstein equation $Dq = kT\mu$. $\frac{S_N(f)}{N^2}$ is the fluctuation in the number of carriers. $\frac{S_c(f)}{c^2}$ is the fluctuation in carriers which only happens in a relatively long n^+-p diode since part of the injected carriers disappear by recombination. $\frac{S_{cn}(f)}{cn^2}$ is the fluctuations in the contact recombination velocity S_{cn} at the ohmic contact ($S_{cn} = 10^7$ cm s^{-1}). In devices where the mobility fluctuation predominates, the mobility fluctuation term $\frac{S_{\mu}(f)}{\mu^2}$ is much larger than other term and the total low frequency noise S_f (f) becomes $\frac{S_{\mu}(f)}{\mu^2}$. If both the number fluctuation and mobility fluctuation dominate, then $S_f(f) \cong \frac{S_{\mu}(f)}{\mu^2} + \frac{S_N(f)}{N^2}$.

2.3.2. Isolating the Noises in the Base-Emitter Region

In this section, we are going to discuss how different external circuit configuration would enhance the noise power of one or more of the noise sources inside a bipolar transistor. By adapting the results in [7] to our npn transistor in a common emitter configuration, we will show that the circuit configuration used in our experiments enhances the noise sources at the base-emitter junction. Figure 2.3 shows the main current flow and the biasing scheme in our npn transistors. We use a common emitter configuration because it employs the natural amplification of the device instead of using an external amplifier which might introduce unwanted noise to our results.

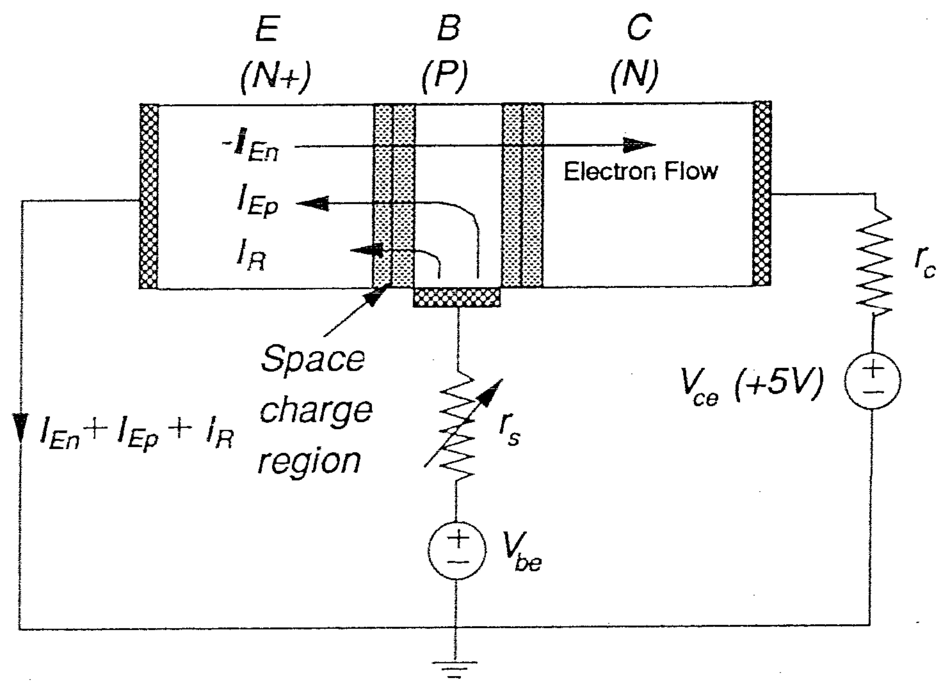

Figure 2.3 - Main current flows and the biasing scheme in our npn transistors

In Figure 2.3, r_S is the variable external source resistance and was set to 10kΩ in our measurements. The collector voltage V_{ce} was kept constant at 5V while the base voltage V_b was kept constant at a level corresponding to the desired collector current. I_{En} is the electric current (from collector to emitter) due to the electron diffusion from the emitter to the collector. I_{Ep} is the current component due to the hole injected from the base into the emitter. I_R is the recombination current component in the emitter base space charge region. In a bipolar transistor, the three noise sources that generate most of the low frequency noises are

1) the fluctuating occupancy of holes or electrons by traps or dislocations in the base or emitter space charge region and in the oxide surface (the fluctuation in current due to this source is represented by δI_R),

2) mobility fluctuations due to holes interacting with phonons cause 1/f noise in the electron current I_{En} diffusing from the emitter to the collector (the fluctuation in

current due to this source is represented by δI_{En}), and

3) mobility fluctuations due to the hole current I_{Ep} injected from the base into the emitter (the fluctuation in current due to this source is represented by δI_{Ep}).

These three possible causes are represented as current sources δI_R, δI_{Ep} and δI_{Ep} in an equivalent circuit first reported in [21]. This circuit is also modified and applied to our npn transistors, as shown in Figure 2.4.

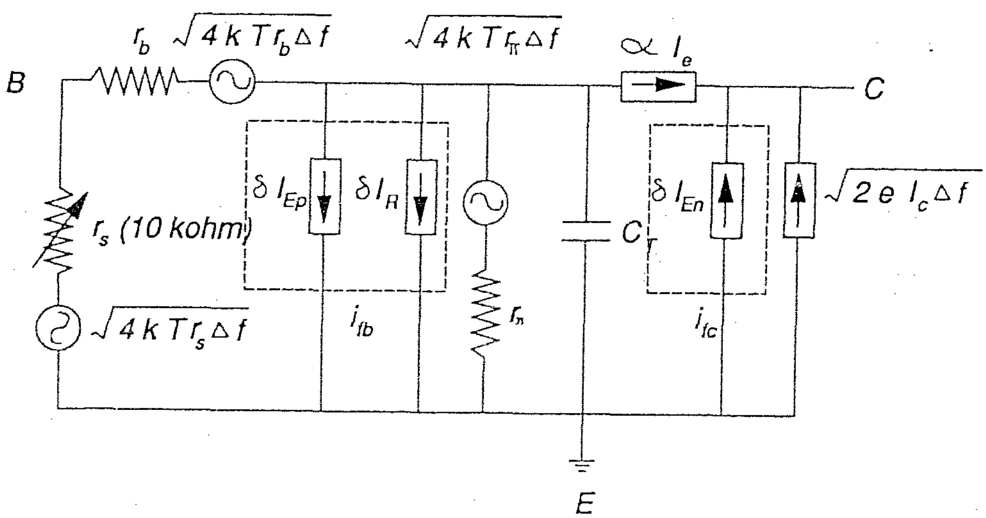

Figure 2.4 - Equivalent circuit for our npn transistors which is a modification of the one reported in [21]

The two base current sources are combined into an equivalent noise source, $i_{fb} = \delta I_R + \delta I_{Ep}$ and the emitter collector current source is renamed as $i_{fc} = \delta I_{En}$. Current and voltage noise spectral contributors such as 4 k T r_b, 4 k T r_s S_{if_b}, $2kT/g_m$ etc shown in Figure 2.5 are obtained from squaring all the noise sources in Figure 2.4. Since all noise spectral contributors in Figure 2.5 are input referred, spectral contributors at the output side were divided by the transconductance of the transistor g_m^2 to obtain the input referred voltage spectral contributors. The overall natural amplification factor $A_{transistor}$ that amplifies the input referred spectral contributors to the measurable voltage noise spectra is

$$A_{transistor}{}^2 = (R_L\, g_m)^2 = (\beta\, R_L / R_\pi)^2 \tag{2.10}$$

Since the collector shot noise power $2\, e\, I_c\, \Delta f$ (3×10^{-21} $A/\sqrt{Hz}$ or -205 dBA for the maximum I_c = 10 mA) is well below the amplified flicker noise and GR noise level ($>10^{-17}$ $A/\sqrt{Hz}$ or -170 dBA), we did not consider shot noise in our calculation.

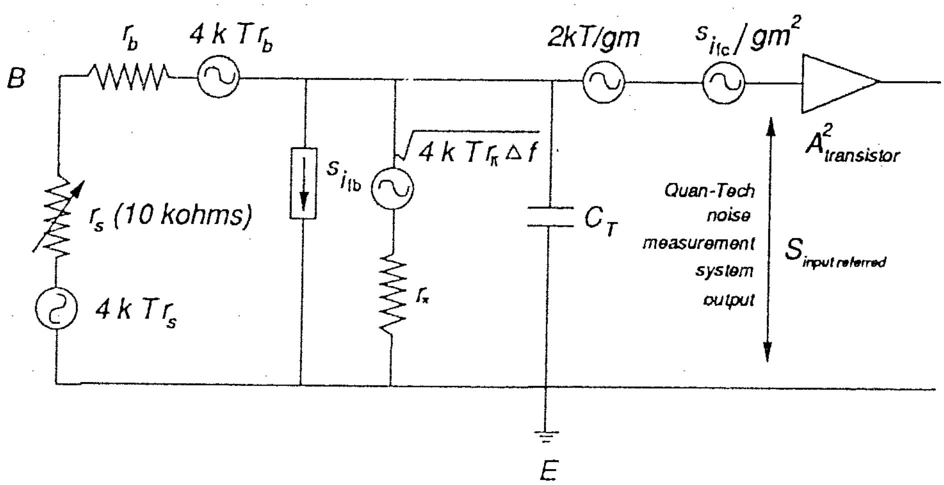

Figure 2.5 - Common emitter circuit with input referred voltage spectral contributors

From Figure 2.5, the voltage noise spectra measurable at the collector output is given by

$$S_{meas} = A^2\left\{ (S_{R_s} + S_{r_b})\left(\frac{r_\pi}{R_s + r_b + r_\pi}\right)^2 + 2kTr_\pi \left(\frac{r_\pi}{R_s + r_b + r_\pi}\right)^2 \right\}$$

$$+A^2\left\{S_{i_{fb}}\left[\frac{(R_s+r_b)\,r_\pi}{R_s+r_b+r_\pi}\right]^2+\frac{2kT}{gm}+\frac{S_{i_{fc}}}{gm^2}\right\}. \quad (2.11)$$

Using a high source resistance configuration (Rs = 10kΩ >> r_b = 100Ω), equation (2.11) reduces to

$$S_{meas}=\beta^2 R_L{}^2\left\{2\,e\,I_B+S_{i_{fb}}+\frac{S_{i_{fc}}}{\beta^2}\right\}. \quad (2.12)$$

The input referred current noise spectra would be the measured current voltage noise spectra divided by $\beta^2 R_L{}^2$:

$$S_{HRs,input\ referred}=\frac{S_{meas}}{\beta^2 R_L{}^2}=2\,e\,I_B+S_{i_{fb}}+\frac{S_{i_{fc}}}{\beta^2} \quad (2.13)$$

At low frequency (f < 100Hz), the 1/f portion of our spectra $\left(S_{i_{fb}}+\frac{S_{i_{fc}}}{\beta^2}\right)$ dominates and is above the shot noise (2 e I_B) level :

$$S_{HRs,input\ referred}=S_{i_{fb}}+\frac{S_{i_{fc}}}{\beta^2}\cong S_{i_{fb}}\quad \text{since } \beta=100 \quad (2.14)$$

Therefore, our high source resistance R_S configuration isolates $S_{i_{fb}}$ at low frequencies. Since we defined I_{fb} as $\delta I_R + \delta I_{Ep}$, we get

$$S_{i_{fb}}=S_{I_R}+S_{I_{Ep}}. \quad (2.15)$$

Therefore, we are effectively measuring type 1 and 3 low frequency noises described previously in section 2.3.2. Therefore the fluctuating occupancy of holes or electrons by traps or dislocations in the base or emitter space charge region or in the oxide surface, and mobility fluctuations due to the hole current I_{Ep} injected from the base into the emitter give rise to the measured noise power.

2.3.3. Theories for Generation-Recombination Noise

Generation-recombination (GR) noise in bipolar transistor is a non-fundamental low frequency noise which arises from the trapping and detrapping mechanism of traps or crystal dislocations which may be in a conducting channel, in a space-charge region, or in a surface oxide. Generation-recombinadion noise can be reduced through better fabrication techniques by which surface and bulk defects, including both the surface trapping centers and the bulk crystal structure dislocations, can be reduced. It has been suggested in [7] suggested that the fluctuating occupancy of carriers in oxide surface traps or in dislocations in the base or emitter space charge region modulates the surface recombination velocity and results in flicker noise. Using this idea, a mathematical model for this type of flicker noise is developed and it will be presented in next section.

GR noise can be caused by electron traps or hole traps. As explained in [2] for trapping centers in the forbidden gap, one distinguishes electron traps when the center interacts mainly with electron in the conduction band and hole traps when the center interacts mainly with holes in the valence band. In addition, recombination centers are distinguished by the fact that both of these processes occur, that is interaction with both electrons from the valence band and holes from the valence band. For electron or hole traps, there is one time constant per trap level, whereas for a recombination center, one has two time constant per type of center. Although there are two time constants per center for a recombination center, usually one of the two g-r spectra is much more pronounced than the other. As will be shown in the experiment section later, our calculation for the trap level in our devices suggests that the traps that exist in our device should be electron traps rather than hole traps. GR noise, S_{gr} (f), is modelled using the McWhorter's model [20] which is a summation of a group of Lorentzian-type of flicker noise spectrum and is

$$S_{gr}(f) = 4 \sum_{i=1}^{N} \overline{\Delta N_i^2} \frac{\tau_i}{1+\omega 2 \tau_i^2}. \tag{2.16a}$$

$$\text{where } \tau_i = \tau_{i0} \exp \frac{q(E_t - E_F)}{kT}, \tag{2.16b}$$

τ_{i0} is a constant, E_t is the energy level of the trap and E_F is the Fermi energy level. For the case of having only one trap, the above two equations are simplified to

$$S_{gr}(f) = 4 \overline{\Delta N^2} \frac{\tau}{1+\omega^2 \tau^2} \tag{2.16c}$$

$$\text{where } \tau = \tau_0 \exp \frac{q(E_t - E_F)}{kT}, \tag{2.16d}$$

The derivation of equation (2.16) is given in Appendix II.

2.3.3.1. Noise Power and the Fermi Level

Using the quasi-equilibrium approximation discussed in [22], we assume that the quasi-Fermi levels remain flat throughout the depletion region of the p-n junction in a bipolar transistor. The band diagram with both the electron quasi-Fermi level (E_{Fn}) and hole quasi-Fermi level (E_{Fp}) for a actively-biased NPN transistor is shown in Figure 2.6.

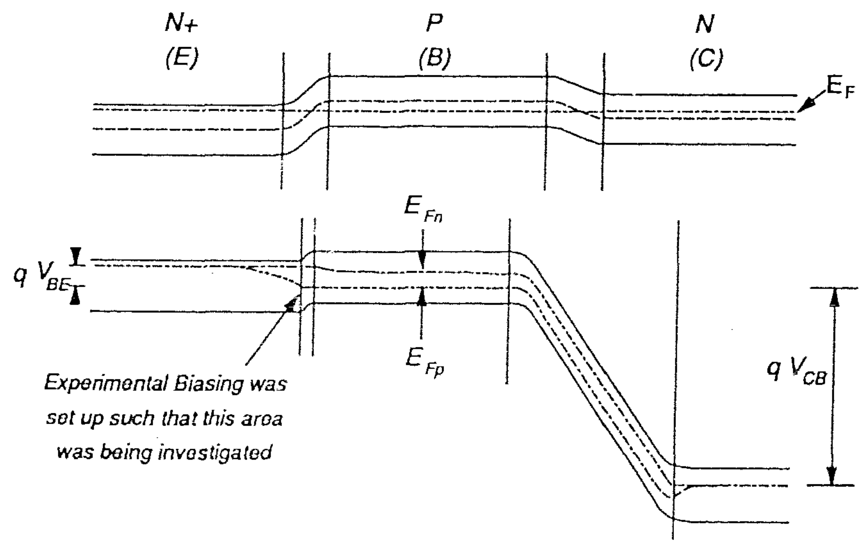

Figure 2.6 - Band diagram of a NPN transistor in thermal equilibrium (top figure)and under bias (bottom figure)

The total number of traps being occupied by carriers depends on the both the Fermi-level and the temperature. The fractional occupancy of traps is obtained from Fermi-Dirac statistics and is

$$f_t = \frac{1}{1 + \exp\frac{q\,(E_t - E_F)}{k\,T}} \qquad (2.17)$$

where E_t is the trap level and E_F is the Fermi-level of the carriers which can be calculated from the following six equations based on the Maxwell-Boltzmann approximation :

$$E_{Fp} = E_i - k\,T \ln \frac{p}{n_i} \qquad (2.18a)$$

$$E_{F_n} = E_{F_i} + k\,T \ln \frac{n}{n_i} \tag{2.18b}$$

$$n_i = N_C \exp\left(\frac{E_{F_i} - E_C}{k\,T}\right) \tag{2.18c}$$

$$N_C = 2 \left(\frac{2\,\pi\, m_e^{*}\; k\,T}{h^2}\right)^{3/2} \tag{2.18d}$$

$$E_F = 1.16 - \frac{7.02 \times 10^{-4}\, T^2}{T + 1108} \tag{2.18e}$$

These equations were used to determine the Fermi levels discussed later in Chapter 3. Since the Fermi level E_F varies with temperature, then f_t also varies with temperature, and, as shown in Figure 2.7, $f_t = 0.5$ when $E_F = E_t$. In other words, the quasi-Fermi level in a p-n junction represents the energy state at which the probability of occupancy of a trap by a mobile carrier is exactly one-half, and therefore, a trap with $E_t = E_F$ would be half of the time empty, and half of the time filled. The trapping and detrapping activities of a half filled trap is strongest and therefore results in the maximum noise power. The shape of the GR noise spectrum in the noise power versus temperature graph is that of a inverted valley. We simply refer this shape as 'hill' shape for simplicity. The "hilltop" (the maximum point) in a GR noise is reached when the Fermi-level crosses the trap level. Figure 2.8 shows the GR spectra corresponding to 5 different trap levels in a neutron-irradiated JFET that was reported in [23].

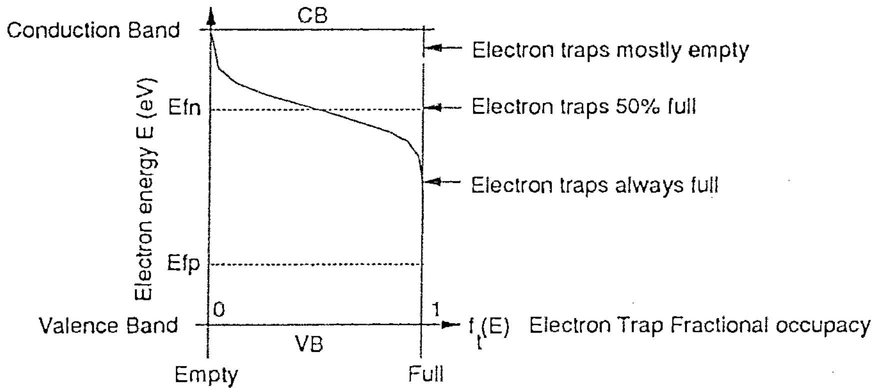

Figure 2.7 - Since the quasi-Fermi level represents the energy state at which the probability of carrier occupancy is exactly one-half, traps with energy near the Fermi-level would have half of the time empty and half of the time filled

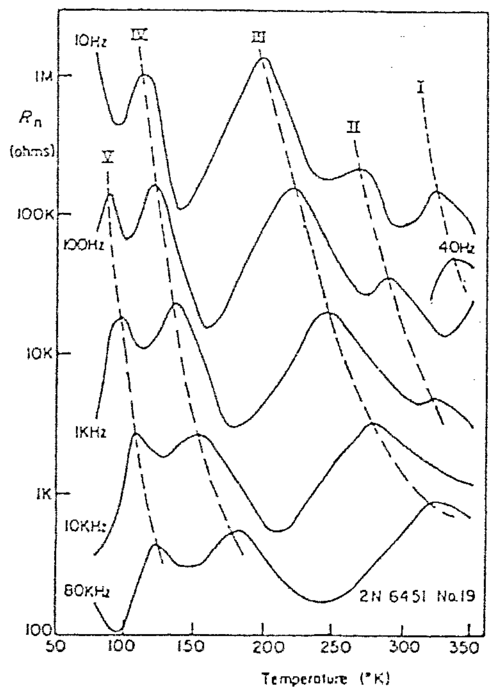

Figure 2.8 - Equivalent noise resistance versus temperature with frequency as a parameter in a neutron-irradiated JFET [K. K. Wang, A. Van der Ziel, and E. R, Chenette, IEEE Trans. Electron, Devices, ED-22, 591 (1975).]

Using the fact that the quasi-Fermi level is a function of temperature, one can directly vary the Fermi-level by varying the temperature. Peaks of GR noise are then observed as Fermi-level crosses any trap energy level [2]. Since holes are injected from the base into the depletion region in our npn transistors, traps inside the depletion region with energies near the hole quasi-Fermi level would have the strongest trapping and detrapping activities and produce the highest GR noise power. At room temperature, hole traps with energy that are a few mV higher than the quasi-Fermi level would be very quiet, since these traps would be full all the time. Hole traps with energy few mV lower than the quasi-Fermi level would also be very quiet, since these traps would be empty all the time. An analogous situation applies to electron traps.

Since a large portion of a GR peak was observed in our experimental data, we should be able to determine the corresponding trap energy levels by calculating the quasi-Fermi levels. Since the high source resistance (R_s) circuit configuration was used in our experiments, both the flicker noise and GR noise measured should originate from the base emitter region similar to that reported in [7]. Furthermore, whether the traps that generate the GR noise are hole traps or electron traps has to be determined from experimental results by calculating the value of the quasi-Fermi level for the experimental conditions used.

2.3.3.2. The Collector Current fluctuation Model based on Fluctuating Occupancy of Traps inside the Depletion Region

From our experiment, we found that the fluctuation in the number of carriers $\overline{\Delta N^2}$ in expression (2.16) depends on both the emitter area and collector current. A one-dimensional collector current fluctuation model based on the fluctuating occupancy of traps inside the depletion region for $\overline{\Delta N^2}$ was developed to provide a physical explanation for the experimental results obtained. This model provides a physical understanding of why the noise power is proportional to the square of the collector current and inversely proportional to the emitter area. It is one-dimensional because field variations in all directions except the one along the conduction channel are neglected. This model is based on the assumption that carrier fluctuation originates from generation-recombination centers in the space-charge region, and that the fluctuation in number of carriers modulates the diffusion current. The fluctuating occupancy of traps in the surface oxide was not included in this analysis because it is believed that the traps in the depletion region affect the collector current more directly than those in the surface oxide through the modulation of the depletion width. Traps in the depletion region of a bipolar transistor should therefore contribute more to the overall noise than those in the surface oxide. In some cases, surface traps can also generate noise with power comparable to that generated from the traps in the depletion region, any other motivation of analysis more than that of providing a physical explanation for the phenomena observed must take the effects of surface traps into consideration. Our theory was developed for the noise generated from the traps in the depletion region only. Van der Ziel has done a detailed derivation for a JFET, readers are suggested to refer to the Appendix A.2. of [2] for more information. For a planar NPN transistor as shown in Figure 2.9, let A be the effective emitter area of the transistor, n_t be the trap density per unit volume, ΔV be an elementary volume element, ΔN_t be the number of trapped electrons in ΔV, f_t be the fractional occupancy of the traps, τ_t be the trapping time constant, N_D be the donor concentration in the emitter region of the npn transistor, and N_A be the acceptor concentration in the base region.

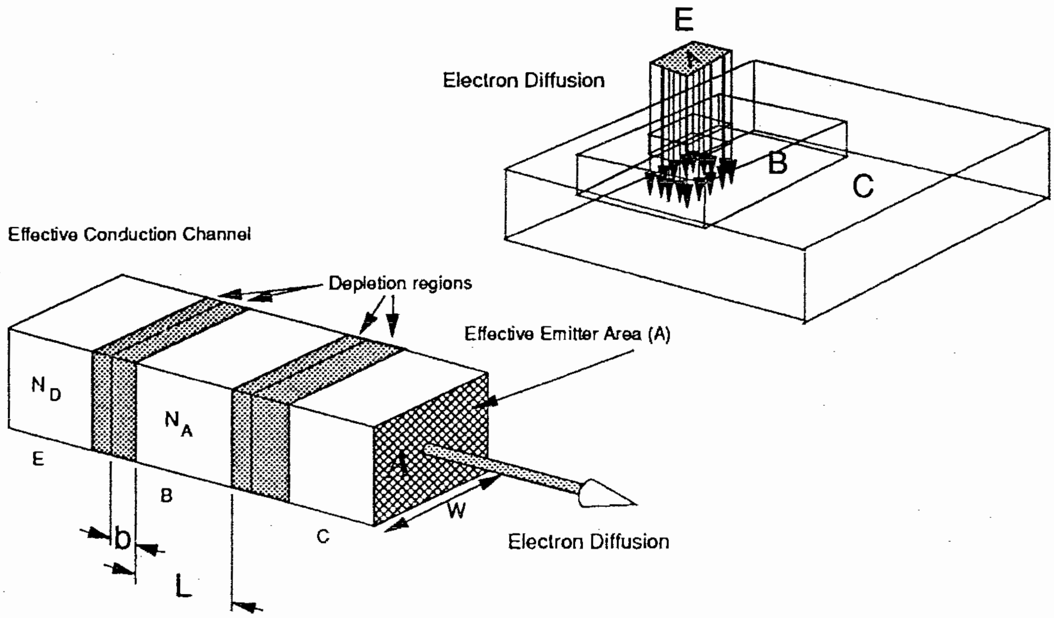

Figure 2.9 - The effective conduction channel in a NPN transistor

Since f_t is the fractional occupancy of the traps [2], then

$$\overline{\Delta N_t} = n_t f_t \Delta V \qquad (2.19a)$$

$$\overline{\Delta N_t^2} = n_t f_t (1 - f_t) \Delta V \qquad (2.19b)$$

If ΔN_t fluctuates by an amount of $\delta\Delta N_t$ then

$$S_{\delta\Delta N_t}(f) = \overline{\Delta N_t^2} \frac{\tau_t}{1 + \omega^2 \tau_t^2} \qquad (2.20)$$

with $\overline{\Delta N_t^2} = 4\, n_t f_t (1 - f_t) \Delta V$. (2.21)

Assuming that the trap fluctuation $\delta\Delta N_t$ in an elementary volume $\Delta V = \Delta x_1$ A in the base depletion region as shown in Figure 2.10, then this fluctuating occupancy of traps

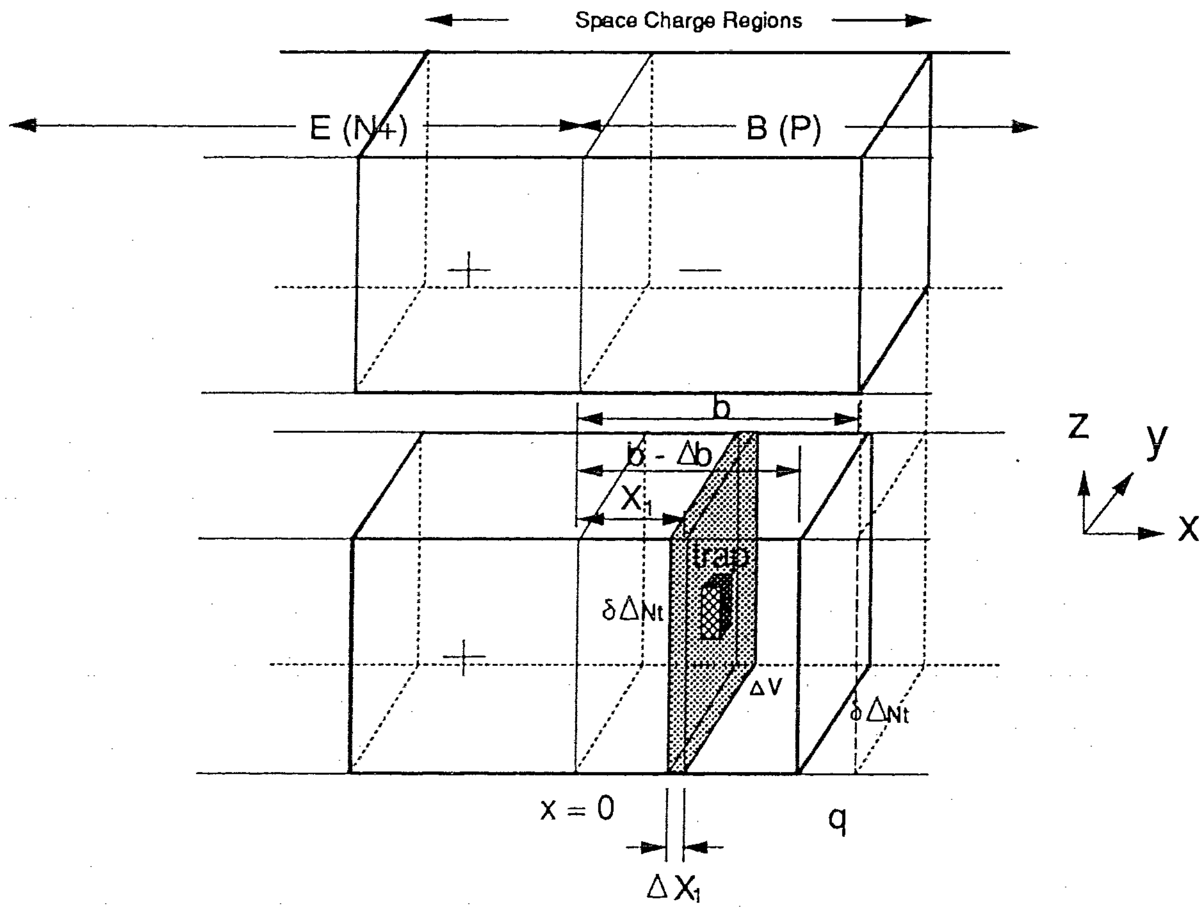

Figure 2.10 - A trap fluctuation $\delta \Delta N_t$ in an elementary volume $\Delta V = \Delta x_1 V$ in the base depletion region

located in the space charge region would modulate the width of the depletion region by an amount of Δb, which affects the amount of diffusion current flowing through the depletion region and modifies the resistance of the conduction channel immediately adjacent to the depletion region. This depletion region width modulation is governed by Possion's equation, as explained below. Applying Possion equation to the base-emitter depletion region results in :

$$\nabla^2\Psi = -\frac{q}{\varepsilon\,\varepsilon_0}\left[N_A - \frac{\delta\Delta N_t}{\Delta V}f(x,y,z)\right] \tag{2.22}$$

where f(x,y,z)=1 inside ΔV, and f(x,y,z)=0 otherwise. Directions x, y and z are defined as showing in Figure 2.10. The first term represents the space charges inside the depletion region and the second term represents the additional charge due to the fluctuating occupancy of traps. For a one-dimensional approximation, we ignore the field variations perpendicular to the collector current. In other words, we have

$$\frac{d^2Y}{dx^2} >> \frac{d^2Y}{dy^2},\ \frac{d^2Y}{dx^2} >> \frac{d^2\Psi}{dz^2}, \tag{2.23}$$

and

$$\frac{d\Psi}{dx} >> \frac{d\Psi}{dy},\ \frac{d\Psi}{dx} >> \frac{d\Psi}{dz}, \tag{2.24}$$

With the approximations, equation (2.22) becomes

$$\frac{d^2\Psi}{dx^2} = -\frac{q}{\varepsilon\,\varepsilon_0}\left[N_A - \frac{\delta\Delta N_t}{\Delta V}f(x)\right] \tag{2.25}$$

where f(x)=1 for $x_1 < x < x_1+\Delta x_1$, and f(x)=0 otherwise. Let Ψ_1 be the potential due to space charge only and Ψ_2 be the potential due to the trap fluctuation only, then the charge density, electric field and potential of our one-dimensional model would be that shown in Figure 2.11 and

$$\nabla^2\Psi = \frac{d^2\Psi}{dx^2} = \frac{d^2\Psi_1}{dx^2} + \frac{d^2\Psi_2}{dx^2} \tag{2.26}$$

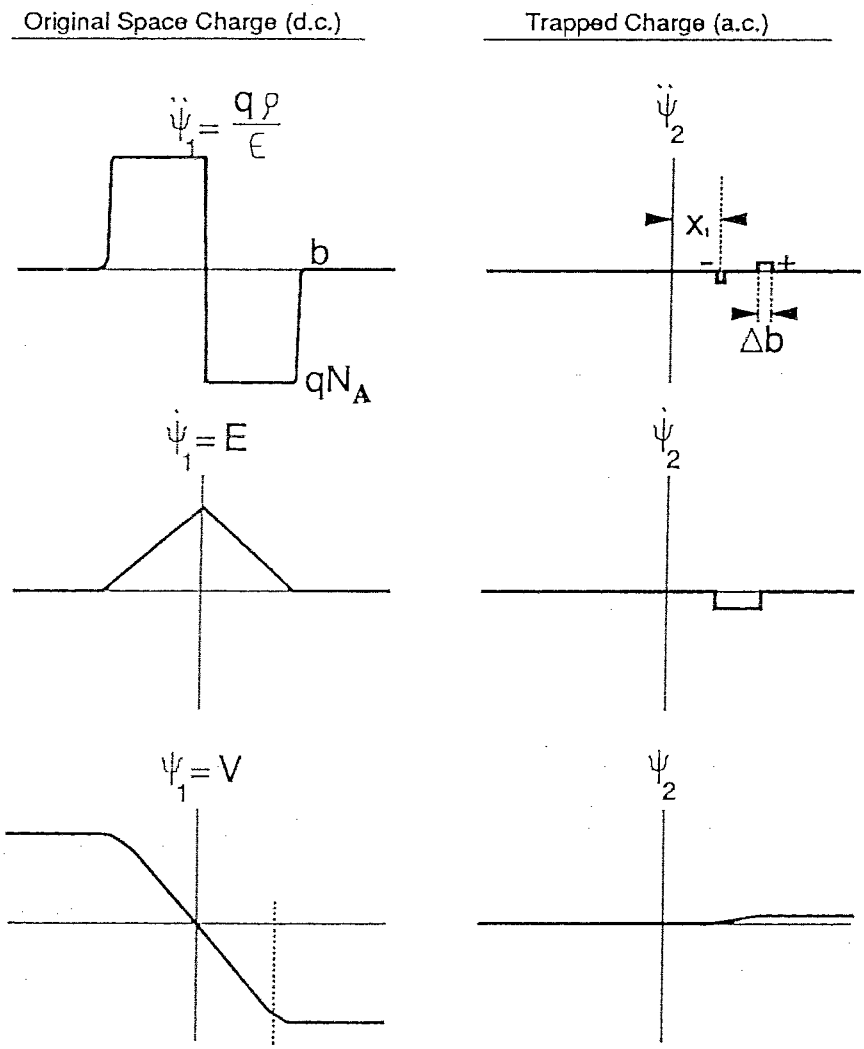

Figure 2.11 - The charge density, electric field and potential of our one-dimensional space-charge region trapping center model

Integrating from x=0 to the end of the space charge region, x=b, and using the boundaries conditions deduced from Figure 2.11, that

$$\Psi_1 = 0 \quad \text{at } x = 0, \tag{2.27a}$$

$$\frac{d\Psi_1}{dx} = \frac{b\,q\,N_A}{\varepsilon\,\varepsilon_0} \quad \text{at } x = 0, \tag{2.27b}$$

$$\Psi_2 = \frac{\delta \Delta N_t}{\Delta x_1 A} (b - x_1) \ \Delta x_1 \text{ at } x = b, \tag{2.27c}$$

then we can solve for $\Psi(x)$, to get

$$\Psi(x) = -\frac{q}{\varepsilon \varepsilon_0} N_A \left(\frac{x^2}{2} - b\,x\right) + \frac{q}{\varepsilon \varepsilon_0} \frac{\delta \Delta N_t}{\Delta x_1 A} (b - x_1) \ \Delta x_1. \tag{2.28}$$

At the depletion boundary, x=b, we have

$$\Psi(b) = -\frac{q}{\varepsilon \varepsilon_0} N_A \frac{b^2}{2} + \frac{q}{\varepsilon \varepsilon_0} \frac{\delta \Delta N_t}{A} \ (b - x_1) \tag{2.29}$$

For a first order approximation, we ignore the influence of the trap on the width of the depletion region at the other side of the junction. Taking the derivatives of $\Psi(b,x_1)$ with respect to b and x_1, we get

$$\begin{aligned} \delta\,\Psi &= \delta b \frac{d\Psi}{dx} + \delta x_1 \frac{d\Psi}{dx_1} \\ &= -\frac{q}{\varepsilon \varepsilon_0} N_A\, b\, \delta b - \frac{q}{\varepsilon \varepsilon_0} \frac{\delta \Delta N_t}{A} \ \delta x_1. \end{aligned} \tag{2.30}$$

Assuming that the base voltage is held constant by an external voltage source (V_{be}) and that the base resistance is zero, we set Ψ=0 to obtain δb in terms of $\delta \Delta N_t \, \Delta x_1$

$$\Delta b = -\frac{\delta \Delta N_t}{N_A A} \frac{\Delta x_1}{b}. \tag{2.31}$$

Equation (2.31) indicates that a trap fluctuation $\delta \Delta N_t$ produces a base-width modulation of $\Delta b = -\dfrac{\delta \Delta N_t}{N_A A} \dfrac{\delta \Delta x_1}{b}$. The negative sign indicates that the size of the depletion region would decrease to compensate the extra charge trapped inside the depletion region. The modulation of the depletion region width directly affect the emitter collector diffusion current which is related to the effective base length L_B by

$$I_c = I_s \exp\left(\frac{q V_{be}}{kT}\right)\left(1 + \frac{V_{ce}}{V_{af}}\right) \tag{2.32}$$

$$\text{where } I_s = \frac{A\, q\, D_n\, n_{op}}{L_B}. \tag{2.33}$$

Taking the derivative of I_c with respect to L_B and noting that $\delta L_B = \delta b$, we get

$$\frac{\delta I_c}{\delta b} = \frac{-A\, q\, D_n\, n_{op}}{L_B^{\,2}} \exp\left(\frac{q V_{be}}{kT}\right)\left(1 + \frac{V_{ce}}{V_{af}}\right) = \frac{-I_c}{L_B} \tag{2.34}$$

Let ΔI_C be the total change in collector current due to all traps, and Δb be the total change in base-width due to all traps. Then, the incremental change in ΔI_C due to an incremental change in Δb is

$$\delta\Delta I_c = \delta\Delta b \frac{\delta I_c}{\delta b} = \frac{\delta x_1\, \delta\Delta N_t}{b\, N_A\, A}\left(\frac{-I_c}{L_B}\right). \tag{2.35}$$

Using Fourier analysis and equation (2.20) and (2.21), we get that

$$\Delta S_{Ic}(f) = \lim_{T \to \infty} \frac{2}{T} \int_{-\infty}^{\infty} \delta\Delta I_c(u)\, \delta\Delta I_c(u+s)\, \exp(-j\omega s)\, ds$$

$$= \frac{4\, I_c^2\, \Delta x_1^3}{b^2\, L_B^{\,2}\, N_A^2\, A}\, n_t\, f_t\, (1 - f_t) \frac{\tau}{1 + \omega^2 \tau^2}.$$

$$\therefore\ \Delta S_{Ic}(f) = \frac{4\, I_c^2\, \Delta x_1^3}{b^2\, L_B^{\,2}\, N_A^2\, A}\, n_t\, f_t\, (1 - f_t) \frac{\tau}{1 + \omega^2 \tau^2}. \tag{2.36}$$

Comparing (2.36) with (2.16), the variance of the fluctuation in the carrier number is

$$\overline{\Delta N^2} = \frac{4\, I_c^2\, \Delta x_1^3}{b^2\, L_B^2\, N_A^2\, A}\, n_t\, f_t\, (1 - f_t). \tag{2.37}$$

The most important relationship obtained from this one-dimensional model is that, from this modulation mechanism, the model suggests that the collector current noise power should be proportional to the square of the collector current and inversely proportional to the emitter area. Experimental results indicate that there is a power relationship between $\Delta S_{i_c}(f)$ and I_c^{power} with the power≅2. For the emitter area dependence, the experimental results were that $\overline{\Delta N^2}$ is inversely proportional to the square of the emitter area, instead of inversely proportional to the emitter area found from the theory. This discrepancy in the power of the emitter area is probably due to the first order approximation used in this model, the non-uniform current flow inside the conduction channel, the neglect of the surface oxide traps and the possibility of the effect of other second order noise mechanism that happen concurrently with the assumed mechanisms. The motivation in developing this model was to provide some physical explanation for the phenomena observed, rather than to provide a precise prediction of the noise level that requires more details than are available with a one-dimensional first order model.

2.3.3.2.1. Determining the Trap level energy from the experimental data using this model

Due to the limited temperature range in the experimental data, only part of the GR feature can be recognized. Curve fitting the experimental data to determine the peak of the GR noise spectra and then calculating the corresponding Fermi-level would give a comparatively large error. However, by differentiating equation (2.36) with respect to the reciprocal of temperature, the trap energy level can be determined from the rising edge of the GR spectrum. The use of the falling edge rather than the peak would allow more data points to be used in the calculation, and the results will therefore be more accurate. First of all, we substitute the trap fractional occupancy in (2.17) into our noise model in (2.36) and let

$$K = \frac{4\, I_c^2\, \Delta x_1^3}{b^2\, L_B^2\, N_A^2\, A}\, n_t. \qquad (2.38)$$

After simplification, we get

$$\Delta S_{Ic}(f) = \frac{q\, K\, \tau_0\, \exp\left(\frac{2\, q\, E_t}{k\, T}\right)}{\exp\left(\frac{q\, E_F}{k\, T}\right)\left(1 + \exp\frac{q\,(E_t - E_F)}{k\, T}\right)^2 \left(1 + 4\,\pi^2\, f^2\, \tau_0^2\, \exp\frac{2\, q\, E_t}{k\, T}\right)} \qquad (2.39)$$

As explained earlier in section 2.3.3, the GR spectrum has the shape of an inverted valley, and the Fermi-level is equal to the trap energy level at the maximum point of a GR noise spectrum which has the factor $\frac{\tau}{1+\omega^2\,\tau^2}$ as the trap activation term. Considering the denominator of the trap activation term at different temperatures, we have that,

on the rising edge of the GR noise spectrum ($T << T_{peak}$), $\omega^2\tau^2 >> 1$, (2.40a)

on the falling edge of the GR noise spectrum ($T >> T_{peak}$), $\omega^2\tau^2 << 1$. (2.40b)

A similar situation occurs in the denominator of the fractional trap occupancy factor

$f_t = \dfrac{1}{1 + \exp\dfrac{q\,(E_t - E_F)}{k\, T}}$ where we get at the peak ($T = T_{peak}$), $\qquad \exp\frac{q\,(E_t - E_F)}{k\,T} = 1,$ (2.41a)

on the rising edge ($T << Tpeak$), $\qquad \exp\frac{q\,(E_t - E_F)}{k\,T} >> 1,$ (2.41b)

and on the falling edge ($T >> T_{peak}$), $\qquad \exp\frac{q\,(E_t - E_F)}{k\,T} << 1.$ (2.41c)

Now applying equations (2.40) and (2.41) to (2.39), we get that on the rising edge, equation (2.39) becomes

$$S_i = \frac{q\,K}{4\,\pi^2\,f^2\,\tau_0^2\,\exp\frac{q\,(2\,E_t - E_F)}{k\,T}}$$

Taking natural log and differentiating with respect to 1/T, we get

$$\frac{d\,(\ln S_i)}{d\,(1/T)} = -\frac{2\,q\,E_t}{K} - \frac{q\,T}{k}\frac{d\,E_F}{d\,T} + E_F\,\frac{q}{k} \tag{2.42}$$

Rearrange this to get,

$$\boxed{E_t = -\frac{T}{2}\,\frac{d\,E_F}{d\,T} + \frac{E_F}{2} - \frac{k}{2\,q}\,\frac{d\,(\ln S_i)}{d\,(1/T)}} \tag{2.43}$$

in which E_F can be calculated from equation (2.18), then $\frac{d\,(\ln S_i)}{d\,(1/T)}$ can be measured from rising edge of a ln (S_i) vs 1/T curve. Therefore, by plotting the GR noise spectrum versus the reciprocal of temperature, one can determine the trap level energy. It will be shown in the experimental section that a trap-level energy that agrees with the quasi-Fermi level method was determined using equation (2.43). On the rising edge, equation (2.39) becomes

$$\ln (S_i) = \ln \ (K \tau_0) + \frac{q \, E_F(T)}{k} \frac{1}{T} \cdot \qquad (2.44)$$

In the experiment section, the slope of $\frac{q \, E_F(T)}{k \, T}$ is shown to closely follow the slope of the experimental data. Furthermore, since K contains the emitter area factor, a plot of the y-intercept in equation (2.44) versus the emitter area allows us to determine the dependence of GR spectrum on emitter area. It will be shown in the experiment section later that a straight line was observed in a log-log plot of GR noise power versus the emitter area, with the noise power being inversely proportional to the square of the emitter area.

2.3.4. Theories for Flicker Noise

2.3.4.1. Fundamental Flicker Noise

Flicker noise in modern bipolar transistor is a fundamental low frequency noise which is mainly caused by the diffusion of carriers. Diffusion noise is the main flicker noise source because the major current component in bipolar transistor is the diffusion current. The collision and scattering between carriers and the lattice phonons during diffusion are the main mechanism that produces mobility fluctuation and the fundamental flicker noise. The diffusing carriers that generate noise could be those carriers diffusing from the emitter to the collector, or those carriers injected from the base into the emitter. There are different kinds of scattering and collision mechanisms in the diffusion process of a bipolar junction device, and each of these mechanisms can lead to a different expression for the diffusion type flicker noise. However, lattice scattering and ionized impurity scattering are the two most important scattering mechanisms in a bipolar transistor. The contribution of each of these mechanism at a given temperature can be estimated by finding the mobility of the charge carriers. The mobility is material and temperature dependent, and is an important parameter for devices in which the main current is that due to drift. At low temperatures, carriers have low thermal kinetic energies and low thermal velocities and have long passage time through ionized impurities. With reduced phonon activities, lattice scattering is reduced relative to ionized impurities scattering. Therefore ionized impurity scattering mechanism is the dominant scattering mechanism in most semiconductor devices at low temperatures. On increasing temperature, the collisions due to ionized impurity scattering become relatively less important when compared to collisions with neutral atoms of the lattice because the lattice atoms vibrate about their mean position with an amplitude that increases with temperature. The higher the temperature, the larger the effective capture area of the lattice atoms. Thus lattice scattering is the key scattering mechanism at higher temperatures. Since the total mobility would be heavily affected by the scattering mechanism with the shortest scattering time, the total mobility would be that of ionized impurity scattering at lower temperatures, and dominated by that due to lattice scattering at higher temperatures. Equations that give a good fit to the experimental data for the mobility of electrons (μ_e) and holes (μ_h) in silicon have been presented in [22] and are described by equations (2.45a) and (2.45b) below

$$\mu_e = 88\, T_n^{-0.57} + \frac{7.4 \times 10^8 \times T^{-2.33}}{1 + [N/1.26 \times 10^{17}\, T_n^{2.4}]\; 0.88 \times T_n^{-0.146}} \tag{2.45a}$$

$$\mu_h = 54.3\, T_n^{-0.57} + \frac{1.36 \times 10^8 \times T^{-2.23}}{1 + [N/2.35 \times 10^{17}\, T_n^{2.4}]\; 0.88 \times T_n^{-0.146}} \tag{2.45b}$$

where $T_n = T/300$. In Figure 2.12, the three solid lines represent the electron and hole mobility calculated from these equations using the doping levels for our transistors. The solid line at the top represents the mobility of the majority electrons diffusing from the emitter to the collector. The other two solid line at the bottom represent the upper bound and low bound of the mobility of the minority hole injected from the base into the collector. The upper bound and lower bound were calculated using the highest and lowest doping concentration in the base respectively. The rising dashed line is the physical models [24] for mobility due to ionized impurity scattering (μ_i) as given in equation (2.46) and is proportional to $T^{3/2}$ while that due to lattice scattering (μ_l) is given by equation (2.47) and is proportional to $T^{-3/2}$.

$$\mu_i = \frac{1.65 \times 10^{19}}{N_i \ln\left[1 + (3 \times 10^{11}/N_i^{\ 2/3})(T\varepsilon/300\varepsilon_0)^2\right]} \left(\frac{T}{300}\right)^{3/2} \left(\frac{\varepsilon}{\varepsilon_0}\right)^2 \left(\frac{m_0}{m^*}\right)^{1/2} \ \mathrm{cm^2/V\text{-}s} \qquad (2.46)$$

$$\mu_l = \frac{2\sqrt{2\pi}\, e\, h^4 \rho\, v_s^{\ 2}\, m_e^{*\,-5/2} (kT)^{-3/2}}{2\, E_{1c}^{\ 2}} \ \mathrm{m^2/V\text{-}s.} \qquad (2.47)$$

Here E_{1c} is a proportionality constant commonly referred as the deformation potential, ρ is the mass density, v_s is the sound velocity in the semiconductor with $v_s^{\ 2} = c/\rho$ and c is the elastic constant. The range of temperature for our measurements is between 273K and 373K as indicated by the region bounded with the two vertical dash lines in the figure. Since the calculated electron and hole mobilities lie within the lattice scattering region (the $T^{-3/2}$ falling portion), our calculation indicates that lattice scattering rather than ionized impurity scattering dominates the scattering process in our device. This is an important conclusion that will be used in formulation of our noise model later.

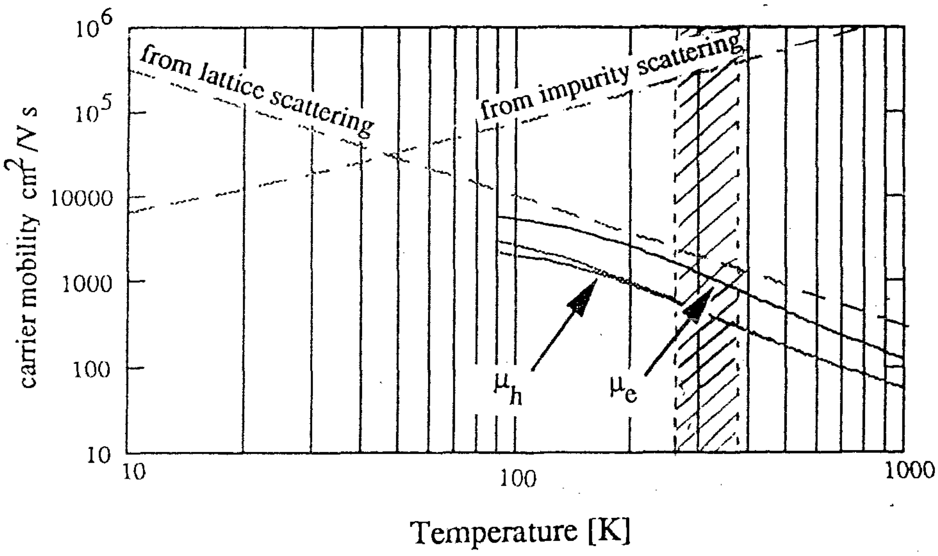

Figure 2.12 - The electron and hole mobility calculated for our devices indicate that lattice scattering rather than ionized impurity scattering dominates

Besides ionized impurity scattering and lattice scattering, there are other high energy collisions that could occur in our devices, but to a smaller extent at room temperature than at higher temperatures. Umklapp process is one of these high energy processes in which an electron gives up a momentum $\frac{h}{a}$ to the lattice or accepts a momentum $\frac{h}{a}$ from the lattice (where a is the lattice spacing and h is the Planck's constant), and is scattered into the next Brillouin zone. Since momentum is not conserved, the collision is inelastic. This inelastic collision is also an integral part of our noise model.

2.3.4.2. Mobility Fluctuation Theory for Diffusion noise

Using the theory developed in [25], the hole current noise spectrum in a short p+-n diode due to mobility fluctuations, which is the current noise spectrum due to the emitter-collector diffusion current I_{Ep} in a p+-n-p transistor could be written as

$$S_{I_{Ep}}(f) = 2\,q\,I_{Ep}\frac{\alpha_p}{4\;f\;\tau_{dp}}\ln\frac{P(0)}{P(w_B)} \tag{2.48}$$

where α_p is the Hooge's constant [14] for holes, $\tau_{dp} = w^2/2\,D_p$ is the diffusion time constant for holes through the base region, w_B is the base width and P(0) and $P(w_B)$ are the hole concentrations per unit length at the emitter side and the collector side of the base, respectively, and $D_p = k\,T\,\mu_p$ is the diffusion constant for holes. Similarly, the current noise spectrum due to electrons injected from the base into the emitter is

$$S_{I_{En}}(f) = 2\,q\,I_{En}\frac{\alpha_n}{4\;f\;\tau_{dn}}\ln\frac{N(0)}{N(w_E)} \tag{2.49}$$

where α_n is the Hooge's constant for electrons, $\tau_{dn} = w^2/2\,D_n$ is the diffusion time constant for electrons through the emitter region, w_E is the emitter width and N(0) and $N(w_B)$ are the electron concentrations per unit length at the base side and the metal contact side of the emitter, respectively. The diffusion time constant τ_{dn} is related to the cutoff frequency of the transistor by

$$f_T = \frac{1}{2\,\tau_{dn}}. \tag{2.50}$$

Assuming $I_{Ep} >> I_R$, then $\frac{I_c}{\beta} = I_b = I_{Ep}$. Using equation (2.50) and modifying (2.49) for our npn transistor, we obtain the equation for the diffusion noise due to mobility fluctuation occurring in the holes injected from the base into the emitter as

$$S_{I_b}(f) = \frac{\pi\,f_T\,q\,I_c\,\alpha_p}{f\;\beta}\ln\frac{P(0)}{P(w_E)}. \tag{2.51}$$

I_b in the original equation is replaced by I_c because the collector current is measured by our system directly. To estimate the ratio $\frac{P(0)}{P(w_E)}$, we follow the method in [14, equation A7] which gives

$$\frac{P(0)}{P(w_E)} < \frac{w_E\, v_s}{D_p} \tag{2.52}$$

where v_s is the saturated drift velocity and, for silicon, is equal to

$$v_s = \frac{2.4 \times 10^5}{1 + 0.8 \exp\left(\frac{T}{600}\right)}. \tag{2.53}$$

Using (2.52) in equation (2.53), we can now calculate a minimum value for the Hooge's parameter for holes as

$$\alpha_p > \frac{\beta\, D_p\, S_{I_b}(f)\, f}{\pi\, f_T\, q\, I_c\, w_E\, v_s}, \tag{2.54a}$$

or

$$\alpha_{p,min} = \frac{\beta\, D_p\, S_{I_b}(f)\, f}{\pi\, f_T\, q\, I_c\, w_E\, v_s}. \tag{2.54a}$$

where the subscript min denotes minimum. By measuring the base current noise S_{I_b} (f), collector current I_C, and knowing the device parameters of the bipolar transistors including the current gain β, the cutoff frequency f_T, the emitter width w_E, then equation (2.54) allows us to calculate the minimum Hooge's parameter for holes. As shown in the experiment section, the Hooge's parameter for holes determined from our experiments has a value between 3 x 10^{-6} to 5 x 10^{-9}, and lies in the range of Hooge's parameter reported by other researchers, as illustrated in next section. Equation (2.54) is valid only when the diffusion noise arising from the base emitter hole diffusion current is the dominant noise source in the base emitter region. We will show later from our experiments that the dominant noise in our transistor is GR noise in base-emitter region. Although the diffusion noise is not the dominant noise source, it still plays an important part in fitting our model with the experimental data.

2.3.4.3. The Hooge's parameter used in the Diffusion Noise Model

The Hooge's parameter appears in equation (2.51) and (2.54) has been proposed by Hooge [26]. Based on data obtained for many different materials, he postulated that

$$\frac{S_I(f)}{I^2} = \frac{\alpha}{N f} \tag{2.55}$$

where N is the effective number of carriers, α is a universal dimensionless constant of about 2×10^{-3} that is only weakly dependent on temperature. However, it is now believed that the Hooge's parameter is not a universal constant and is several orders of magnitude smaller than the proposed value for some devices. As we will show later shown in the experiment section, the Hooge's parameter for holes determined from our experiments has values which range from 3×10^{-6} for small devices with an emitter area of $1.6\mu m^2$ at low temperatures to a value of 5×10^{-9} for large devices with an emitter area of $144\mu m^2$ at high temperatures, and these values agree closely with the Hooge's parameter values reported by other researchers. Different expressions for Hooge's parameter have been reported for different flicker noise mechanisms and depending on the nature of the noise source, the effective Hooge's parameter could be a combination of one or more Hooge's expression given below :

$$
\alpha_H = \begin{cases}
\dfrac{4\alpha_0}{3\pi}\dfrac{\Delta v^2}{c^2} & \text{for collision-free device operation, [27,28]} \\[2ex]
\dfrac{4\alpha_0}{3\pi}\dfrac{6kT}{m^*c^2} & \text{for normal collision process}^2\text{, [14]} \\[2ex]
\dfrac{4\alpha_0}{3\pi}\left(\dfrac{h}{mac}\right)^2 & \text{for Umklapp collision process}^3\text{, [14, 29-31]} \\[2ex]
\dfrac{4\alpha_0}{3\pi}\dfrac{2}{3} & \text{for coherent state flicker noise source,[32-33]} \\[2ex]
\dfrac{4\alpha_0}{3\pi}\dfrac{2E}{m\,c^2} & \text{for fluctuation in carrier injection across junction barrier [34-36]} \\[2ex]
\dfrac{4\alpha_0\;(2e(V_{dif} - V) + 6kT)}{3\pi\left((m_n^*)^{1/2} + (m_p^*)^{1/2}\right)^{1/2}} & \text{for fluctuation across junction barrier, [34-35]} \\[2ex]
\dfrac{4\alpha_0}{3\pi}\,(Ego - |Eg\,|)\dfrac{2}{m^*} & \text{for recombination of electron in the p-region contacts. [37]}
\end{cases}
$$

(2.56a] to (2.56g)

The way to combine the above Hooge's expression is to multiply each expression by an probability factor which is equal to

$$P_i\,(T) = \frac{\mu^2}{\mu_i^2} \qquad \textbf{(2.57)}$$

---

2 Normal collisions are elastic collisions with a Maxwellian velocity distribution.

3 In an Umklapp porcess, an electron can give up a momentum h/a to the lattice or accept a momentum h/a from the lattice, while being scattered into the next Brillouin zone.

where μ_i^2 is the carrier mobility due to a particular type of scattering mechanism. The effective Hooge's parameter α_H can be calculated from the Hooge's parameter for different scattering processes using the following equation,

$$\alpha_H = \sum_i \frac{\mu^2}{\mu_i^2} \alpha_{H_i}. \tag{2.58}$$

A derivation for this expression using Mathiesen's rule is shown in Appendix I. Based on the experiments in [38-40], two probability factors were introduced in [14] for elastic collision process and non-elastic collision process :

$(1 - \exp(\frac{-\theta}{2T})$	for elastic process (normal collision process) and
$\exp(\frac{-\theta}{2T})$	for non-elastic (Umklapp collision process)

where θ is the Debye temperature. Since good fitting to the experimental data using Umklapp collision (non-elastic collision) and normal collision (elastic collision) were obtained in [14], these results will be used in our model, as given by equation (2.58b) below.

$$\alpha_p = \alpha_{elastic} \frac{\mu^2}{\mu_{elastic}^2} + \alpha_{non\text{-}elastic} \frac{\mu^2}{\mu_{non\text{-}elastic}^2} \tag{2.59a}$$

$$= \alpha_{elastic} (1 - \exp(\frac{-\theta}{2T})) + \alpha_{non\text{-}elastic} \exp(\frac{-\theta}{2T}) . \tag{2.59b}$$

Using (2.56b) for normal collision process and (2.56c) for Umklapp collision process and the two probability factors, the expression for the effective Hooge's parameter becomes

$$\alpha_p = \frac{4\,\alpha_0}{3\,\pi}\,\frac{6\,k\,T}{m^*\,c^2}\,(1 - \exp(\frac{-\theta}{2T})) \;+\; \frac{4\,\alpha_0}{3\,\pi}\left(\frac{h}{m^*\,a\,c}\right)^2 \exp(\frac{-\theta}{2T}) \tag{2.60}$$

where θ is the Debye temperature and is equal to 645K for both p-type and n-type silicon and 350K for GaAs.

Chapter 3 Experiment

3.1 Devices Under Test (DUT)

For the experiments, seven bipolar transistors with emitter areas varying from 0.5 x 3.2 μm^2 to 14.4 x 3.2 μm^2 were used, and the noise measurements were performed at ten temperatures between 283K to 373K with more than five biasing currents at each temperature, and at frequencies from 10Hz to 100kHz. Each noise measurement was repeated at least 30 times. Figure 3.1 summarizes our measurement procedures for noise measurement with different frequencies, biasing currents, temperatures and device sizes.

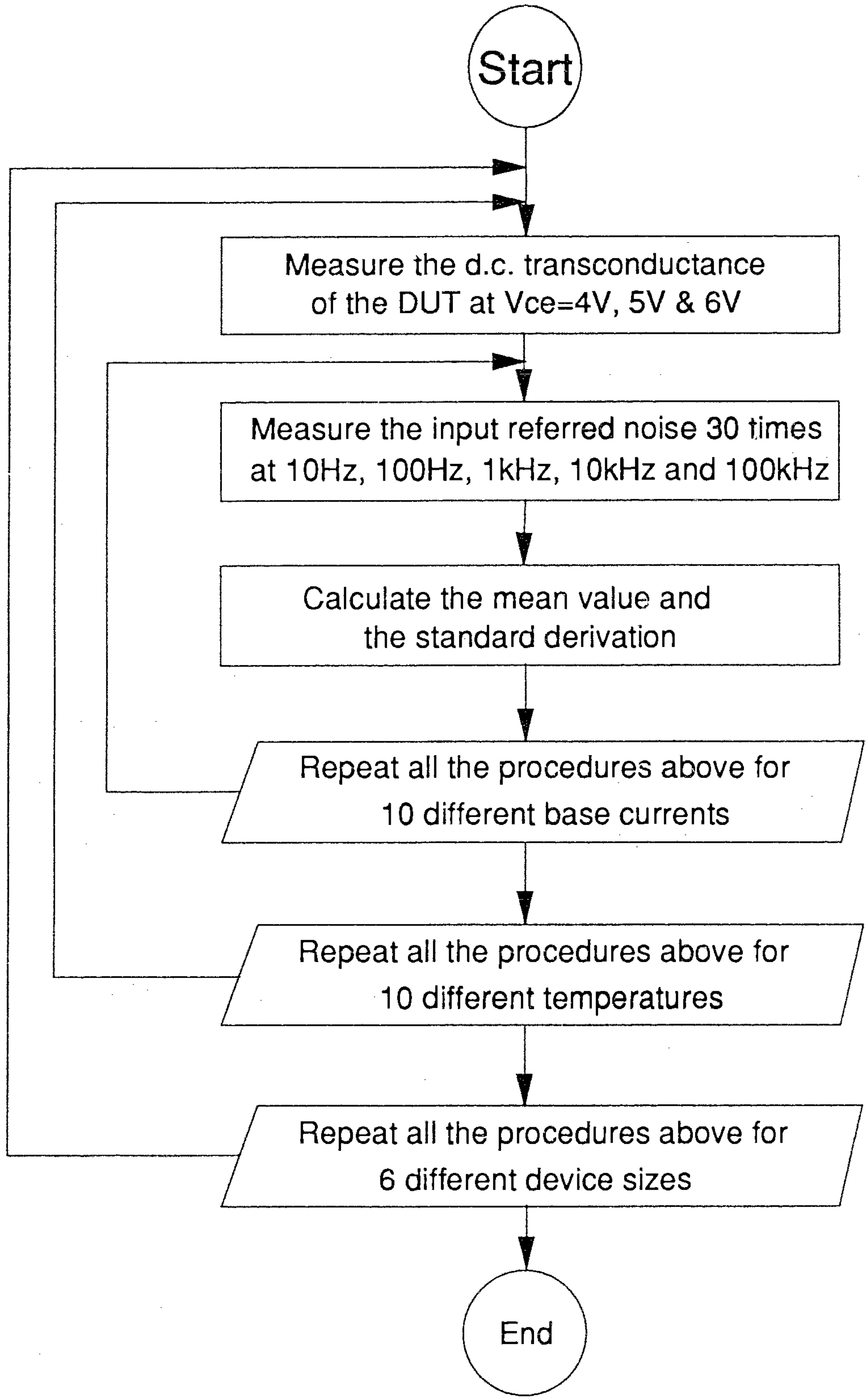

Figure 3.1 - A summary on our measurement procedures for noise measurement with different frequency, biasing current, temperature and device size

The chemical doping profile of the device used is shown in Figure 3.2. The transistors used in the experiment have an Arsenic doped emitter, a Boron-doped p type base and a Phosphorous doped n-type collector. D.C. characteristic measurements including the measurement of the forward and reverse current gains, base, collector and emitter internal resistances were performed on the HP 4145B Semiconductor Parameter Analyzer.

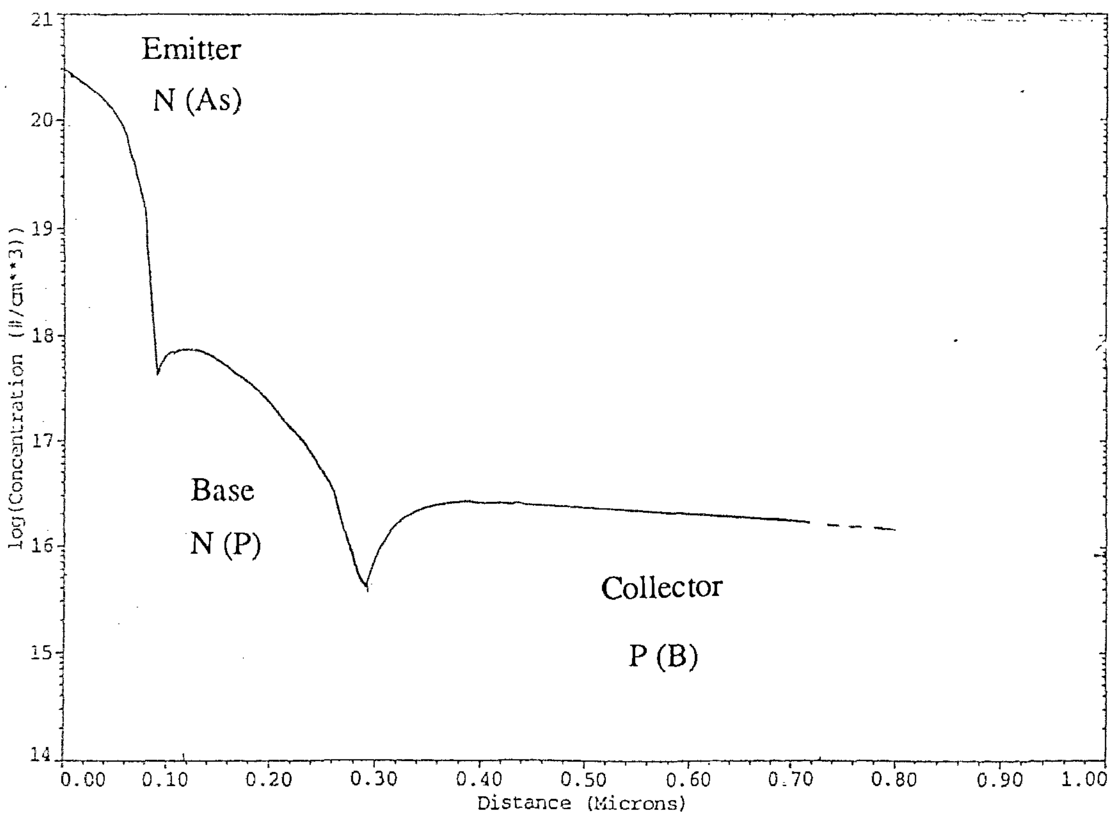

Figure 3.2 - The chemical doping profile of typical npn transistors used in the experiment

3.2 The Noise Measurement System

A block diagram of the measurement system is shown in Figure 3.3. The equipment used to measure input referred noise of the transistors is the Quan-Tech Semiconductor Noise Analyzer model 5173 which biases the device's collector voltage to 5V and a constant collector current level as shown in Figure 3.4. Input referred noise power were measured at five frequencies (10Hz, 100Hz, 1kHz, 10kHz and 100kHz) simultaneously using five bandpassed noise measuring units.

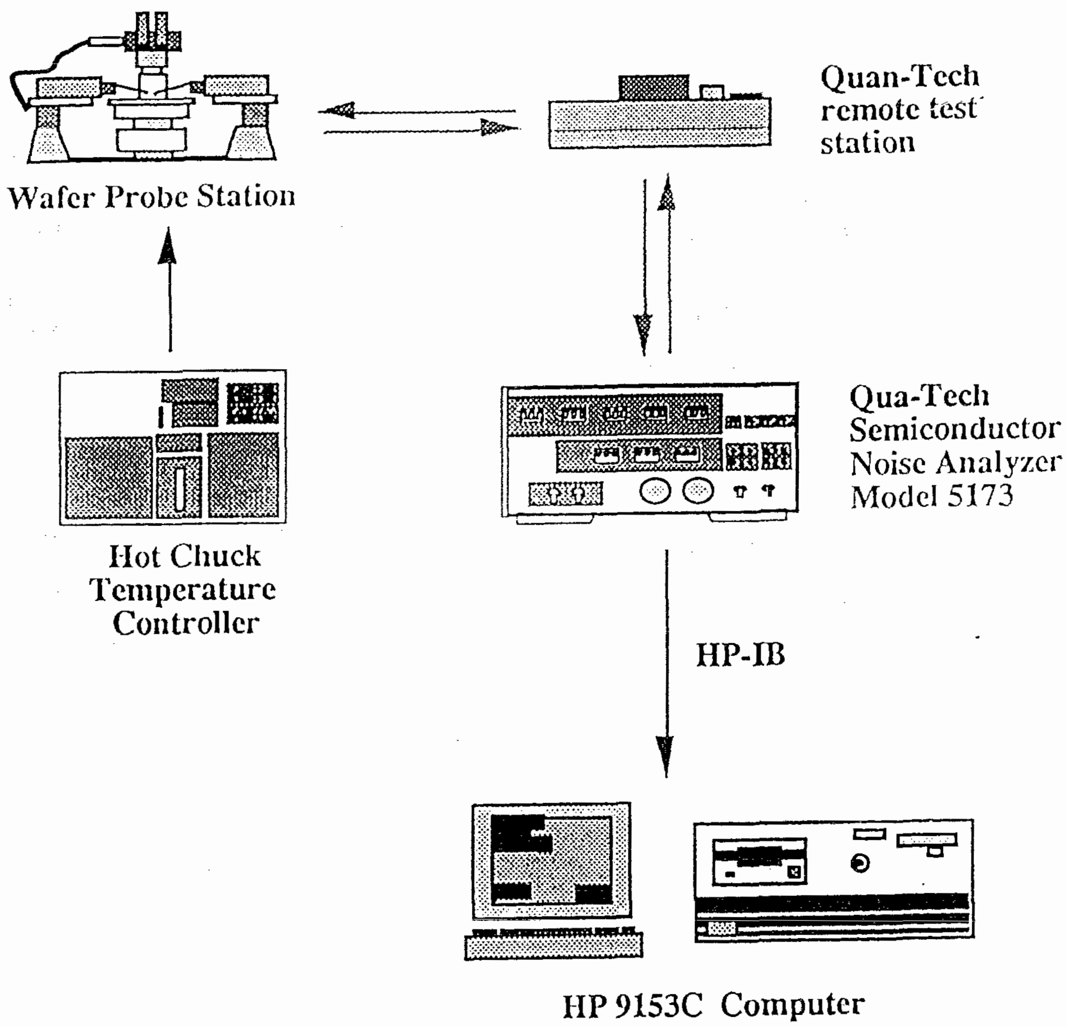

Figure 3.3 - Block diagram of the noise measurement system

The bipolar junction transistors being measured were placed in the prober station illustrated in Figure 3.3 which is connected to the Quan-Tech remote test station and the hot chuck temperature controller. The hot chuck temperature controller heats the hot chuck using d.c. current. The measured noise data were collected and statistically analyzed with an HP computer. Due to the high sensitivity of the Quan-Tech measurement system, each measurement required a period of at least 50 seconds to stabilize the noise readings. External interference including the effect of someone walking by the equipment would affect the measurements results. The system's transient response and the effect of external interference were investigated and the results were summarized in Figure 3.5.

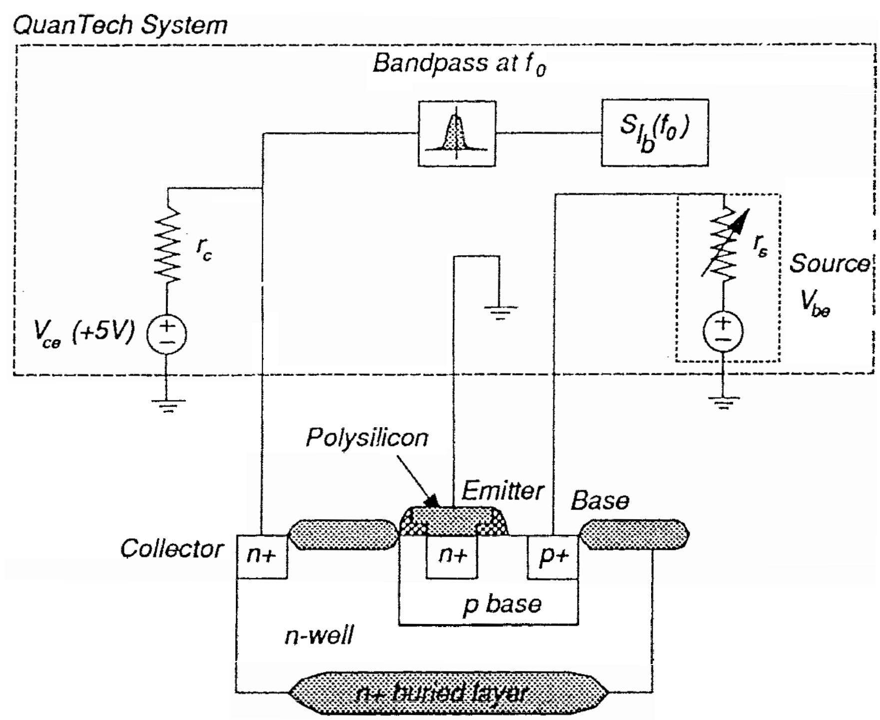

Figure 3.4 - The biasing scheme and circuit configuration of the noise measurement

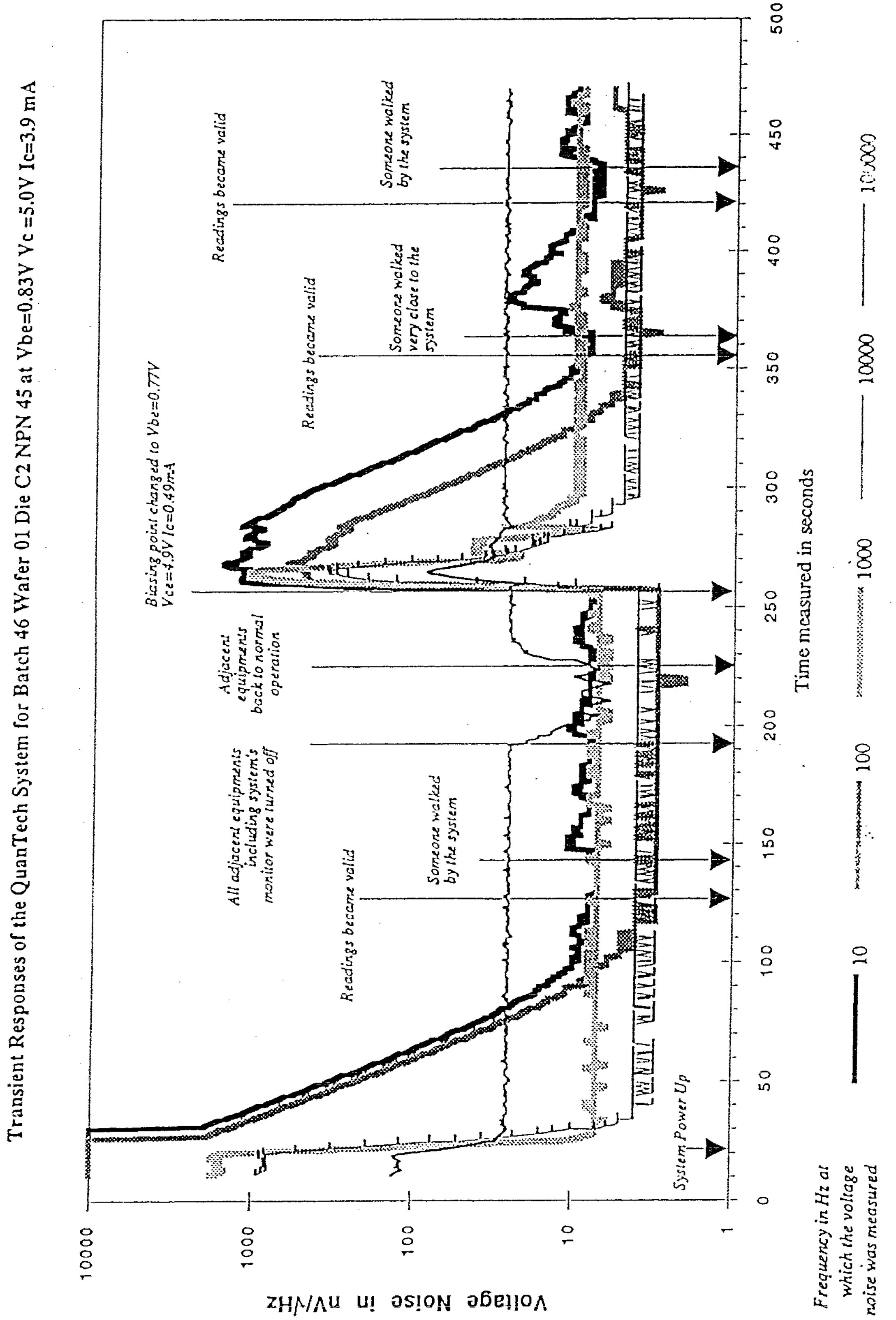

Figure 3.5 - The QuanTech system's transient response and the effect of external interference.

3.3 The Analysis Procedures

Figure 3.6 illustrates the analysis procedures for our noise data. Input referred current noise collected at the five measurement frequencies was plotted in a graph of noise power versus frequency as shown in graph A. Assuming our noise data are $1/f^{\beta}$ type with $\beta = 1$,

$$S_x(f) = \frac{\alpha}{f^{\beta} N} \tag{3.1a}$$

then

$$\frac{\alpha}{N} = f_0 \, S_x(f_0) \tag{3.1b}$$

Since f_0 can be any frequency, by setting $f_0 = 1$, then

$$\frac{\alpha}{N} = f_0 \, S_x(f_0) = f_1 \, S_x(f_1) = ... = S_x(\,1\text{Hz}\,) \tag{3.1c}$$

Equation (3.1c) indicates that multiplying all noise data by their measuring frequencies is the same as normalizing all noise data to 1Hz. This idea allows us to draw conclusion from data measured at different frequencies. By repeating the measurement in graph A at ten different base currents, and normalizing all noise data to 1Hz, the dependence of the input referred noise power on base current was determined as shown in graph B. The y-intercept (KF) in this log-log graph is actually the noise power normalized to a base current of 1A because the base current is 1A at the y-intercept. Since KF is the noise normalized to 1Hz and a base current of 1A, KF is used to compare the noise level of different devices. The slope of the line (AF) indicates the exponential dependence of the

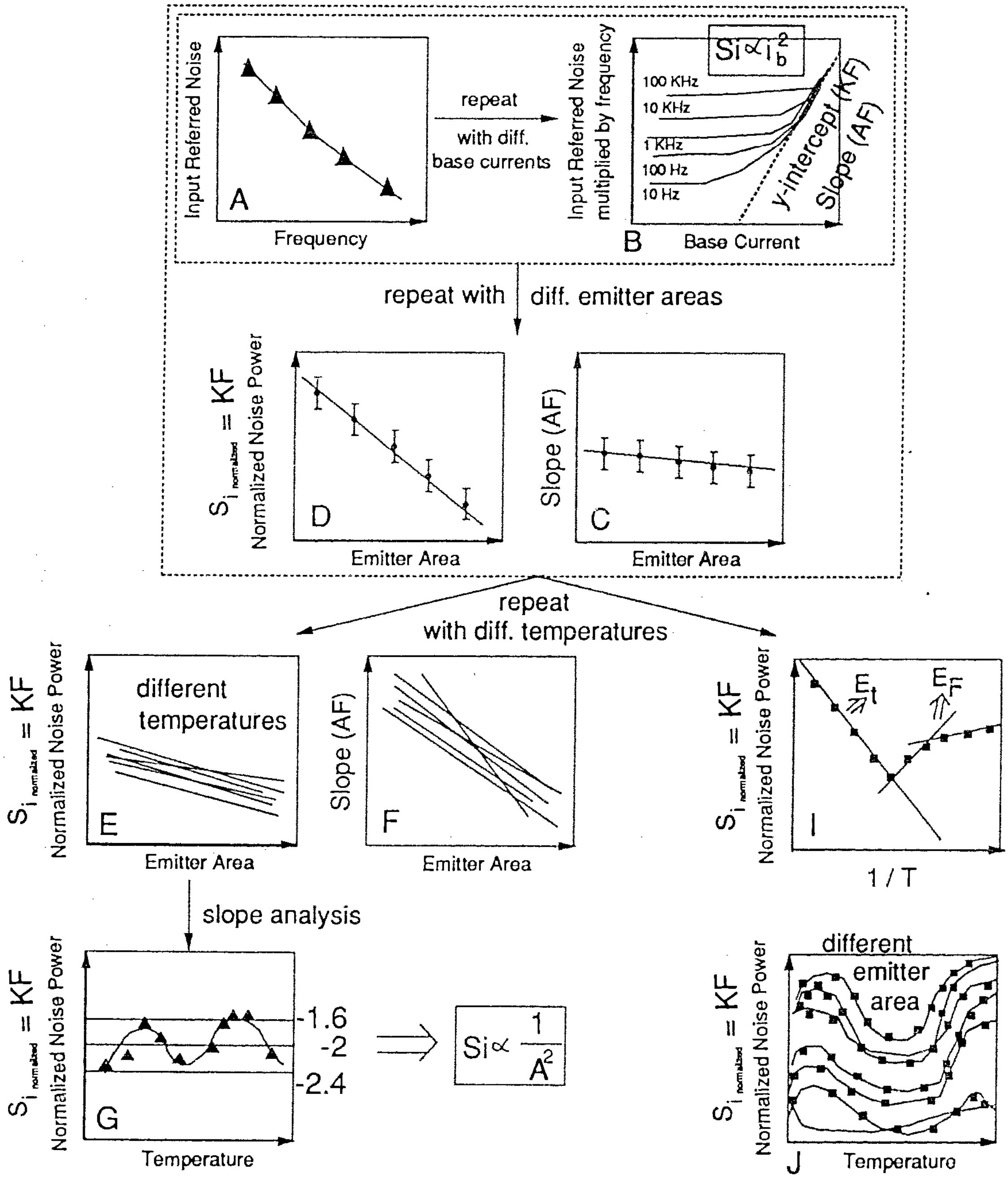

Figure 3.6 - Analysis procedures for the measured noise data

noise power on the base current. By repeating the above procedures for seven different emitter areas, the variation of the y-intercept (KF) and the slope (AF) can be found as shown in graphs C and D. It will be shown in the result section that AF is found to be varying slightly with the emitter area and has an average value of approximately 2. The measured noise power is therefore closely proportional to the square of the base current for all emitter areas. All the above procedures were repeated for 10 different temperatures between 273K and 373K, as shown in graphs E and F. By analyzing the variation of the slope of each line in these graphs, the variation of the slope of the lines in these graphs can be plotted as a function of temperature as shown in graph G. Furthermore, the normalized current noise KF is found to be inversely proportional to the square of emitter area from graph G. Using the model developed in this research, the trap activation energy can also be found by plotting the normalized noise data versus the reciprocal temperature as shown in graph I. A GR noise profile can also be observed for different emitter areas by plotting the normalized noise data versus temperature as shown in graph J. Finally, improvements of the noise model were made based on the results in graph B and C, and this improved noise model was used to fit experimental results shown in graph A (variation with frequency), graph I (variation with temperature) and graph J (variation with both emitter area and temperature).

Chapter 4 Results and Discussion

4.1 D.C Characteristics

The d.c. and noise measurement results are presented in this chapter, and comments will be made and conclusions will be drawn. A typical i_c-V_{be} characteristic and forward beta plot of one of the transistor used in this research were shown in Figure 4.1 and 4.2 respectively. Noise measurement were made only in the linear region of the i_c-V_{be} characteristic before the onset of high level injection and after the region where the recombination current dominates.

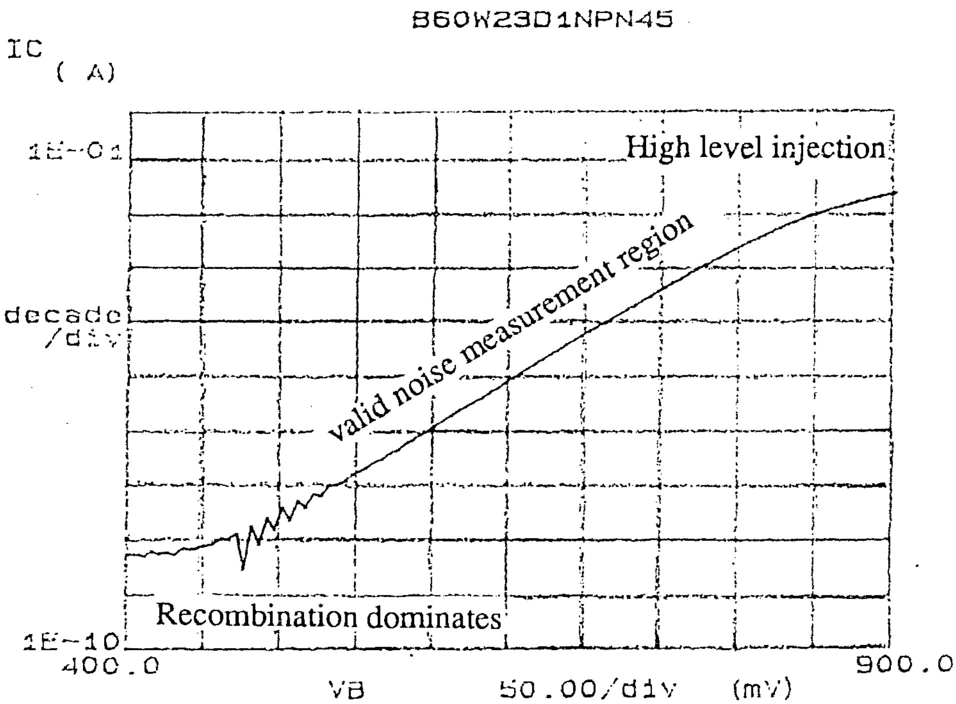

Figure 4.1 - A typical i_c-V_{be} characteristic of the transistors used

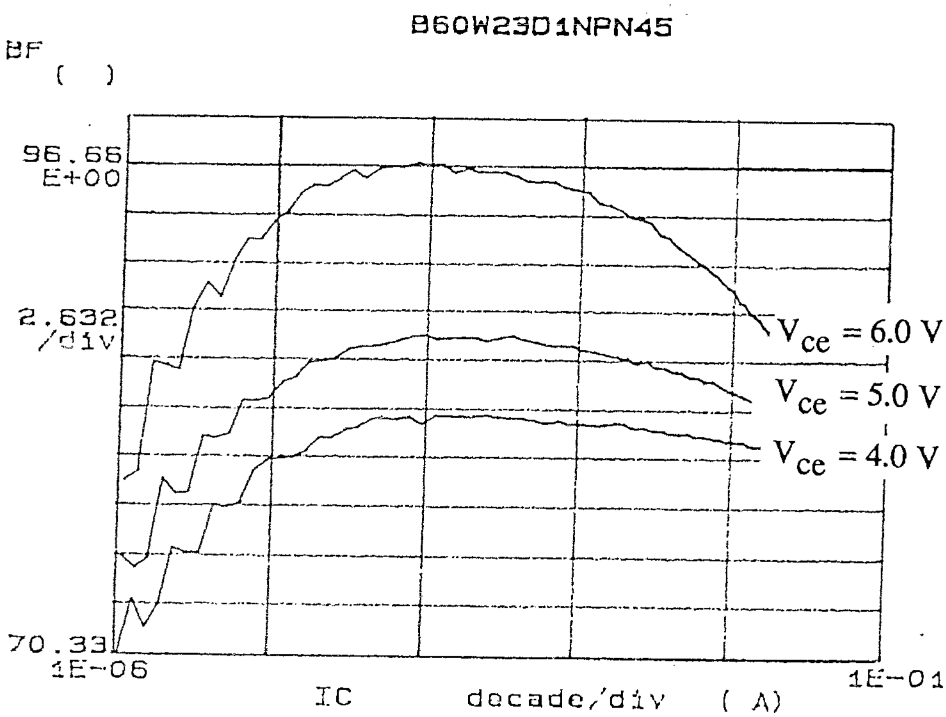

Figure 4.2 - A typical plot of forward current gain β versus Ic characteristic of the transistors used

4.2 Variation with Collector Current

An example of the input referred noise spectra measured at different collector currents is shown in Figure 4.3. The low frequency noise spectra were found to have a $1/f^{\beta}$ dependence with $\beta \cong 0.8$. The noise spectrum decreases as the collector current decreases, following the trend of the flicker noise model. The flicker noise in our measurements is much higher than the white noise and the corner frequency is beyond the measurable frequency range of 100kHz.

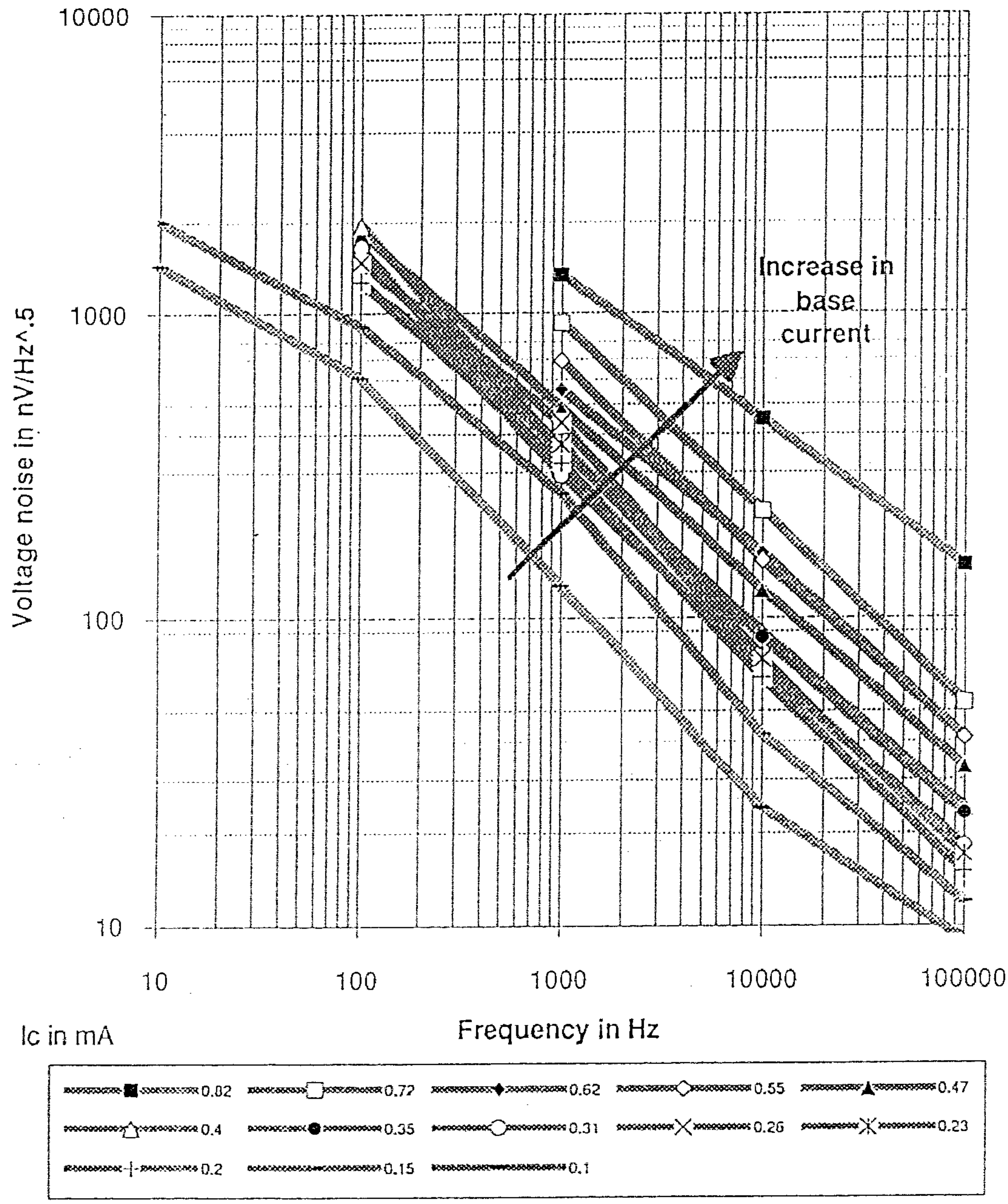

Figure 4.3 - **Typical input referred voltage noise spectra measured at different collector currents**

Using the external base resistance and the forward beta measured for each collector current, the measured voltage noise and collector current were converted into current noise and base current respectively. Then by normalizing the noise data at different frequencies to 1 Hz, the data was plotted in a graph of log (normalized current noise) vs. log (base current). Figure 4.4 is a typical log-log graph of normalized current noise vs. base current. There are two separate regions in this graph :

1) the white noise region where the flicker noise is drowned out by the white noise and,
2) the flicker noise region where the flicker noise dominates.

In this region, the current noises of different frequencies overlap with each other since they are all normalized to 1Hz. Due to the nature of the flicker noise, the noise levels at high frequencies are lower than those at lower frequencies. When the base current decreases, the current noise at 100 kHz levels off into the white noise region faster than those at lower frequencies.

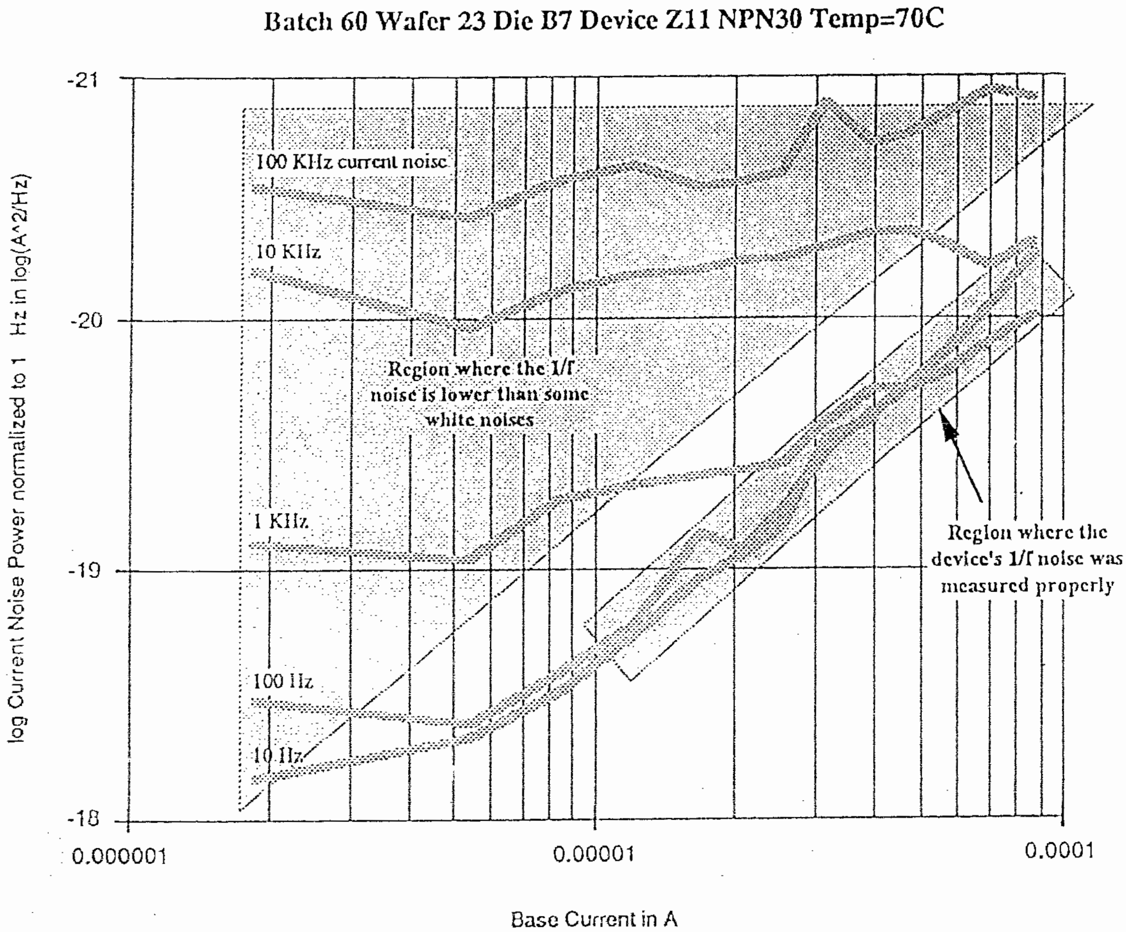

Figure 4.4 - A typical graph of log input referred current noise normalized to 1 Hz vs log base current.

The flicker noise region where noise curves of different frequencies overlapped is the region where AF (the slope of the flicker noise region) and KF (the y-intercept of the flicker noise region) should be calculated. These flicker noise parameters relate to the flicker noise power by

$$S_i\,(1\mathrm{Hz}) = KF\,\frac{i^{AF}}{f^{\gamma}} \quad \text{where } \gamma \cong 1 \text{ and } AF \cong 2 \tag{4.1}$$

A possible dependence between the noise power and the base current is

$$S_i \propto i_b^{\,2} \tag{4.2}$$

Figure 4.5 illustrates how AF and KF are extracted from the noise data by performing a linear fit on the data points in the 1/f noise region. AF was determined from the slope of the best fit line and was found to be 1.36 [log A/ log (A^2/Hz)] for a device with an emitter area of 96 μm^2 measured at 70C. KF was determined from the y-intercept and was found to be 2.987E-14 A^2/Hz. As shown in Figure (3.5), within one standard deviation of the current noise data, AF should lie within 1.05 to 1.40. The noise data at 100 Hz was used to determine AF and KF for most devices. Figure 4.5 illustrates how AF and KF are extracted from the noise data by performing a linear fit on the data points in the 1/f noise region.

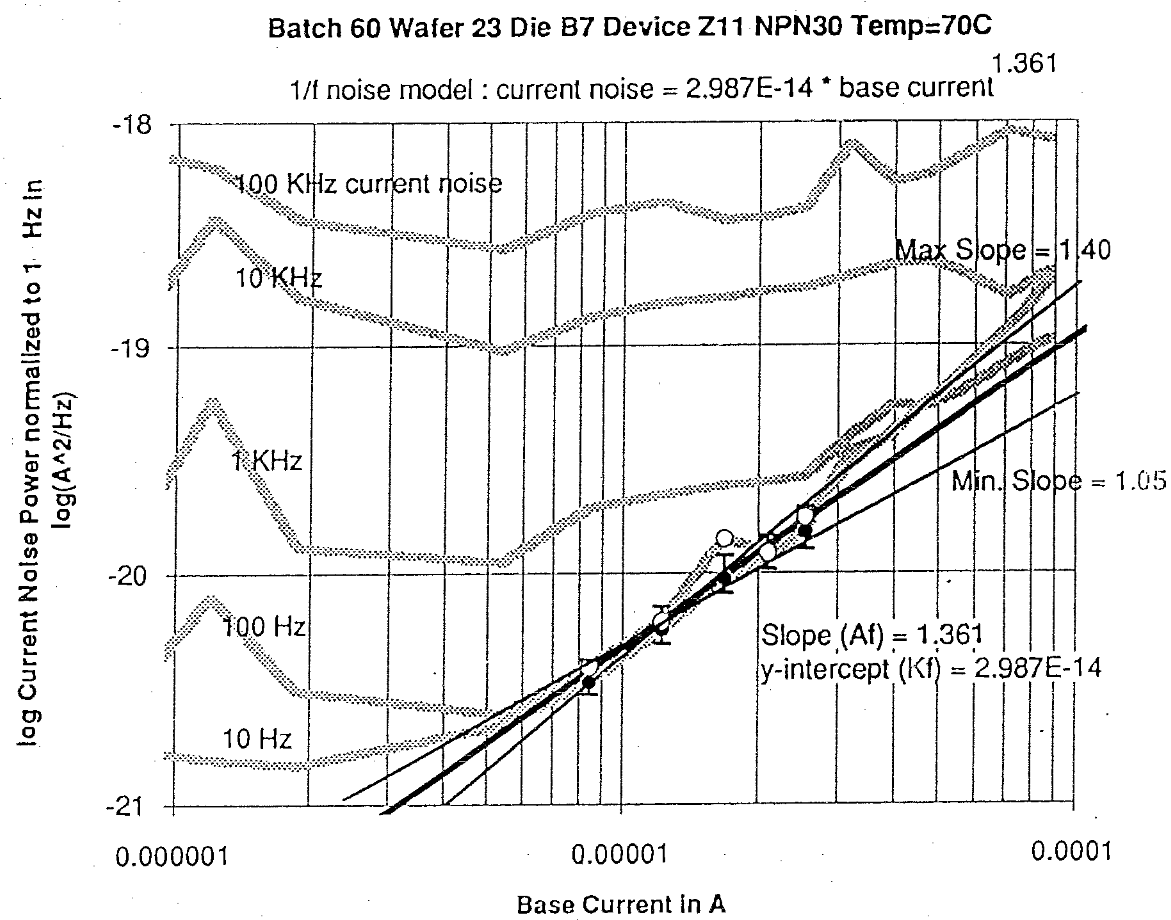

Figure 4.5 - AF and KF were extracted from the noise data by performing a linear fit on the data points in the 1/f noise region

4.3 Variation with Emitter Area

The above measurement and analysis procedure were applied to devices with different emitter areas. AF's measured from different device sizes were then plotted vs device size as shown in Figure 4.6a. A linear relationship was observed in the graph of log AF vs log device size. A least square line fitting process was then applied to this graph to determine the relationship between AF and the device size.

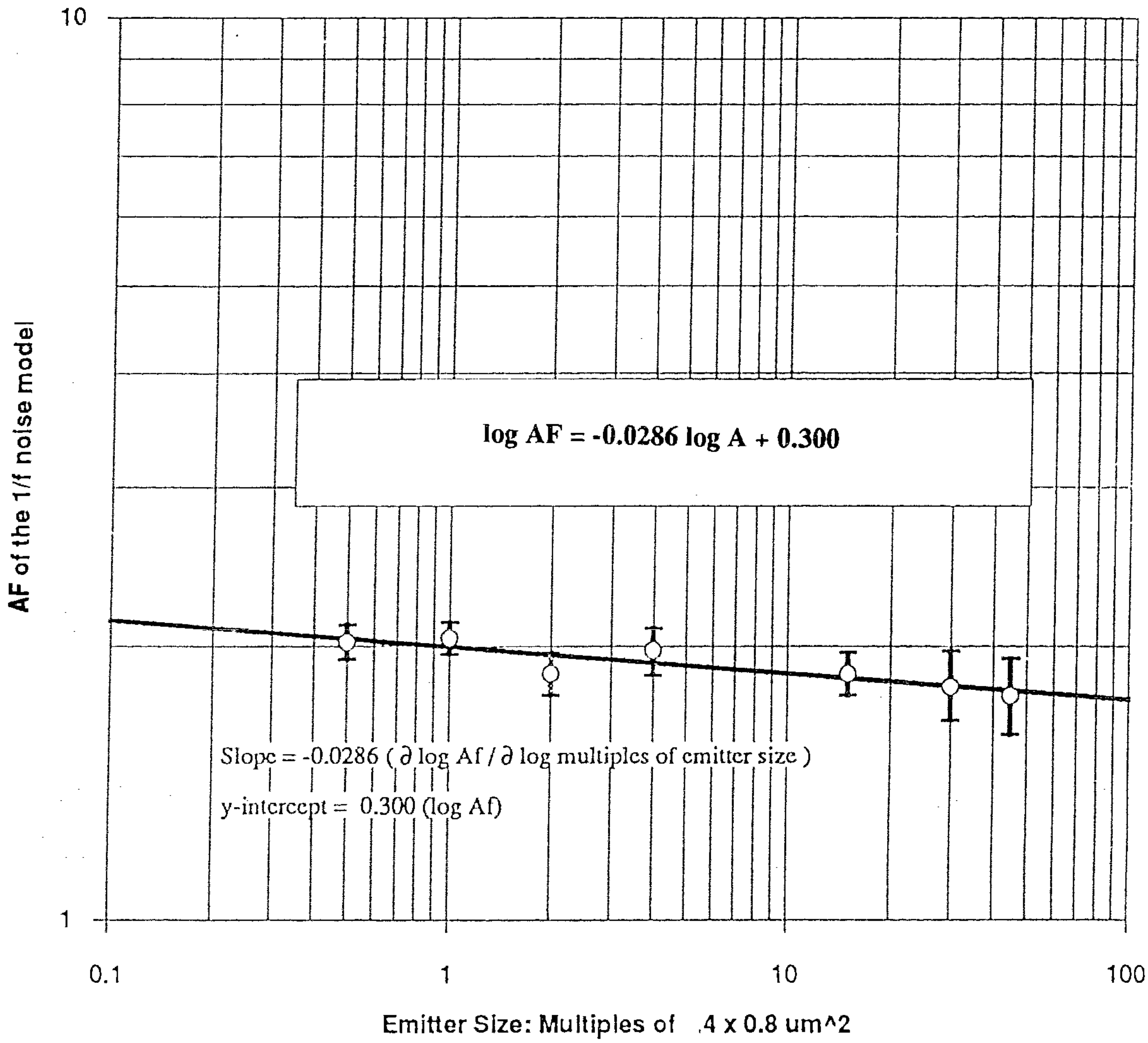

Figure 4.6 AFs measured from different device sizes were then plotted vs device size to determine how AF varies with the device size. A linear relationship was observed in the graph. A weak emitter area dependence was observed in the AF measured.

Based on these data, the relationship of AF with device size was

log AF = -0.029 log A + 0.30 (4.3)

where A is the device size in multiples of (3.2 μm^2). It can be concluded from this graph that AF, which is the exponential dependence of the noise power with the base current, only weakly depends on the emitter area. Similarly, as shown in Figure 4.7, KF's determined were plotted on a graph of log Kf vs log device size in which a linear relationship was observed. Based on these data, the relationship of KF with device

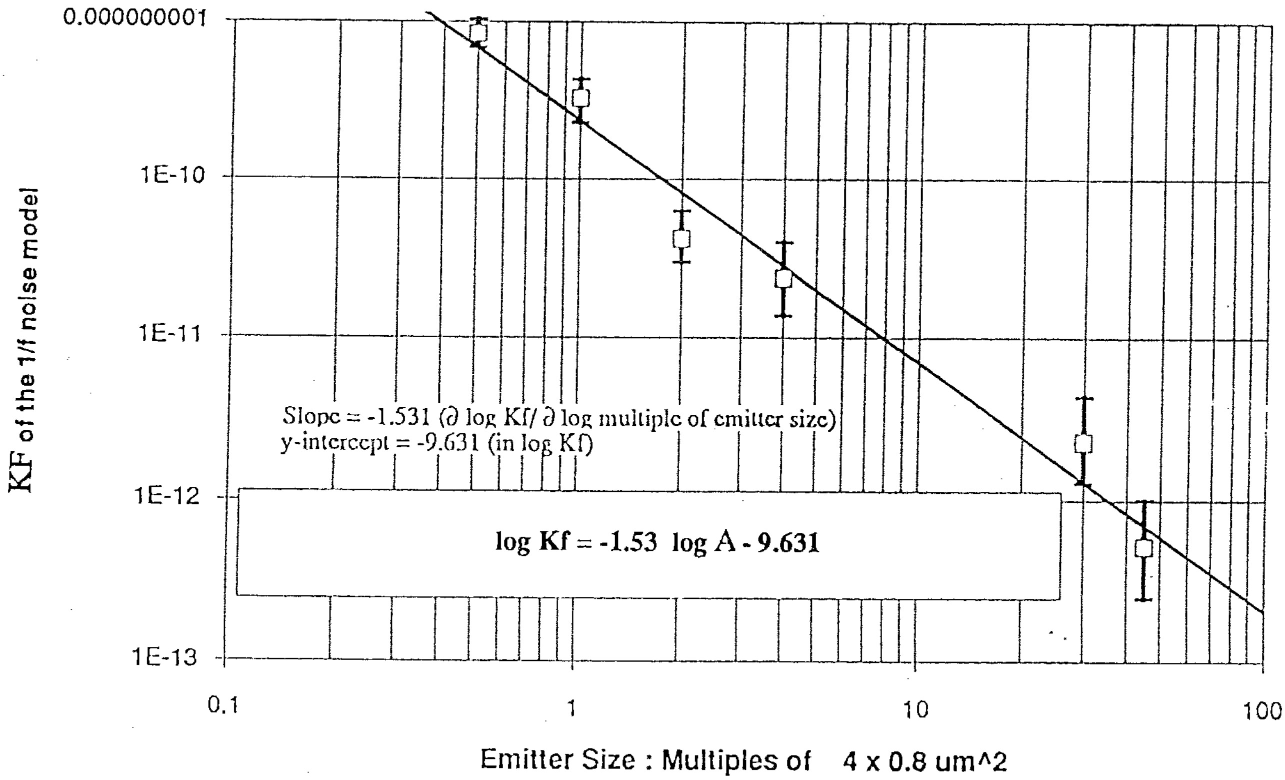

Figure 4.7 KFs measured from different device sizes were then plotted vs device size to determine how AF varies with the device size. A linear relationship was observed in the graph. A weak emitter area dependence was observed in the AF measured.

emitter size was found to be

$$\log KF = -1.53 \log A - 9.63 \tag{4.4}$$

where A is a multiple of 3.2 μm^2. Notice that KF, the noise power normalized to 1Hz and 1A, is strongly dependent on the emitter area.

4.4 Variation with Temperature

The same procedures for finding the AF and KF with varying device size was then repeated at 10 different temperatures: 10C, 20C, 30C, 40C, 50C, 70C, 85C, 86C, 92.5C and 100C. Figure 4.8 and Figure 4.9 show the best fit models for both AFs and KFs measured with respect to device size at different temperatures. For clarity purposes, only those that 0C, 50C and 100C are shown in the figures.

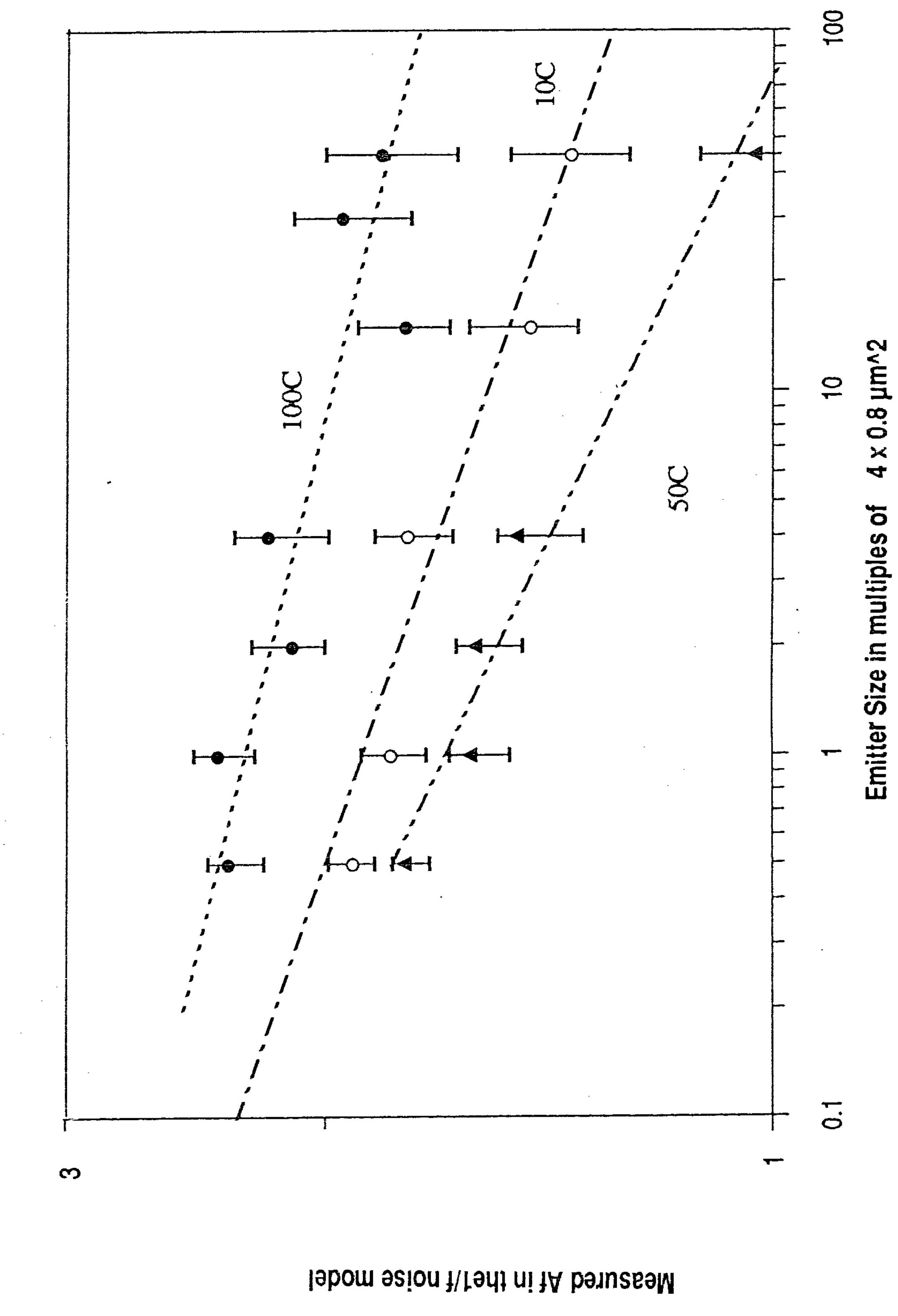

Figure 4.8 Best fit models for AFs measured for different device sizes at 0C, 50C and 100C.

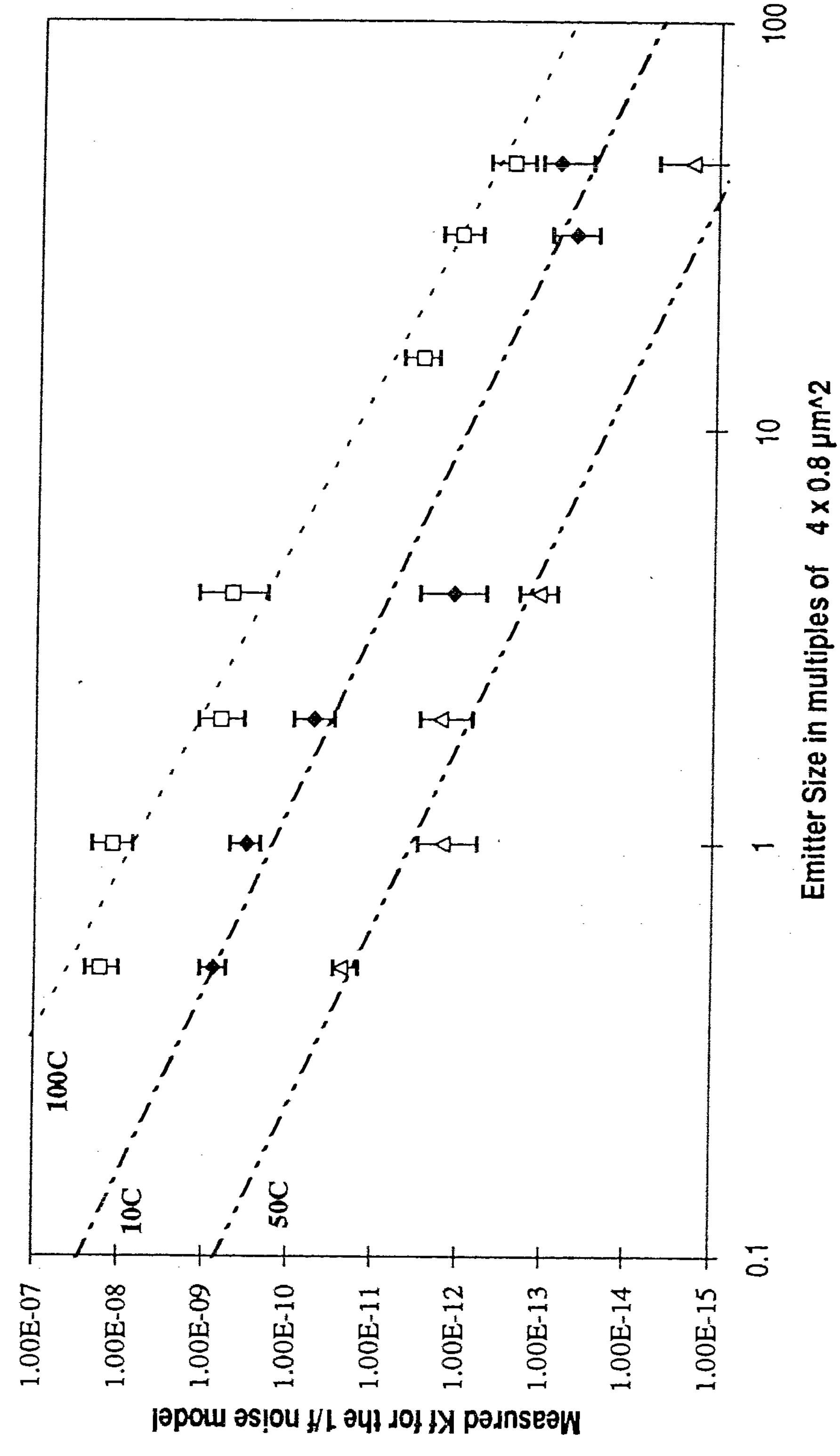

Figure 4.9 Best fit models for KFs measured for different device sizes at 0C, 50C and 100C.

Table 4.1 summarizes the least square slopes and the error ranges measured for KFs at different temperatures. Figure 4.10 shows the distribution of these values at different temperatures. An average slope of -2 indicates that the noise power is inversely proportional to the square of the emitter area.

$$S_i \,\alpha\, \frac{1}{A^2} \tag{4.5}$$

This experimental finding has a significant effect on the noise performance of small emitter area BJTs, for example, a reduction in area by results in almost an order of magnitude increase in the current noise power. This results will be used in the development of a noise model for our npn transistors. Note that the magnitudes of the least square slopes reach a minimum at 30C and 86C.

Temperature	Least Square Slope	Max. Slope	Min. Slope
10 C	-2.33	-2.10	-2.67
20 C	-2.21	-2.10	-2.43
30 C	-1.95	-1.73	-2.07
40 C	-1.96	-1.83	-2.43
50 C	-2.29	-2.00	-2.4
70 C	-1.83	-1.56	-2.27
85 C	-1.73	-1.60	-2.06
86 C	-1.53	-1.46	-1.77
92.5 C	-2.06	-1.96	-2.5
100 C	-2.21	-2.03	-2.43

Table 4.1 The least square slopes and the error ranges measured for KFs at different temperatures.

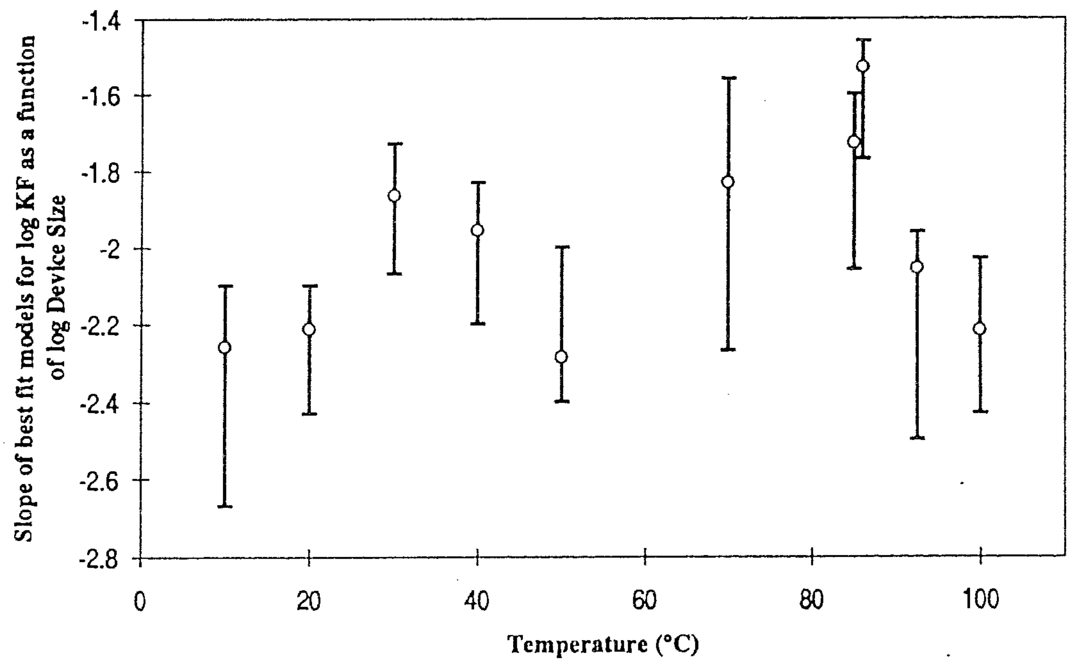

Figure 4.10 The slopes of the best fit models for KFs vary with temperature. KF is the noise power normalized to 1Hz and 1A, the slope value shown here represents the exponential dependence between the noise and the emitter area. A average slope of -2 indicates that the noise power is inversely proportional to the square of the emitter area.

According to the our theory, a plot of the noise spectrum versus the reciprocal temperature would give the trap level energy on the falling linear portion and the quasi-fermi level at the rising curve. Figure 4.11 shows a typical example of this kind of plot in which the straight line on the left side corresponding to the rising edge of a GR noise peak and the curve on right side corresponding to the falling edge of a GR noise peak. Fitting a straight line into the data points on the left side in Figure 4.11 and using equation (2.43), an trap energy of 0.837 eV was determined.

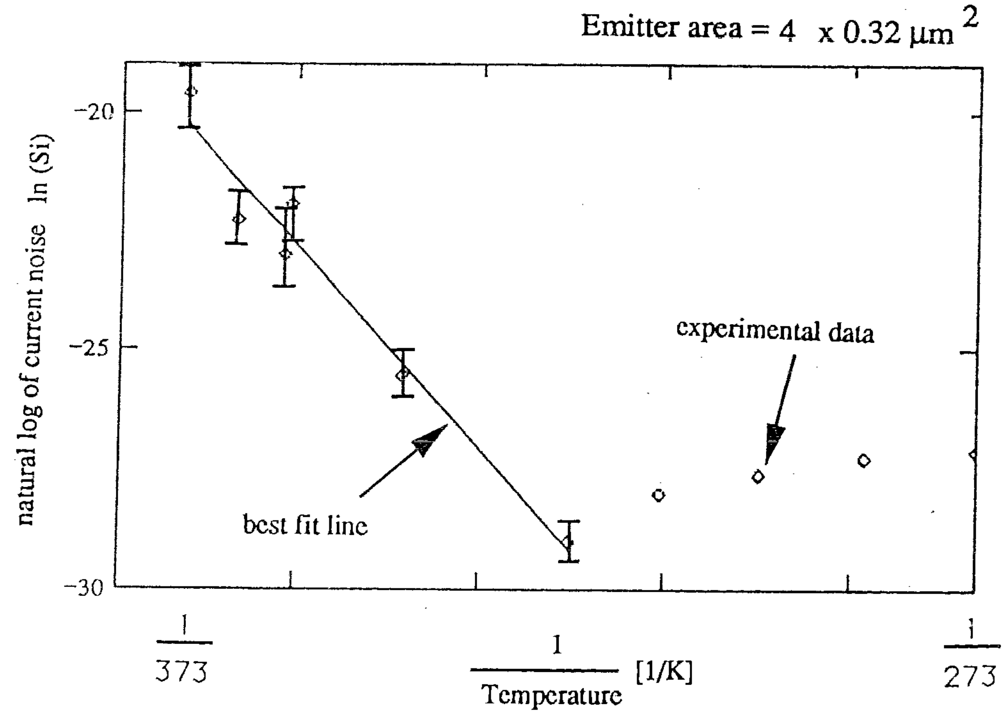

Figure 4.11 In a plot of the noise spectrum for a npn transistor with an emitter area of 12.8 μm^2 versus the reciprocal of the temperature, an trap level energy of 837 meV above the valence band was determined.

The activation energies determined from similar line fitting for all transistors with different emitter areas as listed in Table 4.1 below

Emitter Area [μm^2]	Trap Energy [meV]
0.5 x 3.2	822 ± 7.2
1 x 3.2	912 ± 12.3
2 x 3.2	810 ± 14.6
4 x 3.2	837 ± 6.3
15 x 3.2	801 ± 16.4
30 x 3.2	781 ± 13.2
45 x 3.2	785 ± 6.1
Average :	821 ± 5.4

Table 4.2 The activation energies transistors with different emitter areas

Using $N_A = 7 \times 10^{17}$ cm^{-3} for the base and $N_D = 1 \times 10^{19}$ cm^{-3} for the emitter. and assuming complete ionization of the dopants at temperature higher than 50C, the Fermi level for hole and electron are calculated as 121 meV and 943 meV above the valence band. According to our theory, the slope of the right side of Figure 4.11 should be equal to $\frac{q}{kT}$ Ef (T). In order to verify our theory, we plot the function $\frac{q}{kT}$ Ef (T) + C, where C is a constant for vertical offset, on the same graph with our experimental data . The theory is verified if we find the slope of $\frac{q}{kT} E_f(T) + C$ matches with the experimental data. Figure 4.13 compares the experimental data with our theory. The solid line is $\frac{q}{kT}$ Ef (T) using Fermi-Dirac approximation for calculating $E_f(T)$ for intermediate temperatures. The dashed line is $\frac{q}{kT} E_f(T) + C$ using the function for $E_f(T)$ for low temperatures. These results indicate that our theory and the experimental data are in good agreement.

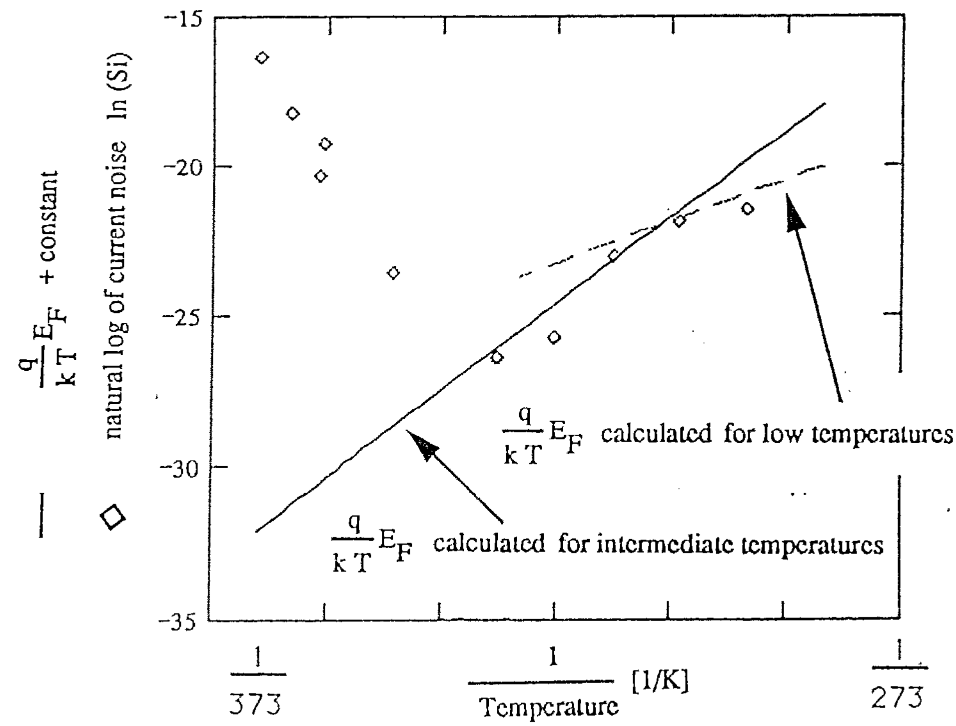

Figure 4.12 Compare the function $\frac{q}{kT}E_F(T) + C$ predicted from our theory with the actual experimental data. The dark line is $\frac{q}{kT}E_F(T) + C$ using Fermi-Dirac approximation for calculating $E_F(T)$ for intermediate temperatures. The dash line is $\frac{q}{kT}E_F(T) + C$ using the function for $E_F(T)$ for low temperatures.

Using the trap energy of 821 meV above the conduction band determined from experiment and an appropriately selected time constant in our noise model which is discussed in detail in next chapter, good agreement between the original data and model results as shown in Figure 4.13 are obtained. In this figure, we can only model one of the two GR noise peaks because the falling edge of the other GR noise does not contain information on the trap level energy .

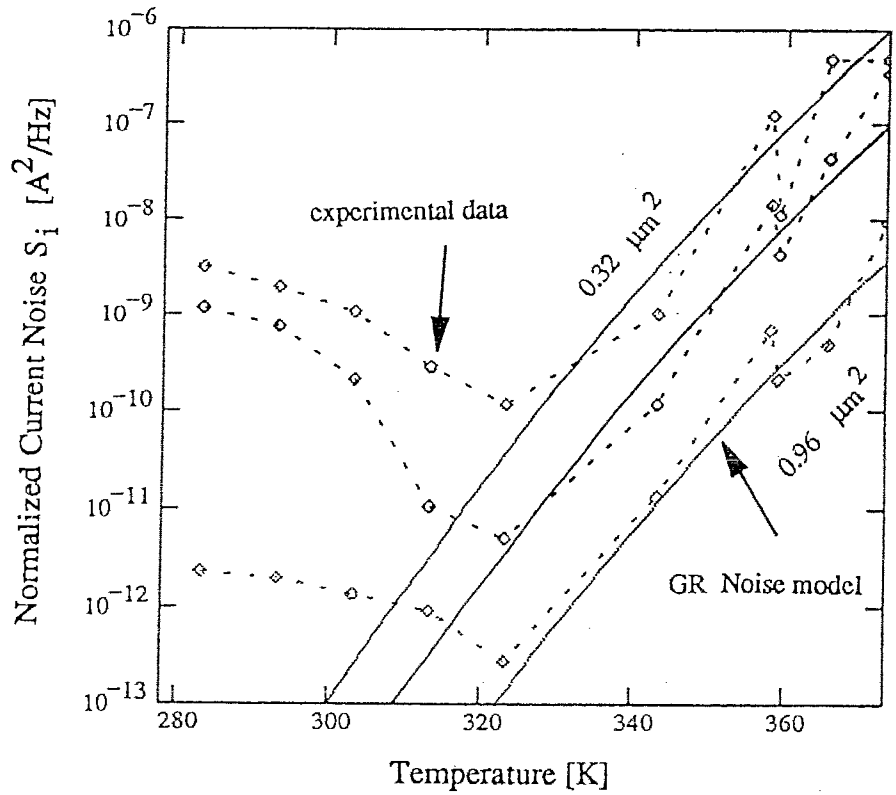

Figure 4.13 Using the trap activation energy of 0.88 eV determined from experiment, a good agreement between the original data and model results are observed

4.5 Hooge's Parameter for Holes

Using equation (2.54), the minimum values of the Hooge's parameter for holes for different device sizes and temperatures are calculated and summarized in Table 4.3.

α_p	1.6 μm^2	3.2 μm^2	6.4 μm^2	12.8 μm^2	48 μm^2	96 μm^2	144 μm^2
283 K	3.37E-06	2.49E-06	7.85E-07	3.02E-08		2.83E-09	4.94E-09
293 K	2.73E-06	2.21E-06	6.11E-07	3.49E-08	5.34E-09	1.66E-09	
303 K	1.51E-06	5.37E-07	3.35E-07		1E-08	1.24E-09	3.95E-09
313 K	6.21E-07	6.39E-08	1.42E-07	6.65E-09	2.21E-09	4.46E-10	1.14E-09
323 K	3.43E-07	4.74E-08	5.43E-08	6.05E-09			7.87E-10
343 K	9.2E-07	2.27E-07		3.99E-08	3.06E-09		5.65E-10
358 K	1.11E-05	2.5E-06	8.28E-07	8.54E-07	4.16E-08	8.01E-09	3.4E-09
359 K	3.85E-06	1.37E-06	3.78E-07	1.3E-07	2.05E-08	6.09E-09	3.12E-09
365.5 K	3.39E-05	4.74E-06	6.12E-07	1.94E-07	3.04E-08	1.04E-08	3.48E-09
373 K	1.97E-05	1.22E-05	2.1E-06	1.11E-06	4.31E-08	6.8E-09	2.81E-09

Table 4.3 The minimum values of the Hooge's parameter for holes for different device sizes and temperatures

The Hooge's parameters summarized above are in good agreement with the values reported by other researchers: 8.5 x 10^{-7} for n-type silicon at 300K in [14], 9 x 10^{-7} for n-channel MOSFET in [40], 9.3 x 10^{-8} for the base region of pnp BJT in [41] and 7.1 x 10^{-8} for n-channel JFETs in [15,44]. A comparison of our Hooge's parameters determined from experiment with the values reported by other researchers is shown in Figure 4.14.

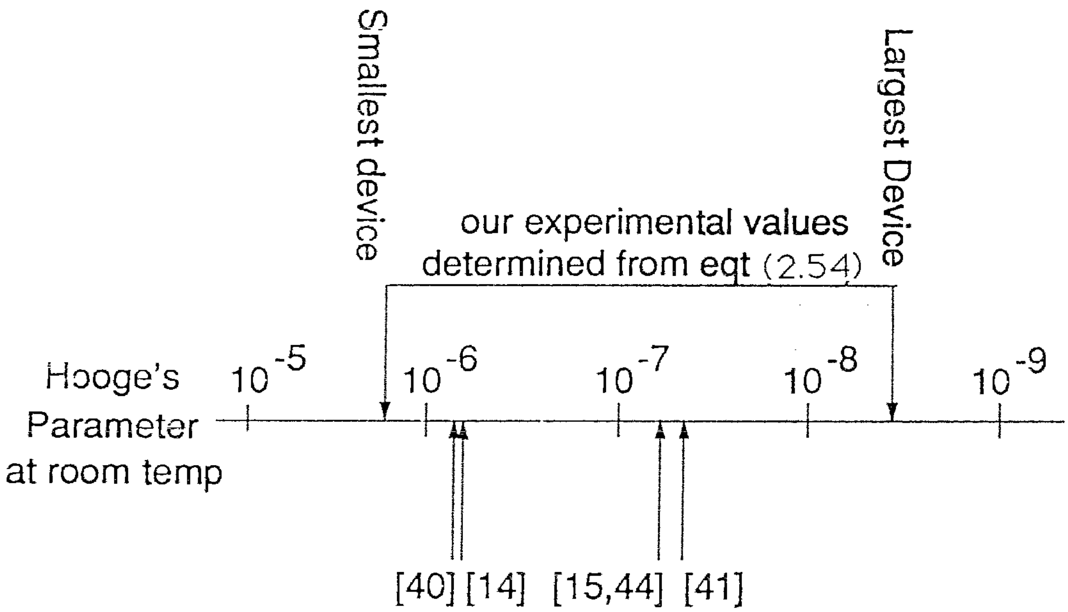

Figure 4.14 A comparison of our Hooge's parameters determined from experiment with the values reported by other researchers

Chapter 5 Noise Model and Modelling Results

5.1 Nature of the Model

Our flicker noise model for bipolar transistor is a semi-empirical noise model which is consisted of two parts :

1) the fundamental noise part for flicker noise mobility fluctuations and
2) the non-fundamental part for GR noise.

A precise physical noise model is difficult to obtain because the theoretical model in [25] only provides a lower limit for the Hooge's parameter. However, as will be demonstrated in the next section, the combination of fundamental flicker noise and a number of non-fundamental GR noise produces good fitting to a large number of experimental data. Once the fitting parameters are determined, this simulation model can closely fit noise data with different frequency, biasing current, temperature and emitter area. The first two independent variables are supported by the simulation model developed here, while the latter two are made possible after this research work. The fundamental part of our noise model is a term that increase slowly with temperature while the non-fundamental part depends heavily on temperature.

5.2 Physical and Fitting Parameters for the Model

Before the noise model can be used for the noise simulation of a given bipolar transistor, the device parameters for the device must be extracted and the fitting parameters have to be determined. The meanings of the inputs parameters for both the flicker noise model and the GR noise model are given in Tables 5.1 and 5.2 respectively.

Fundamental Flicker Noise (Diffusion Noise)		
Device Parameters	T_F	Transit time = τ_e (electron life time) / β_{dc}
	W_E, W_B	Emitter and base width
	N_D, N_A	Donor and acceptor concentration
	A_E	Emitter area
	C_f	Fitting parameter for fundamental flicker noise (<=Emitter Area^2). Account for the area dependence constant and the fact that our physical model give only an lower bound for the Hooge's parameter rather than the exact value

Table 5.1 Meaning of the inputs to the flicker noise model

Non-fundamental GR Noise (for each trap)		
Device Parameters	τ_0	pre-exponential time constant
	E_t	trap energy level
	A_E	Emitter area
	C_{nf}	Fitting parameter for non-fundamental flicker noise power (independent of f, T, I_c)

Table 5.2 Meanings of the inputs to the GR noise model

5.3 Definition of the Noise Model

As described in last section, the actual model is a summation of the fundamental flicker noise model and a non-fundamental GR noise models and the noise power is

$$S(f, I_b, T, A_E) = S_d(f, I_b, T, A_E) + \sum_{i=1}^{n} S_{gr_i}(f, I_b, T, A_E) \tag{5.1}$$

where n is the number of traps involved. The definition of the two models are defined in Table 5.3 and 5.4 below.

Flicker Noise Model Definition

$$S_d = \frac{\pi\, f_T\, q\, I_B \ln\frac{P(0)}{P(w_E)}\, \alpha_p\, C_f}{f\, A_E^{\,2}}$$

where

$\alpha_p = \alpha_{elastic}\,(1 - \exp(\frac{-\theta}{2T})) + \alpha_{non\text{-}elastic}\,\exp(\frac{-\theta}{2T})$ is the Hooge's parameter,

$\alpha_{elastic} = \alpha_{normal} = \frac{4\,\alpha_0}{3\,\pi}\,\frac{6\,k\,T}{m^*\,c^2}$ is the Hooge's parameter for elastic collision,

$\alpha_{non\text{-}elastic} = \alpha_{umklapp} = \frac{4\,\alpha_0}{3\,\pi}\left(\frac{h}{m^*\,a\,c}\right)^2$ is that for non-elastic collision,

$f_T = \frac{g_m}{2\,\pi\,C_{be}}$ is the cutoff frequency,

$g_m = \frac{q\,I_c}{k\,T}$ is the transconductance of the transistor,

$C_{be} = \frac{q\,I_c\,T_F}{k\,T}$ is the junction capacitance of the transistor

$\frac{P(0)}{P(W_E)} = \frac{D_h}{W_E\,V_s}$ is the hole concentration ratio at the emitter boundaries,

$D_h = \frac{kT}{q}\,\mu_h$ is the diffusion constant for holes,

$$\mu_h = 543\ T_n^{-0.57} + \frac{407\ T^{-2.23}}{1 + \left[\frac{N_d}{235 \times 10^{17}\, T_n^{\,24}}\, 0.88\, T_n^{-0.146}\right]}$$ is the hole mobility

with $T_n = T/300$ and $V_s = \frac{2.4 \times 10^5}{1 + 0.8\exp(\frac{T}{600})}$ is the saturation velocity.

Table 5.3 Definition of the Flicker Noise Model for Bipolar Junction Transistors

GR Noise Model Definition (for Bipolar Junction Transistors)
$$S_{gr_i} = \frac{C_{nf}\, I_C{}^m}{A_E{}^n} \, \frac{\tau_i}{1+(2\,\pi\, f\, \tau_i)^2} \, f_{t_i}\,(1 - f_{t_i})$$ where $f_{t_i} = \dfrac{1}{1 + \exp \dfrac{q\,(E_{t_i} - E_F)}{k\,T}}$ is the trap fractional occupancy, $\tau_i = \tau_{0_i} \exp\left(\dfrac{q\,E_{a_i}}{kT}\right)$ is the trapping time constant $E_{a_i} = (E_C - E_{t_i})$ for electron trap and $(E_{t_i} - E_V)$ for hole trap, m and n are device dependent constants and are determined to be 2 for our devices.

Table 5.4a Definition of the GR noise model for Bipolar Junction Transistors

GR Noise Model Definition (for Junction Field Effect Transistors)
$$S_{gr_i} = C_{nf} \, \frac{\tau_i}{1+(2\,\pi\, f\, \tau_i)^2}$$ where $\tau_i = \tau_0 \exp\left(\dfrac{q\,E_a}{kT}\right)$ is the trapping time constant, $E_a = (E_C - E_t)$ for electron trap and $(E_t - E_V)$ for hole trap, C_{nf} is a constant independent of temperature.

Table 5.4b Definition of the GR noise model for JFETs

The GR noise model for JFETs in Table 5.4b is different from that of a BJT in Table 5.4a since the trap occupancy factor f_t $(1 - f_t)$ in a JFET is treated as a temperature independent constant as shown in [45] and [46]. The differences in the treatment of f_t $(1 - f_t)$ comes from the structural and operational difference of the two devices.

5.4 Definition of parameters used in the Models

The meanings the symbols used in the model definitions are given in Table 5.4 and Table 5.5 :

Constants and variables used in the Fundamental Flicker Noise Models		
Symbol	**Type**	**Meaning and value**
f	variable	frequency [Hz]
T	variable	temperature [K]
I_B	variable	base current [A]
A_E	variable	emitter area [m^2]
C_f	fitting parameter	noise power offset from theoretical minimum
N_d	device parameter	emitter donor concentration at the base-emitter junction
W_E	device parameter	effective emitter width
T_F	device parameter	transit time in SPICE = 1.6×10^{-11} s
q	constant	electron charge = 1.60210×10^{-19} C
θ	constant	Debye temperature = 645 K (Si)
α_0	constant	fine structure constant = 1/137 (Si)
k	constant	Boltzmann constant = 6.6256×10^{-34} J/K
h	constant	Planck constant = 1.38054×10^{-23} J/K
m^*	constant	effective mass = $0.946 \times 9.1091 \times 10^{-31}$ kg
c	constant	speed of light in vacuum = 2.997925×10^{-8} m/s

Table 5.5a Constants and variables used in the fundamental flicker noise model

Constants and variables used in the Non-fundamental GR Noise Models (for each trap)		
Symbol	**Type**	**Meaning and value**
f	variable	frequency [Hz]
T	variable	temperature [K]
I_C	variable	collector current [A]
A_E	variable	emitter area [m^2]
C_{nf}	fitting parameter	noise power offset
τ_0	device parameter	pre-exponential time constant [s]
E_t	device parameter	trap energy level [eV]
E_c	device parameter	conduction band energy level [eV]
E_v	constant	valence band energy level = 0 eV
q	constant	electron charge = 1.60210 x 10^{-19} C
k	constant	Boltzmann constant = 6.6256 x 10^{-34} J/K

Table 5.5b Constants and variables used in the non-fundamental GR noise model for JFET

5.5 Applying the Models to Noise Data

Figure 5.1 illustrates the idea of using both the GR noise and the flicker noise spectrum to construct a noise model for our experimental data. The symbols in this figure are the trend of our experimental results obtained from a 4^{th} degree polynomial curve fitting. Figure 5.2 shows our actual experimental data measured from a device of emitter area 3.2 μm^2 and the modelling results using parameters shown in Figure 5.2b. The GR noise model in Figure 5.2 uses the activation energy (820eV) determined previously in the experimental section. As seen in these figures, the fundamental flicker noise is a weak temperature-dependent function while the GR noises depend heavily on temperature and appear as 'hills'.

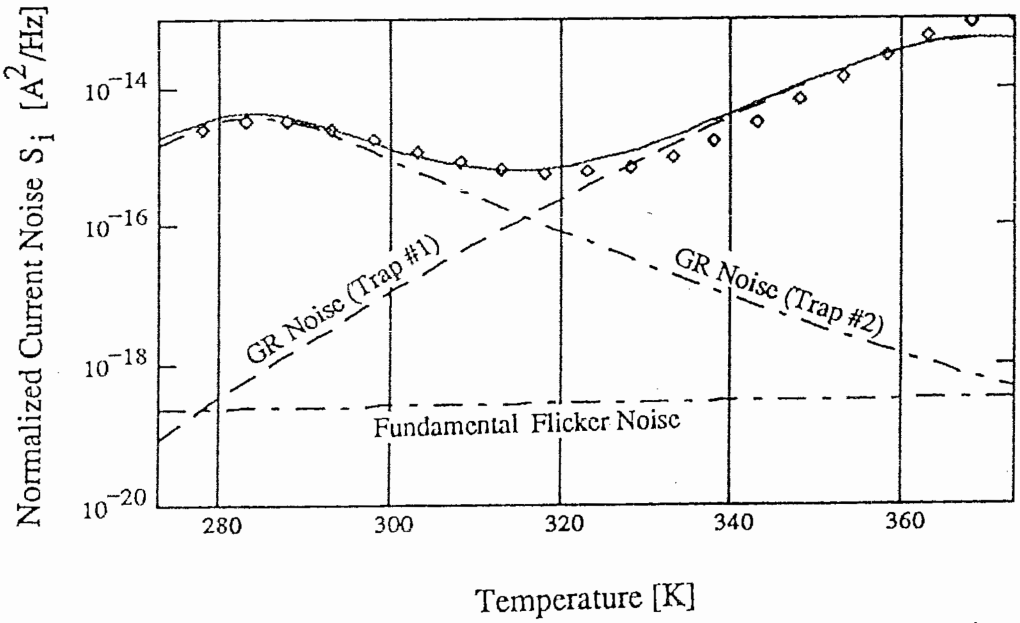

Figure 5.1a - Two GR noise spectra were used together with the fundamental flicker noise to fit the experimental data

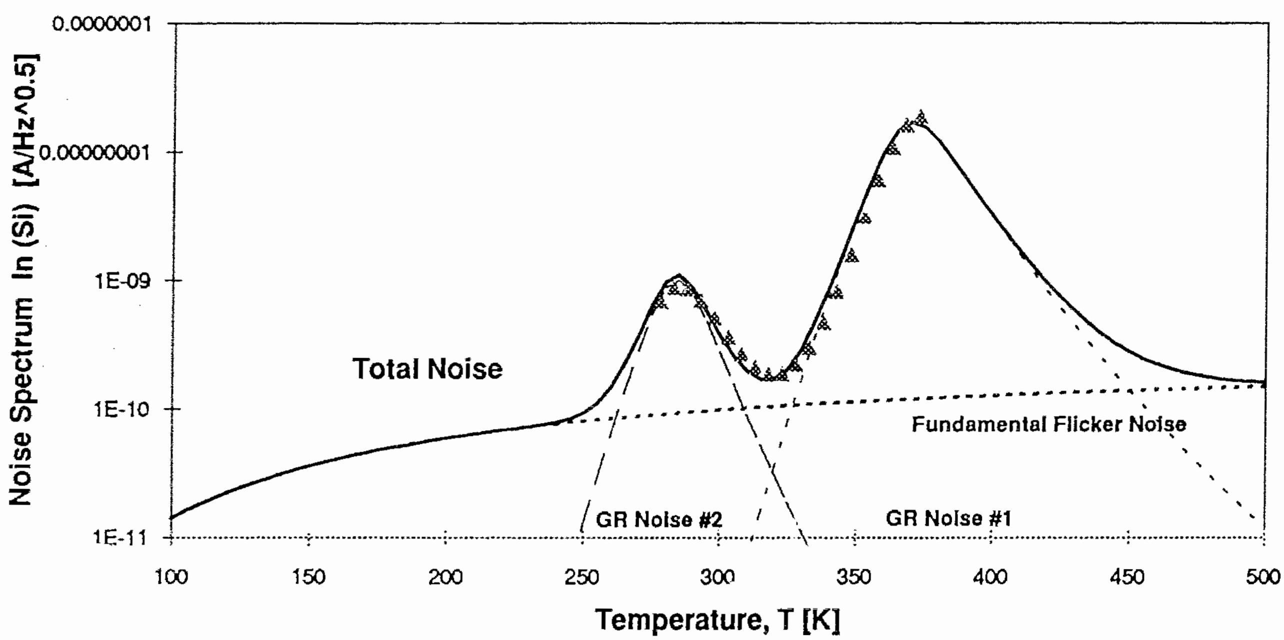

Figure 5.1b - A plot identical to Figure 5.1a except for a wider temperature range being used

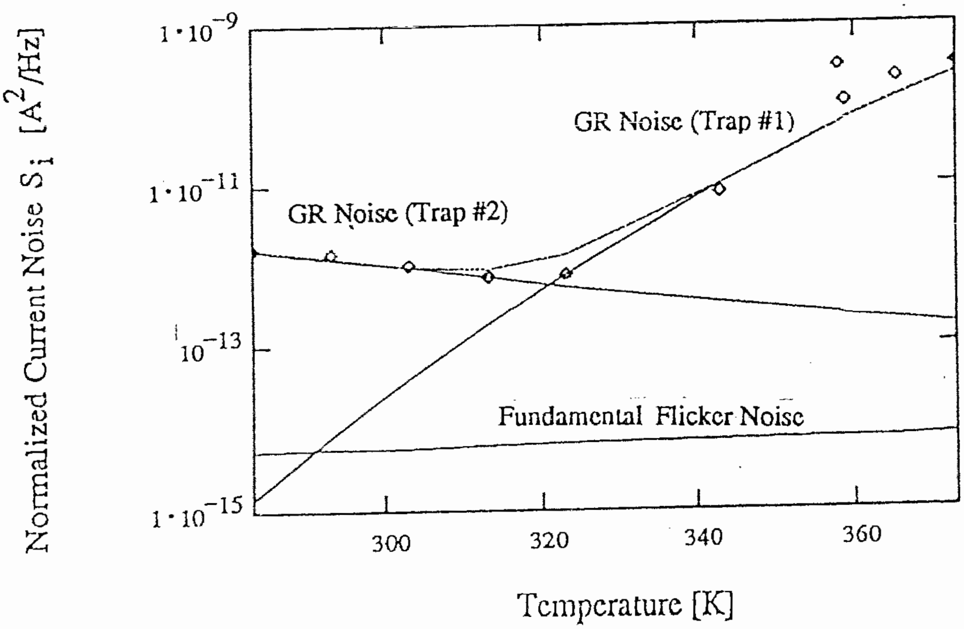

Figure 5.2a An GR noise spectra with Et = 880 meV was used together with another GR noise spectra and the fundamental flicker noise to fit the experimental data

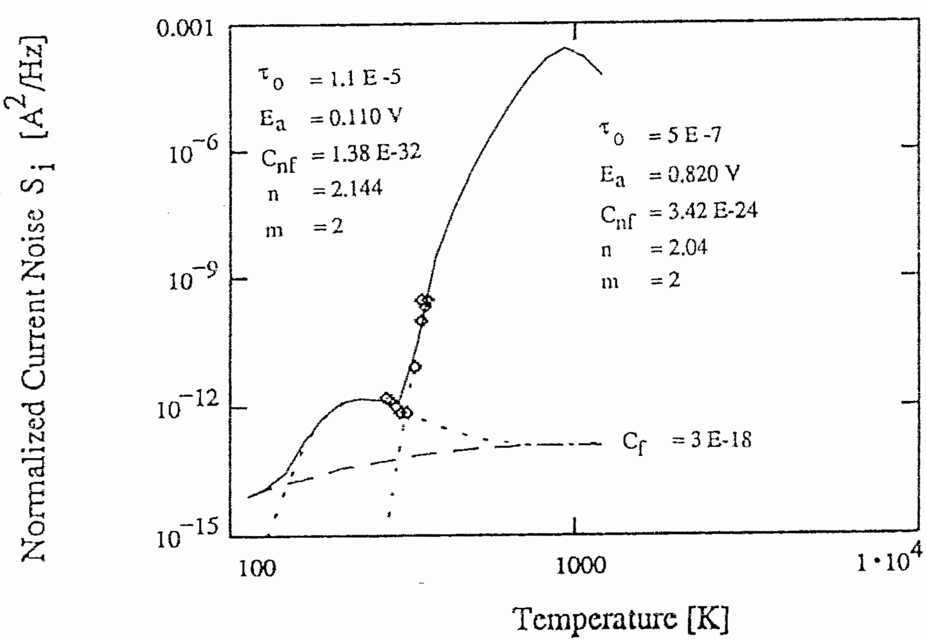

Figure 5.2b - A plot identical to Figure 5.2a except for a wider temperature range being used

The corresponding noise spectrum was shown in Figure 5.3 in which the triangles are the experimental data. It can be seen in this graph that the two GR noises have Lorentzian shape and add two 'bumps' to the 1/f noise spectrum.

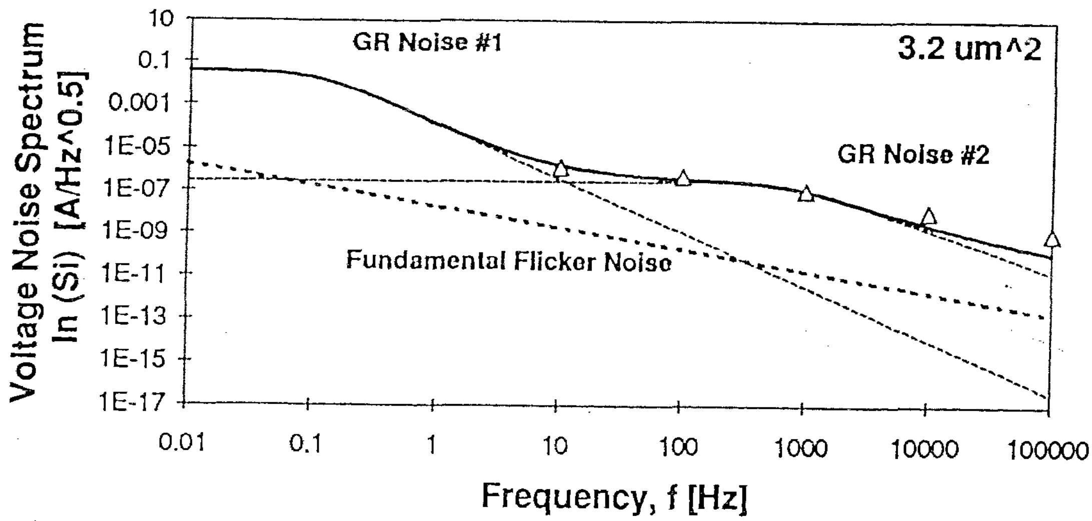

Figure 5.3 - Simulated and experimental noise spectrum corresponding to the data in previous figure.

Figure 5.4 show the variation of the noise spectrum with the emitter area. Solid lines in this figure are simulation results obtained by setting the emitter area variable in the model used in Figure 5.1 to 0.5 x 3.2 μm^2, 2 x 3.2 μm^2, 4 x 3.2 μm^2 and 30 x 3.2 μm^2. The measured noise data are represented by the symbols in the figure.

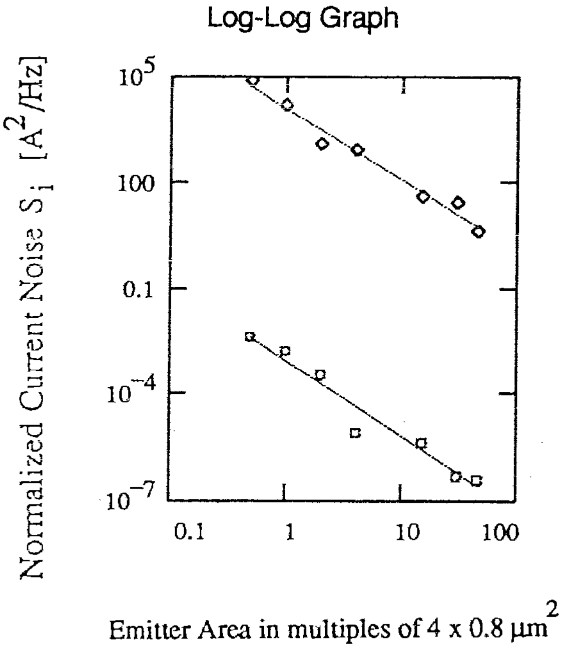

Figure 5.4 - Variation of the noise spectrum with the emitter area.

Using the experimental data for a neutron-irradiated JFET in [23], we tested the agreement between published data and the results generated from our noise model. Figure 5.5 shows the five GR noise spectra obtained from our noise model using the five trap activation energy obtained in [23]. The fundamental flicker noise was also used since mobility fluctuations due to lattice scattering occurs in a JFET as the electrons move from the source to the drain. Similar scattering mechanism implies similar temperature dependence. In this figure, the dash line with crosses are our model without using fundamental flicker while the solid line is our model with both the GR noise and the flicker noise. From the fitting results, the normalized current noise power is found to be proportional to A^m where m = -2.04. The values of C_{nf} was determined to be 1.39 x 10^{-32} for the first trap and 3.42 x 10^{-24}.

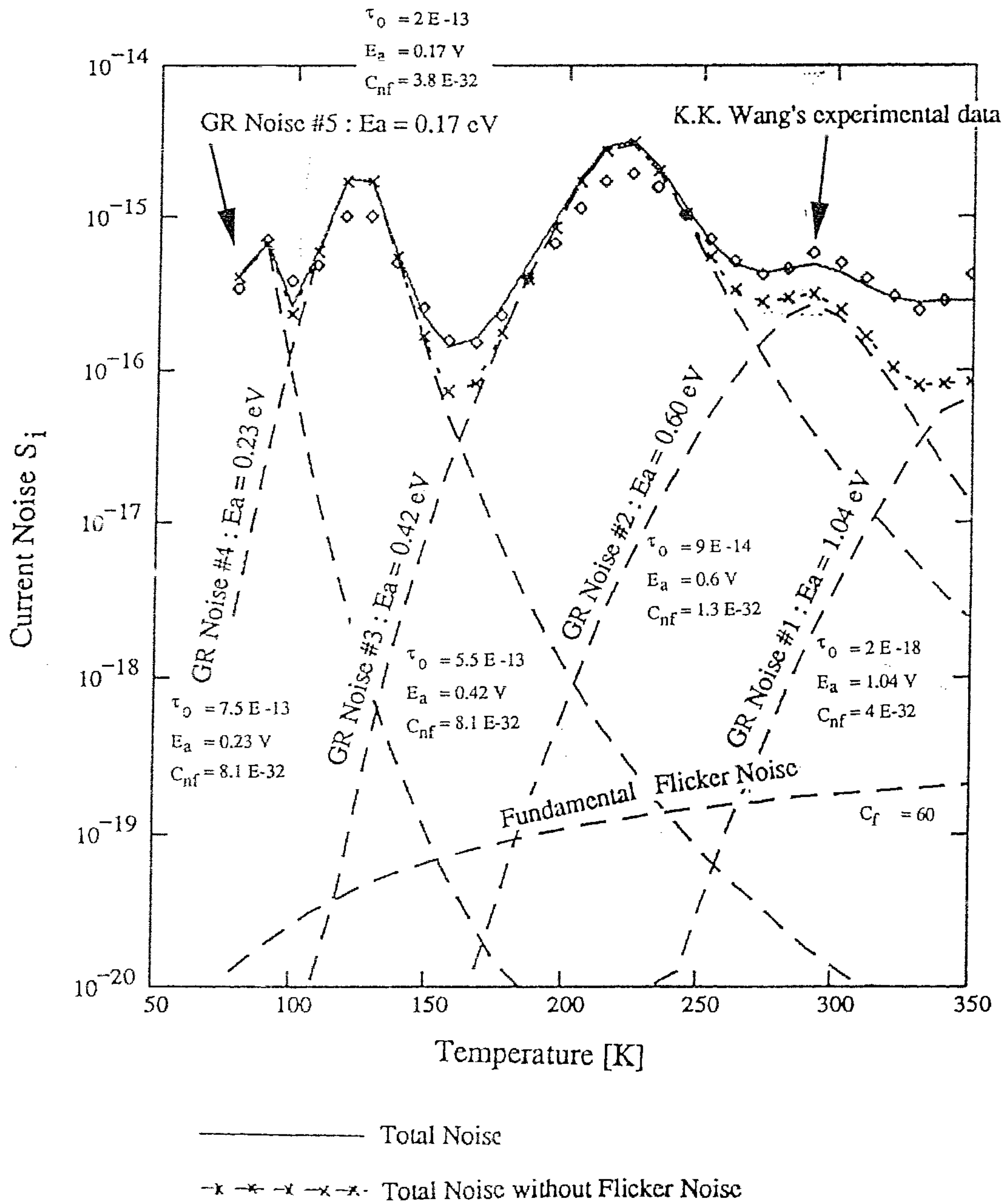

Figure 5.5 - **K. K. Wang's experimental data for a neutron-irradiated JFET [23] was used to test the noise model's ability to fit other GR noise data.**

In Figure 5.6, the lines shows the simulation results obtained from the same model by setting the frequency variable to 10Hz, 100 Hz, 1kHz, 10kHz and 100kHz. The symbols shown in the figure are experimental data from [23]. The values of C_{nf} used in the model range from 1 x 10^{-13} to 2 x 10^{-12}.

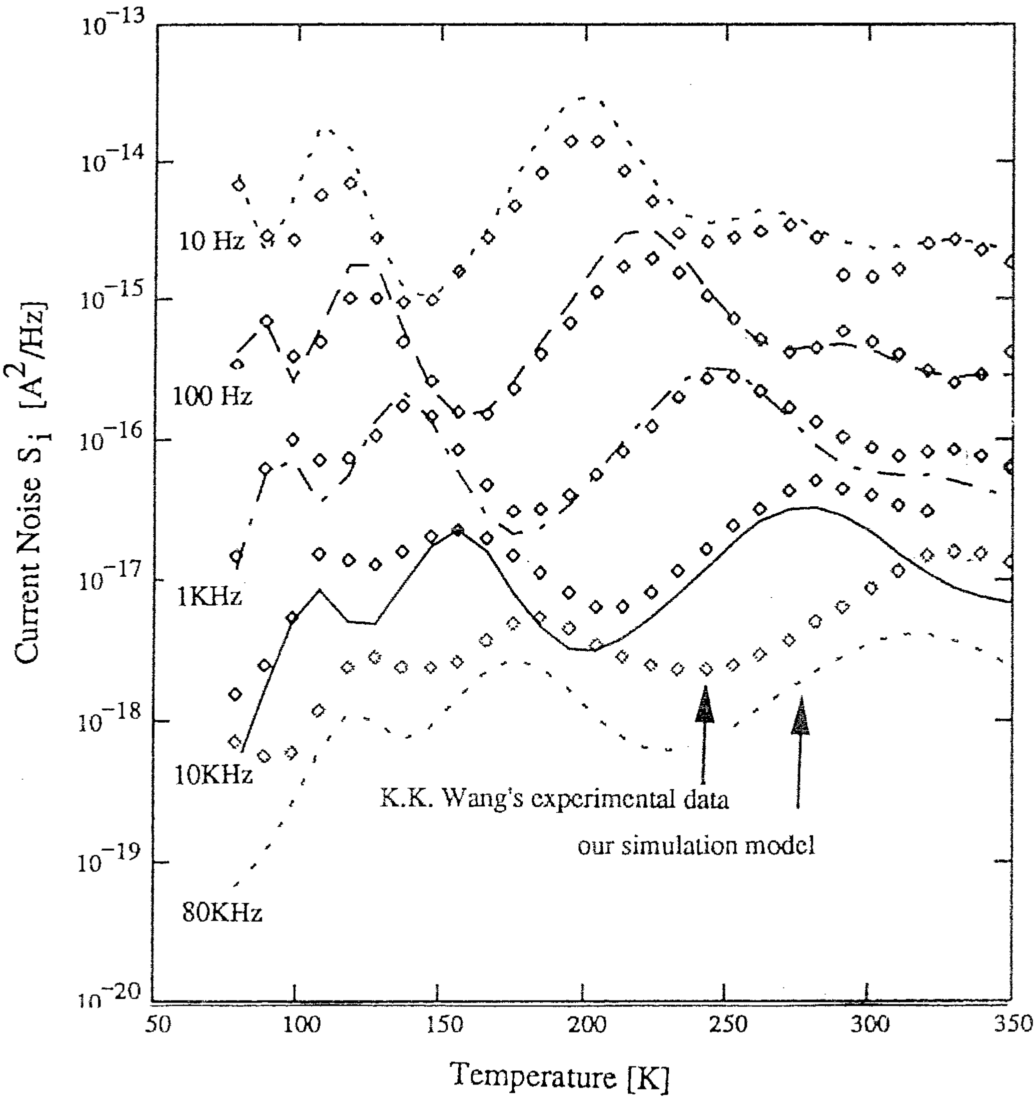

Figure 5.6 - Complete experimental data in [23] for a neutron-irradiated JFET was used to test the noise model's ability to fit other GR noise data with respect to the noise variation with frequency.

Furthermore, the experimental data reported in [41] was used to test the base current dependence of our noise model. The simulation result represents by the top solid line as shown in Figure 5.7 was constructed by adding one GR noise spectrum to the flicker noise spectrum. The other two spectra were obtained by setting the variable I_b in the noise model to 3 μA and 1 μA. From this comparison, one can see the agreement between the experimental noise results from [41] and the noise model's prediction is extremely good.

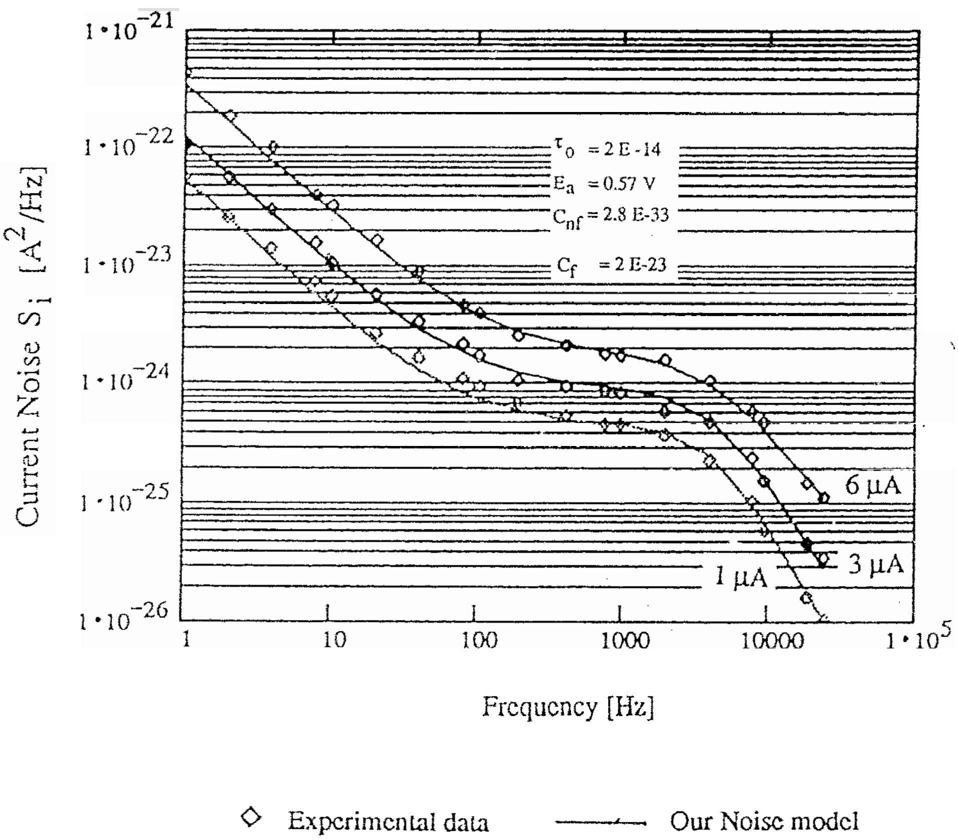

Figure 5.7 - Experimental data reported in [41] was used to test the base current dependence of our noise model.

Based on above fitting examples, one can see that the noise model presented in this chapter is capable of fitting a wide range of data and produce a good prediction of the noise power with varying frequency, temperature, emitter area and biasing current levels.

Chapter 6 CONCLUSIONS

In this thesis, a low frequency noise model for bipolar junction transistors that can predict the variation of the noise power with different operating conditions was developed. This model consists of a fundamental flicker noise and a non-fundamental GR noise. Together with the current and emitter area dependence determined from the experiments, these two noise sources were combined into a single expression that gave good agreement with a wide range of low frequency noise data in BJTs as a function of frequency, temperature, base current and emitter area.

From the experiments, the variation of the current noise power spectra $S_{i_b}(f)$ with the base current i_b shows that $S_{i_b}(f)$ is proportional to i_b^{γ} with γ close to 2. Curve fitting the experimental carrier number fluctuation $\overline{\Delta N^2}$ using the GR noise model showed that $S_{ib}(f)$ is proportional to the square of the collector current, and inversely proportional to the square of the emitter area. This experimental finding indicates that in smaller emitter area BJTs a reduction in area by 3 results in almost an order of magnitude increase in the current noise power.

A collector current fluctuation model due to fluctuating occupancy of the traps in the depletion region was developed in this research in order to provide an physical explanation for the current and emitter area dependence observed. Predictions based on this model were in good agreement with experimentally deduced relationships between the current noise power variation with emitter size and base current. A simple way of measuring the trap level energy from the noise data was derived from this model and was experimentally verified.

In summary, this research work improved the understanding of the noise characteristics of bipolar transistor studied and provides a noise model that is simple enough to be used for simulation purposes, and detailed enough to describe the variation of low frequency noise with frequency, temperature, base current and emitter area

REFERENCES

[1] Owen Stephenson, "Measurement of White and 1/f Noise in Semiconductor Devices," *ENGR 446, Technical Report, Northern Telecom Electronics Ltd, Ottawa,* pp 4, (1988)

[2] Aldert van der Ziel, "Noise in Solid State Devices and Circuits," *Wiley-Interscience Publication,* (1986)

[3] X. L. Wu, A. Van der Ziel, A. N. Birbas and A. D. Van Rheenen, "Burst-Type Noise Mechanism in Bipolar Transistor," *Solid State Electronic,* Vol-32 (11), pp 1039-1042, (1989)

[4] Aldert Van der Ziel, "Unified Presentation of 1/f Noise in Electronics Devices : Fundamental 1/f Noise Sources," *Proceeding of the IEEE,* Vol-76, (3) pp 233-258, (1988)

[5] K. S. Ralls et al," *Phys. Rev. Lett.,* Vol-52, pp 228-231, (1984)

[6] Aldert Van der Ziel, "Proposed Discrimination Between 1/f Noise Sources in Transistors," *Solid State Electronics,* Vol-25 (2), pp 141-143, (1982)

[7] J. Kilmer, A. van der Ziel, and G. Bosman, "Presence of Mobility Fluctuation 1/f Noise Identified in Silicon P+NP Transistors," *Solid State Electronics,* Vol-26 (1), pp 71-74, (1983)

[8] X. Zhu, A. Pawlikiewiz, and A. van der Ziel, "1/f Noise in N+PN Microwave Transistor," *Solid State Electronics,* Vol-28 (5), pp 473-477, (1985)

[9] A. van der Ziel, "Formulation of Surface 1/f Noise Processes in Bipolar Junction Transistors and in P-N Diodes in Hooge-Type Form," *Solid State Electronics,* Vol-32 (1), pp 91-93, (1989)

[10] P. F. Lu, "Low Frequency Noise in Self-Aligned Bipolar Transistors," *Journal of Applied Physics,* Vol-62 (4) pp 1335-1339, (1987)

[11] S.M. Stork, M. Arienzo, and C.Y. Wong, "," *IEEE Trans. Electron Devices,* Vol-ED-32 pp 1766, (1985)

[12] G. L. Patton, J.C. Bravman and J.D. Plummer, "," *IEEE Trans. Electron Devices,* Vol-ED-33 pp 1754, (1986)

[13] D. Doyle and W. Lane, "Scaling of Bipolar Transistor Analog Properties for Mixed Analog/Digital BiCMOS," *J. Proc. of BCTM,* pp 307-310, (1989)

[14] Aldert van Der Ziel, P. H. Handel, Xichen Zhu and Kuang Hann Duh, "A Theory of the Hooge Parameters of Solid-State Devices," *IEEE Transactions on Electron Devices,* Vol-ED32 (3), pp 667-671, (1989)

[15] A. Pawlikiewiicz and Van der Ziel, "Temperature Dependence of the Hooge Parameter in n-Channel Silicon JFET's," *IEEE Electron Device Letter,* Vol EDL-6 (10), pp 500-501, (1986)

[16] A. H. Pawlikiewicz, A. van der Ziel, G. S. Kousikan d' C. M. Van Vliet, "On the Temperature Dependence of the Hooge Paraemeter α_H in n and p-channel Silicon JFET," *Solid State* Electronics, Vol 31 (2), pp 233-236, (1988)

[17] M. J. Deen, X.M. Li, Y. Zhu, Z.X. Yan and T.M. Kleinpenning, "1/f Noise Model for MOSFETs in Saturation," *Proceedings of the International Conference on Noise in Physical Systems and 1/f Fluctuations,*Kyoto, Japan, pp 281-284(1991)

[18] Xichen Zhu and Aldert Van der Ziel, "The Hooge Parameters of n+-p-n and p+-n-p Silicon Bipolar Transistors," *IEEE Transaction on Electron Devices,* Vol-ED-32 (3), pp 658-661, (1985)

[19] Xichen Zhu and Aldert Van der Ziel, "The Hooge Parameters of n+-p-n and p+-n-p Silicon Bipolar Transistors," *IEEE Transaction on Electron Devices*, Vol-ED-32 (3), pp 658-661, (1985)

[20] A. L. McWhorter, "1/f Noise and Related Surface Effects in Germanium," *Lincoln Laboratory Report 80*, Boston, May (1955)

[21] J. L. Plumb and E.R. Chenette, *IEEE Transaction*, Vol-ED-10, 304, (1963)

[22] David L. Pulfrey and N. Garry Tarr, "Introduction to Microelectronics Devices," *Prentice Hall, New Jersey*, pp 130, (1989)

[23] K. K. Wang, A. van der Ziel, and E. R. Chennette, *IEEE Transaction on Electron Devices*, ED-22, pp 591, (1975)

[24] Shyh Wang, "Fundamentals of Semiconductor Theory and Device Physics," Prentice Hall, New Jersey, pp 215, (1989)

[25] T. G. M. Kleinpenning, *Physica*, Vol-98B, pp 289, (1980)

[26] F.N. Hooge, *Physic Letter*, Vol-A (29), pp 139, (1969)

[27] A. Van der Ziel, R. J. J. Zijstra, and H. S. Park, "Discrimination between 1/f Noise Models in Junction Field Effect Transistors and Metal-Oxide Field Effect Transistor, Numerical Results," *Journal of Applied Physics*, Vol-52, pp 4300, (1981)

[28] A. Van der Ziel, R. J. J. Zijstra, H. S. Park and S.T. Liu, "Alternate Explanation of 1/f Noise in an Implanted MOSFET," *Solid-State Electron.*, Vol-27, (1984)

[29] P.H. Handel, "1/f Noise, an 'Infrared' Phenomenon," *Phys. Rev. Lett.*, Vol-34, pp 1492, (1975)

[30] P.H. Handlel, "Quantum Approach to 1/f Noise," *Phys, Rev. Lett.*, Vol-22, pp 745, (1980)

[31] G. K. Kousik, C.M. van Vliet, G. Bosman, and P.H. Handel, "Quantum 1/f noise associated with ionized impurity scattering and electron-phonon scattering in condensed matter," *Adv. Phys.*, Vol-34, pp 663, (1985)

[32] P.H. Handel, "Any Particle Represented by a Coherent State Exhibits 1/f Noise," *Noise in Physical Systems and 1/f Noise, M. Savelli, G. Lecoy, an dJ.P. Nougier, Eds, New York, NY, Elsevier*, pp 97, (1983)

[33] P.H. Handel, "Coherent State Quantum 1/f Noise and the /Quantum 1/f Effect," *Noise in Physical Systems and 1/f Noise, A.d'Amico and P. Mazetti*, Eds. New York, NY:Elsevier, pp 465 (1986)

[34] A. van der Ziel and P.H.Handel,"1/f Noise in n+-p Diodes," *IEEE Trans. Electron. Devices*, Vol-ED 32, pp 1805, (1985)

[35] A. van der Ziel and P.H. Handel,"1/f Noise in n+-p Junctions calculated with Quantum 1/f Theory," *Noise in Physical Systems and 1/f Noise*, A. d'Amico an P. Mazetti, Eds. New York, NY: Elsevier, pp 481, (1986)

[36] A. van der Ziel, *Noise in Solid State Devices and Circuits*, New York, NY: Wiley, (1986)

[37] A. van der Ziel, P. H. Handel, X.L. wu, and J. B. Anderson, "Review of the Status of Quantum 1/f Noise in n+-p HgCdTe Photodiode Detectors and Other Devices," *J. Vac.Sci. Tech-nol.*, Vol-A4, (4), pp 2205, (1986)

[38] A. Pawlikiewicz and A. van der Ziel, *IEEE Electron. Dev. Lett.*, Vol-EDL (6), pp 497, (1985)

[39] C. M. van Vliet, *Symposium on Quantum 1/f Noise, Minneapolis*, (unpublished), (1985)

[40] Kuang Hann Duh and Aldert van der Ziel, "Hooge Parameters for Various FET Structures," *IEEE Transactions on Electron Devices*, Vol-ED32, (3), (1985)

[41] J. Kilmer, A. van der Ziel an G. Bosman, "Mobility Fluctuation 1/f Noise in Silicon p+-n-p Transistors," *Solid-State Electronics*, Vol-28, (3), pp 287-288, (1985)

[42] P. H. Handel, "Relativistic Correction of the Hooge Parameter for Umklapp 1/f Noise," *Physica*, Vol 141B, pp 145-147, (1986)

[43] M. J. Deen, A. Ng, Y. Zhu, A. M. Seabaugh and O. Berolo, "Low Frequency Noise in Double Barrier Resonant Tunneling Diodes," *Proceedings of the International Conference on Noise in Physical Systems and 1/f Fluctuations*,Kyoto, Japan, pp 195-198, (1991)

[44] A. H. Pawlikiewicz, A. van der Ziel, G. S. Kousik, and C.M. van Vliet, "On the Temperature Dependence of the Hooge Parameter α_H in n and p-channel silicon JFETs," *Solid-State Electronics*, Vol-31, (2), pp 233-236, (1988)

[45] Aldert Van Der Ziel, "Noise: Sources, Characterization, Measurement," *Prentice Hall, New Jersey,* (1970)

[46] Aldert van der Ziel, "Noise in Solid State Devices and Circuits," *Wiley-Interscience Publication*, pp 138-140 (1986)

Appendix I - Derivation of the Effective Hooge's parameter

Assuming all momentum gain by the carrier in the electric field ξ is lost in the lattice during a collision, then

$$q\, t_{col}\, \xi\, (-\overline{x}) = m_n^* V_d\, \overline{x} \quad \text{(A1.1)}$$

where $\overline{x}$ is the direction of current flows. Equivalently,

$$V_d\, \overline{x} = \mu\, \xi\, \overline{x} \quad \text{(A1.2)}$$

$$\text{where } \mu = \frac{q\, t_{col}}{m_n^*} \quad \text{(A1.3)}$$

Matthiesen's rule states that the frequency of collision is given by the sum of frequencies of each individual scattering mechanism and

$$f_{col} = f_1 + f_2 + \dots\dots + f_N, \quad \text{(A1.1)}$$

therefore,

$$\frac{1}{t_{col}} = \frac{1}{t_1} + \frac{1}{t_2} + \dots\dots + \frac{1}{t_N} \quad \text{(A1.2)}$$

multiplying each side by $\frac{q\, t_{col}}{m_n^*}$, we have

$$\frac{1}{\mu_{col}} = \frac{1}{\mu_1} + \frac{1}{\mu_2} + \dots\dots + \frac{1}{\mu_N} \quad \text{(A1.3)}$$

Taking the derivative of the above equation, we get

$$\frac{\delta\mu}{\mu_{col}^2} = \frac{\delta\mu}{\mu_1^2} + \frac{\delta\mu}{\mu_2^2} + \dots\dots + \frac{\delta\mu}{\mu_N^2}$$

$$\frac{\Delta\mu}{\mu_{col}^2} = \sum_i \frac{\Delta\mu_i}{\mu_i^2}$$

$$\Delta\mu = \sum_i \frac{\mu_{col}^2}{\mu_i^2} \Delta\mu_i \tag{A1.5}$$

$$\frac{S_{\Delta\mu}(f)}{\overline{\mu}^2} = \sum_i \frac{\mu_{col}^2}{\mu_i^2} \frac{S_{\Delta\mu_i}(f)}{\overline{\mu}_i^2} \tag{A1.6}$$

From Hooge's equation,

$$\alpha_H = \frac{S_{\Delta\mu}(f)}{\overline{\mu}^2} f N$$

$$= \sum_i \frac{\mu_{col}^2}{\mu_i^2} \frac{S_{\Delta\mu_i}(f)}{\overline{\mu}_i^2} f N. \tag{A1.6}$$

Therefore,

$$\alpha_H = \frac{\mu^2}{\mu_1^2} \alpha_{H1} + \frac{\mu^2}{\mu_2^2} \alpha_{H2} + \dots + \frac{\mu^2}{\mu_2^2} \alpha_{HN}$$

$$= \sum_i \frac{\mu^2}{\mu_i^2} \alpha_{Hi} \tag{A1.7}$$

Since the factor $\frac{\mu^2}{\mu_i^2}$ indicates how much a certain flicker noise source in average contributes to the overall flicker noise, it is actually a probability factor that depends on temperature.

Appendix II - Derivation of McWhorter's model for GR noise

The Derivation of McWhorter's model [7]

Non-fundamental flicker noise arises from traps, crystal defects, dislocations etc. The emission and capture of carriers by the processes of generation and recombination is described by the following differential equation

$$\frac{d\,\Delta N}{dt} + \frac{\Delta N}{\tau} = H(t) \tag{A2.1}$$

where ΔN is the fluctuation of the number of carriers, τ is the lifetime of the captured carriers, H(t) is a random number fluctuation and therefore a white noise. Expanding the terms into Fourier series, we have

$$H(t) = \sum_{i=\infty}^{-\infty} \alpha_n \exp(j\omega_n t), \tag{A2.2}$$

$$\Delta N(t) = \sum_{i=\infty}^{-\infty} \beta_n \exp(j\omega_n t), \tag{A2.3}$$

where $\omega_n = \frac{2\pi n}{T}$ and n = 0, ±1, ±2, ... Substitute equation (A2.2) and (A2.3) into (A2.1) and since $\frac{d}{dt} = j\,\omega_n$ for a harmonic wave, we have

$$j\,\omega_n \sum_{n=\infty}^{-\infty} \beta_n \exp(j\omega_n t) + \frac{1}{\tau} \sum_{n=\infty}^{-\infty} \beta_n \exp(j\omega_n t) = \sum_{n=\infty}^{-\infty} \alpha_n \exp(j\omega_n t), \tag{A2.4a}$$

$$\text{where } \beta_n = \frac{\alpha_n}{j\omega_n + \frac{1}{\tau}}. \tag{A2.4b}$$

For any signal E(t) which has a Fourier series of $\sum_{n=\infty}^{-\infty} \gamma_n \exp(j\omega_n t)$, the power spectrum of E(t), $S_E(f) = \lim_{T \to \infty} 2\,T\,\overline{\gamma_n \gamma_n^*}$. Therefore we have $S_H(f) = \lim_{T \to \infty} 2\,T\,\overline{\alpha_n \alpha_n^*}$ and

$S_i(f) = \lim_{T \to \infty} 2\,T\,\overline{\beta_n \beta_n^*}$. Using equation (A2.1), we have

$$\lim_{T \to \infty} 2\,T\,\overline{\beta_n \beta_n^*} = \lim_{T \to \infty} 2\,T\,\overline{\left(\frac{\alpha_n}{j\omega n + \frac{1}{\tau}} \; \frac{\alpha_n^*}{-j\omega n + \frac{1}{\tau}}\right)}$$

$$= 2\,T \lim_{T \to \infty} \overline{\alpha_n \alpha_n^*} \; \frac{\tau^2}{1 + \omega^2 \tau^2}. \qquad \textbf{(A2.5)}$$

From (A2.5), we have,

$$S_N(f) = S_H(f)\,\frac{\tau^2}{1 + \omega^2 \tau^2} \qquad \textbf{(A2.6)}$$

Since in our case, as illustrated from our experiment, the driving force h(t), which is the random fluctuation in the number of carriers, is area and current dependent, the spectrum of the driving force H(t). For f=0, since H(t) is a white noise, in the case of BJT, $S_H(f) = S_H(0)$. Using this

$$S_{\Delta N^2}(f) = \int_0^\infty S_H(f)\, df$$

$$= \int_0^\infty S_H(0)\,\frac{\tau^2}{1 + \omega^2 \tau^2}\, df$$

$$= S_H(0)\,\tau \int_0^\infty \frac{\tau}{1 + \omega^2 \tau^2}\, df$$

$$= \frac{S_H(0)\,\tau}{4}$$

Therefore $S_{gr}(f) = 4\,\overline{\Delta N_i^2}\,\frac{\tau}{1 + \omega^2 \tau^2}$. For n trap centers, we simply add their powers together and obtain the McWhorter model of $S_{gr}(f) = 4 \sum_{i=1}^{n} \overline{\Delta N_i^2}\,\frac{\tau_i}{1 + \omega^2 \tau_i^2}$.

Appendix III - Derivation of Equation (2.19)

The Derivation of Equation (2.19) (from [2])

Let n_T be the number of surface traps, n be the number of trapped electrons, n_0 be the number of trapped electrons at equilibrium, a be the generation rate constant and b be the recombination rate constant. $(n_T - n)$ is the number of empty traps. Then the generation rate (trapping rate) is proportional to the number of empty traps and the recombination rate (release rate) is proportional to the number of trapped electrons,

$$g(n) = a\,(n_T - n) \text{ and} \tag{A3.1}$$

$$r(n) = b\,n. \tag{A3.2}$$

At equilibrium,

$$g(n) = r(n),$$

$$n_o = \frac{a}{a+b} n_T = \frac{1}{1 + (n_T - n_o)/n_o} = f_T\, n_T\,. \tag{A3.3}$$

This gives equation (2.19a). From (A2.1),

$$\tau = \frac{1}{a+b}\,. \tag{A3.4}$$

Furthermore, using (A3.3)

$$\overline{\Delta N_t^2} = \frac{b}{a+b} n_o = \frac{a\,b}{(a+b)^2} n_T = n_T\, f_T\,(1 - f_T) \tag{A3.4}$$

This gives equation (2.19b).

APPENDIX A4 NOISE MODELLING USING MATHCAD

****

************* Noise Modelling using MATHCAD 3.0 in Microsoft Windows **************

********************** Author : Anthony Ng Date Written : May-01-92 ***********************

************************ Semiconductor Device Research Group ****************************

************ Engineering Science Department, Simon Fraser University, B.C. *************

****

================== A4.1 DEFINE CONSTANT =====================

Electron charge: $q := 1.602 \cdot 10^{-19}$ C

Fine structure constant: $\alpha 0 := \dfrac{1}{137}$

Planck's constant : $h := 6.632 \cdot 10^{-34}$ $J \cdot s$

Boltzmann's constant : $k := 1.38 \cdot 10^{-23}$ $\dfrac{J}{K}$

Speed of light : $c := 3 \cdot 10^{8}$ m/s

Effective mass of carrier: $m := 1.00 \cdot 9.1 \cdot 10^{-31}$ Kg

Lattice spacing: $a := 6.20 \cdot 10^{-10}$ m

==== A4.2 Calculate the factor G(T) = $\dfrac{\beta \cdot D_p}{\left[\pi \cdot f_T \cdot q \cdot w_E \cdot v_s\right]}$ required in ========

======= the calculation of α_p which is described in equation (2.54) ======

Define d.c. Current Gain $\beta(T)$

$$A := \begin{bmatrix} \ln(100) & 1 \\ \ln(300) & 1 \end{bmatrix} B := \begin{bmatrix} \ln(6) \\ \ln(70) \end{bmatrix} \begin{bmatrix} m \\ c \end{bmatrix} := A^{-1} \cdot B \qquad m = 2.236$$

$$T := 100, 200 .. 1000$$

$$\beta 1\_25 := 120 \quad c1 := \ln(\beta 1\_25) - m \cdot \ln(300) \beta 1(T) := \exp(m \cdot \ln(T) + c1) \alpha 1(T) := \frac{\beta 1(T)}{\left[1 + \beta 1(T)\right]}$$

$$\alpha(T) := \alpha 1(T) \; \beta(T) := \beta 1(T)$$

Notice: almost all results come from B7, not A1. Betas are 118,116,143,124,126, 119 from 45 to 0.5

Graph of current gain Beta vs. Temp

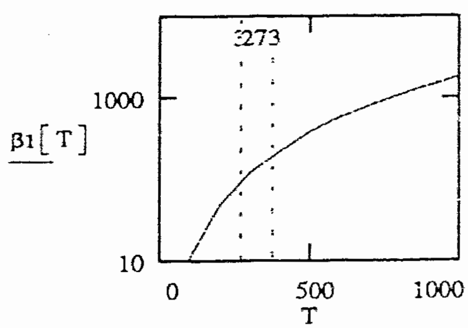

Graph of Common Base Current Gain Factor vs. Temp

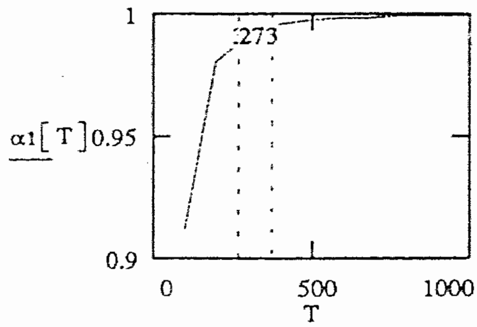

Define the Base-Emitter Capacitance Cbe :

$q := 1.60210 \cdot 10^{-19}$ $k := 1.38054 \cdot 10^{-23}$ $TF1 := 1.6 \cdot 10^{-11}\,s$ $IS1 := 2.657 \cdot 10^{-10}\,A$

$Ib1A := 1$ $Ic1A(T) := Ib1A \cdot \beta(T)$ sicne Ib is normalized to 1A in our calculation.

$Cbe(T, Ic) := \frac{q}{(k \cdot T)} \cdot TF1 \cdot Ic \;(F)$ Assume device operating under normal active mode, thus Cbe >> Cbc

Graph of Base-Emitter Capacitance vs. Temperature

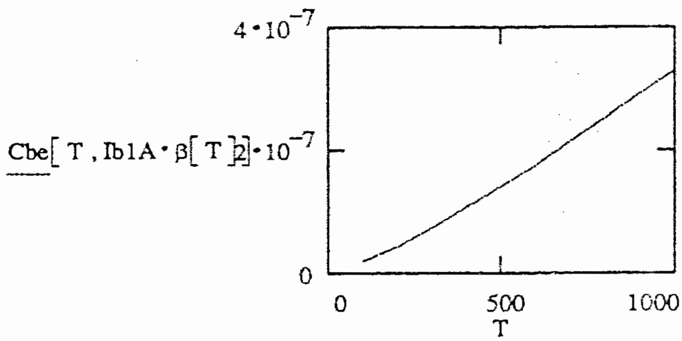

Define the Transconductance gm and the Transistor Cutoff Frequency f_T

$gm(T, IC) := \frac{q}{(k \cdot T)} \cdot IC \left[\frac{A}{V}\right]$ $fT(T, IC) := \frac{gm(T, IC)}{[2 \cdot \pi \cdot Cbe(T, IC)]}$ (Hz)

Graph of Transconductance vs. Temperature

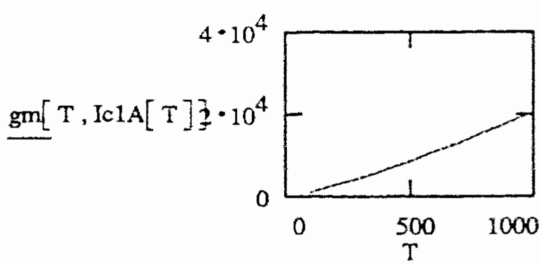

Graph of Transistor Cutoff Frequency vs. Temperature

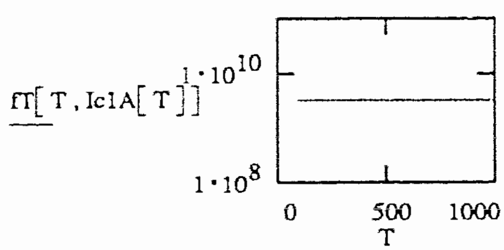

Define Carrier Saturation Velocity Vs for Silicon :

$$Vs(T) := \frac{2.4 \cdot 10^{7}}{\left[1 + 0.8 \cdot \exp\left[\frac{T}{600}\right]\right]} \quad \frac{cm}{s}$$

Graph of Carrier Saturation Velocity Vs vs Temperature

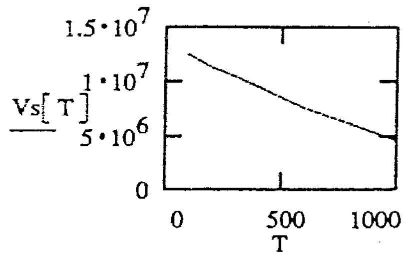

Define the Electron Diffusion Constant Dn(T) :

$$Tn(T) := \frac{T}{300}$$

Total Impurity concentration =Nd $:= 7 \cdot 10^{17}\ cm^{-3}$ $\quad Na := 1 \cdot 10^{18}\ cm^{-3}$

Calculate the Quasi-electron Fermi Level

$m0 := 9.1091 \cdot 10^{-31}$ $me\_eff := 1.38 \cdot m0$ for electron in Si $\quad mh\_eff := 0.946 \cdot m0$

$$Eg(T) := 1.16 - \frac{\left[7.02 \cdot 10^{-4} \cdot T^{2}\right]}{(T + 1108)} cm^{-3} \qquad Nc(T) := 2 \cdot \frac{\left[\frac{\left[2 \cdot \pi \cdot me\_eff \cdot k \cdot T\right]}{h^{2}}\right]^{1.5}}{10^{6}}$$

$$ni(T) := Nc(T) \cdot \exp\left[\frac{\left[\frac{-Eg(T)}{2}\right] \cdot q}{k \cdot T}\right] \qquad Efi(T) := \frac{Eg(T)}{2} + \frac{3 \cdot k \cdot T}{4} \cdot \ln\left[\frac{mh\_eff}{me\_eff}\right]$$

$$Efp(T) := Efi(T) - \frac{k \cdot T}{q} \cdot \ln\left[\frac{Na}{ni(T)}\right] \qquad Efn(T) := Efi(T) + \frac{k \cdot T}{q} \cdot \ln\left[\frac{Nd}{ni(T)}\right]$$

$t := 10, 40 .. 700$

Graph of the Intrinsic Fermi Level and the Hole Fermi Level vs. Temperature

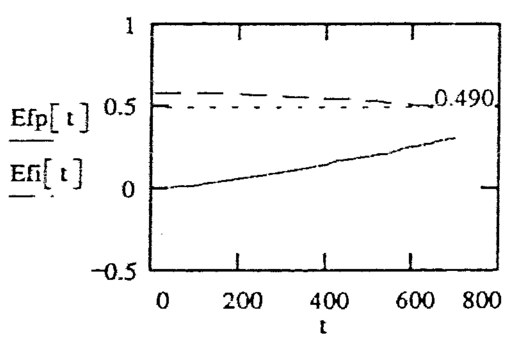

Calculate the Impurity Scattering and Lattice Scattering factors

$$\varepsilon 0 := 8.8542\cdot 10^{-12} \qquad \varepsilon := 16\cdot \varepsilon 0$$

$$ui(T,Ni) := \frac{10.65\cdot 10^{19}}{\left[Ni\cdot \ln\left[1+\frac{3\cdot 10^{11}}{Ni^{\frac{2}{3}}}\cdot\left[\frac{T\cdot\varepsilon}{[300\cdot\varepsilon 0]}\right]\right]\right]}\cdot\left[\frac{T}{300}\right]^{\frac{3}{2}}\cdot\left[\frac{\varepsilon}{\varepsilon 0}\right]^{2}\cdot\left[\frac{m0}{me\_eff}\right]^{\frac{1}{2}}$$ where Ni is the ionized impurity conc in cm^-3

$$\rho := 2.33\cdot 10^{6} \qquad c := 2.997925\cdot 10^{8} \qquad vs := \sqrt{\frac{c}{\rho}}$$

$$ul(T,Elc) := \frac{2\cdot\sqrt{[2\cdot\pi]}}{2}\cdot\frac{q\cdot\left[\frac{h}{[2\cdot\pi]}\right]^{4}\cdot\rho\cdot vs^{2}}{Elc^{2}}\cdot me\_eff^{\frac{-5}{2}}\cdot(k\cdot T)^{\frac{-3}{2}}$$

Calculate the Electron and Hole Mobilities $Na := 1.5\cdot 10^{16} \quad Na\_max := 2.5\cdot 10^{16} \quad Nd := 2\cdot 10^{16}$

$$un(T,Nd) := \left[88\cdot Tn(T)^{-0.57}+\frac{7.4\cdot 10^{8}\cdot T^{-2.33}}{1+\left[\frac{Nd}{\left[1.26\cdot 10^{17}\cdot Tn(T)^{2.4}\right]}\cdot 0.88\cdot Tn(T)^{-0.146}\right]}\right]$$

$$uh(T,Na) := 54.3\cdot Tn(T)^{-0.57}+\frac{1.36\cdot 10^{8}\cdot T^{-2.23}}{1+\left[\frac{Na}{\left[2.35\cdot 10^{17}\cdot Tn(T)^{2.4}\right]}\cdot 0.88\cdot Tn(T)^{-0.146}\right]}$$

$$Dh(T,Na) := \frac{k\cdot T}{q}\cdot uh(T,Na) \qquad Dn(T,Nd) := \frac{k\cdot T}{q}\cdot un(T,Nd)$$

Graph of Electron Mobility (un), Hole Mobility (uh), Mobility due to Lattice Scattering (ul) and Mobility due to Impurity Scattering (ui) vs. Temperature

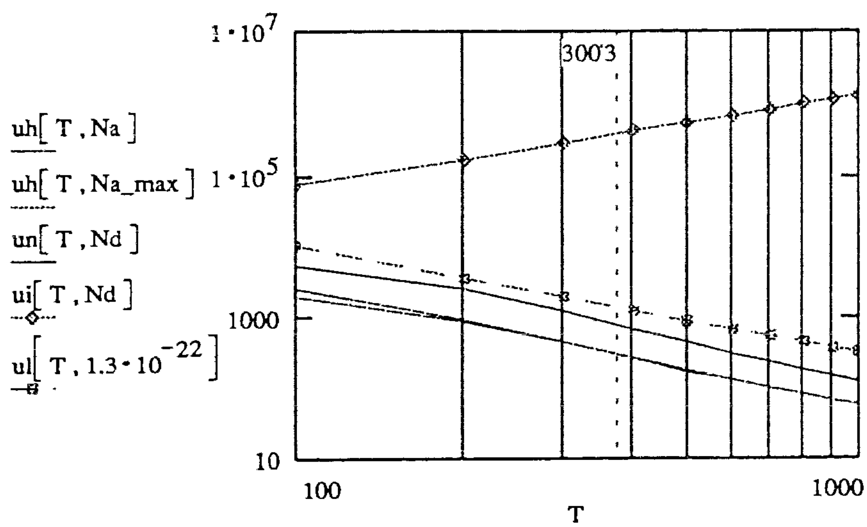

Graph of Electron Diffusion Coefficient vs. Temperature

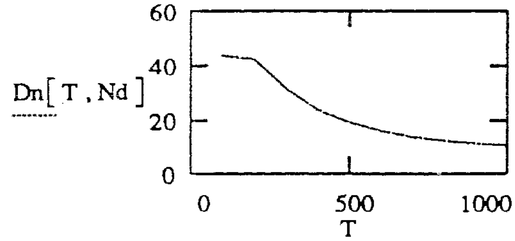

Define the minimum value of hole conc. at the two ends of the emitter (p_ration $=\ln\left[\dfrac{P(0)}{P(N)}\right]$)

Emitter Width : $We := 1.9 \cdot 10^{-5}$ cm

$$p\_ratio(T, We) := \frac{We \cdot Vs(T)}{Dh(T, Na)}$$

Graph of the minimum ratio of hole conc at the two ends of emitter vs. Temperature

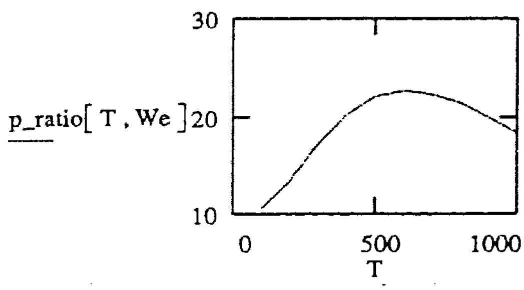

Calculate $G(T) = \dfrac{\beta \cdot D_p}{\left[\pi \cdot f_T \cdot q \cdot w_E \cdot v_s\right]}$

$$G(T, IEp, WE) := \pi \cdot fT[T, IEp \cdot \beta(T)] \cdot q \cdot \ln(p\_ratio(T, WE))$$

Graph of G(T) used in the Calculation of the Hooge's Parameters vs. Temp

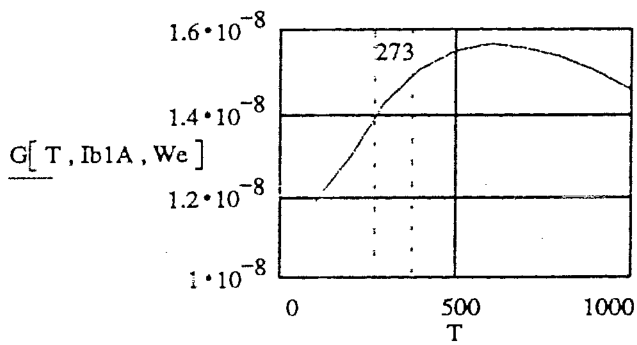

Ef(T) :=

==================== A4.3 GR NOISE MODELLING ======================

****

Complete GR Noise Model (for each trap in BJT)

All energy level refers to valence band

$$\tau[\tau 0, Ea, T] := \tau 0 \cdot \exp\left[\frac{(q \cdot Ea)}{k \cdot T}\right]$$

$$\Delta E1(Et, T) := Eg(T) - Et \quad = Ec - Et$$

$$ft(Et, T) := \frac{1}{\left[1 + \left[\exp\left[\frac{(q \cdot ((Et - Ef(T))))}{k \cdot T}\right]\right]\right]}$$

For Electron Trap :

$$SGR1[Cnf, \tau 0, Et, T, f, \eta] := Cnf \cdot \frac{\tau[\tau 0, \Delta E1(Et, T), T]}{\left[1 + \left[[2 \cdot \pi \cdot f] \cdot \tau[\tau 0, \Delta E1(Et, T), T]\right]^2\right]} \cdot ft(Et, T) \cdot (1 - ft(Et, T))$$

For Hole Trap :

$$SGR2[Cnf, \tau 0, Et, T, f, \eta] := Cnf \cdot \frac{\tau[\tau 0, Et, T]}{\left[1 + \left[[2 \cdot \pi \cdot f] \cdot \tau[\tau 0, Et, T]\right]^2\right]} \cdot ft(Et, T) \cdot (1 - ft(Et, T))$$

****

A4.3.1 Verifying Mohammed I. Abdala et al's Method ("The Excess Noise in GaAs MESFET", Noise in Physical Systems and 1/f Fluctuation ICNF 1991, pp 187)

The Si * f method

$$s := 0, 1 .. 50 \quad \omega_s := 10^{\frac{s}{10}}$$

$$a_1 := 105863 \quad \tau_1 := \frac{1029}{1000000}$$

$$B := 16002$$

$$a_2 := 91468 \quad \tau_2 := \frac{98}{1000000}$$

$$y1_s := \frac{\left[a_1 \cdot [\tau_1] \cdot \omega_s\right]}{\left[1 + \left[[\omega_s \cdot \tau_1]\right]^5\right]} \quad y2_s := \frac{\left[a_2 \cdot [\tau_2] \cdot \omega_s\right]}{\left[1 + [\omega_s]^2 \cdot [\tau_2]^2\right]} \quad y_s := y1_s + y2_s + B$$

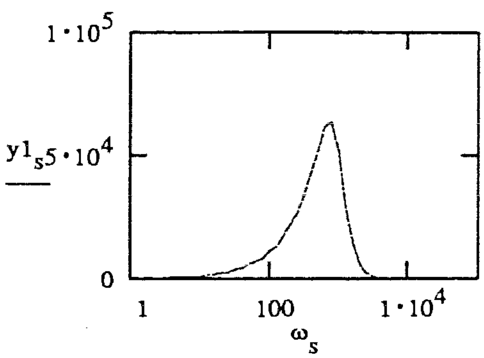

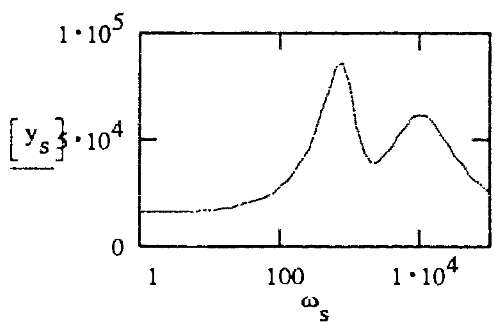

The g-r noise spectrum

$$\mathrm{max\_i} := 100 \quad i := 10, 11 .. 100 \quad \tau := \frac{1029}{1000000}$$

$$f_i := 10^{\left[i \cdot \frac{\left[\log\left[10^7\right] - \log\left[10^0\right]\right]}{\mathrm{max\_i}} + \log[1] \right]} \quad \omega_i := 2 \cdot \pi \cdot f_i \quad A := 1$$

$$SN(\omega, \tau) := 4 \cdot A \cdot \frac{\tau}{\left[1 + (\omega \cdot \tau)^2\right]} \quad S_i := SN\left[\omega_i, \tau\right]$$

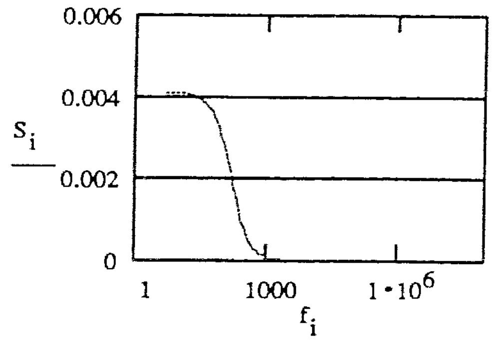

A4.3.2 Using Noise Model in Section 5.3 to Fit Experimental Data Measured for our Bipolar Transisotrs

Emtter Area :

$$A := (0.5 \quad 1 \quad 2 \quad 4 \quad 15 \quad 30 \quad 45)^T \cdot 3.2 \cdot \left[10^{-6}\right]^2$$

Parameters of the two traps for all six sizes :

$$\tau 0 := \begin{bmatrix} 8 \cdot 10^{-16} \\ 2.3 \cdot 10^{-3} \end{bmatrix} \quad Ea := \begin{bmatrix} 0.88 \\ 0.110 \end{bmatrix} \quad f0 := 1000 \qquad Ic := \beta(300) \qquad x := 0$$

$$Cnf := \begin{bmatrix} 6.4 \cdot 10^{-18} & 3.41 \cdot 10^{-18} & 1.37 \cdot 10^{-18} & 2.73 \cdot 10^{-18} & 7.68 \cdot 10^{-18} & 1.54 \cdot 10^{-18} & 1.73 \cdot 10^{-18} \\ 2.13 \cdot 10^{-31} & 8.53 \cdot 10^{-31} & 3.41 \cdot 10^{-31} & 9.56 \cdot 10^{-31} & 3.84 \cdot 10^{-31} & 7.68 \cdot 10^{-31} & 3.46 \cdot 10^{-31} \end{bmatrix}$$

Read in Experimental ResultsNoise versus Temperature

$$j := 0, 1 .. 9 \; N := \mathrm{READPRN}(\mathrm{SI\_T2}) \qquad T_j := \left[N^{\langle 0 \rangle}\right]_j + 273 \qquad TT_j := T_j$$

****

GR Noise Definition for Model for BJT

$$\tau[\tau 0, Ea, T] := \tau 0 \cdot \exp\left[\frac{(q \cdot Ea)}{k \cdot T}\right]$$

$$ft(Et, T) := \frac{1}{\left[1 + \exp\left[\frac{(Efp(T) - Et) \cdot q}{(k \cdot T)}\right]\right]}$$

$$SGR[Cnf, \tau 0, Ea, T, f, Ic, A] := Cnf \cdot \frac{Ic^2}{A^2} \cdot \frac{\tau[\tau 0, Ea, T]}{\left[1 + [[2 \cdot \pi \cdot f] \cdot \tau[\tau 0, Ea, T]]^2\right]} \cdot ft(Ea, T) \cdot (1 - ft(Ea, T))$$

****

Define two frequency normalized g-r noises :

$Ic(T) := 1 \cdot \beta(T)$ All data were normalized to Ib = 1A, therefore Ic = 1 β

$$Sgr0(x, T, f) := \frac{SGR\left[Cnf_{0,x}, \tau 0_0, Ea_0, T, f, Ic(T), A_x\right]}{f}$$

SIMULATION RESULTS FOR X=0,1,3
GRAPH OF Ln (Si) vs Temp

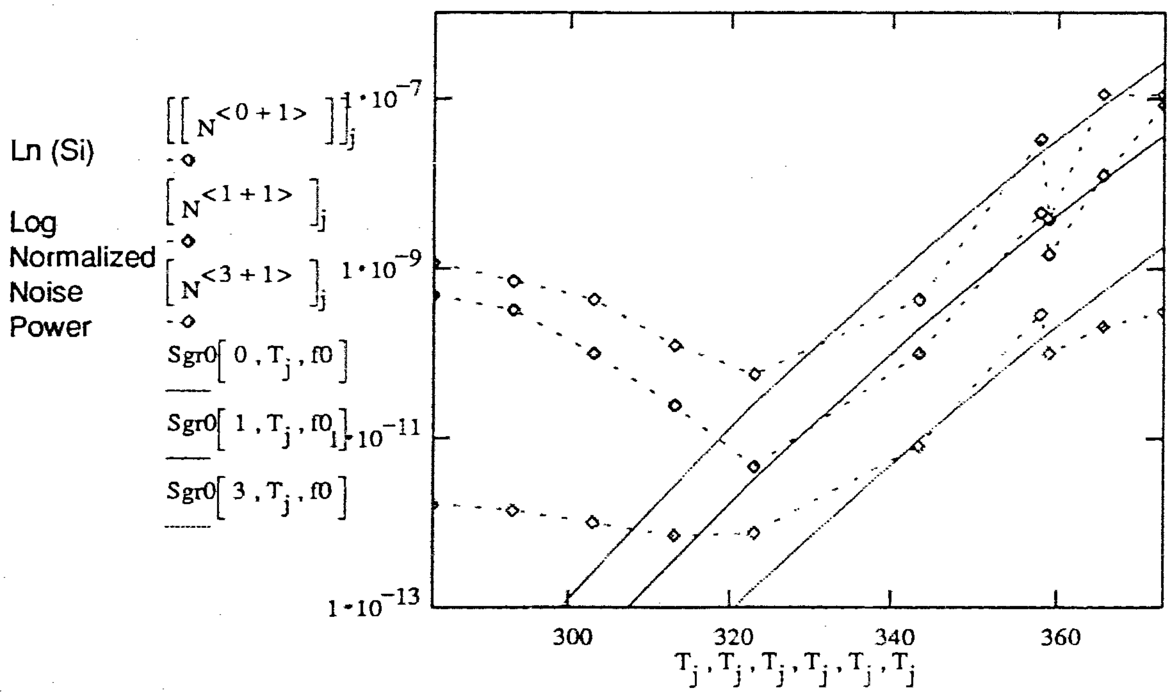

A4.3.3 Using newly derived Method to calculate the Activation Energy Et from the Risng Slope

T << Tpk, 1/T >> 1/Tpk : d ln Si/ d 1/T = - 2 q Et / k + q / kT d Ef /d T ln T + EF q/ k

$$r := \begin{bmatrix} 4 & 3 & 5 & 5 & 4 & 4 & 4 \\ 8 & 8 & 9 & 8 & 9 & 9 & 9 \end{bmatrix}^T \quad x := 6 \quad start := r_{x,0} \quad end := r_{x,1} \quad j := 0, 1 .. (end - start)$$

$$j0 := 0, 1 .. 9 \qquad x1_j := \frac{1}{TT_{j+start}} \qquad z1_j := \ln\left[\left[N^{<x+1>}\right]_{j+start}\right]$$

$$a0 := slope(x1, z1) \quad b0 := intercept(x1, z1) \quad c0 := corr(x1, z1)$$

$$a0 = -1.892 \cdot 10^4 \quad b0 = 24.286 \quad c0 = -0.957$$

Graph of Normalized Noise versus Reciprocal Temperature
Determine the Trap Energy Level

(Ec - Et) for electron trap and (Et - Ev) for hole trap

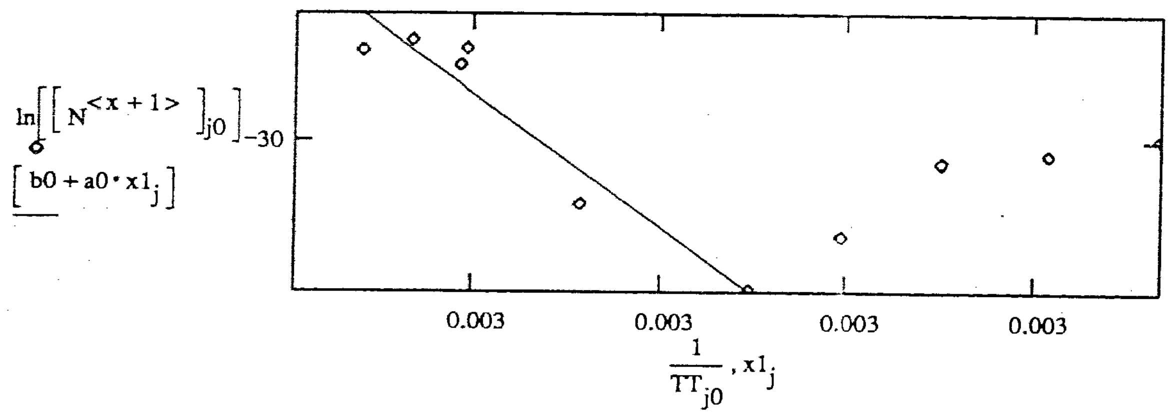

$$Et(T) := \frac{-T}{2} \cdot \left[\frac{d}{dT} Efp(T)\right] + \frac{Efp(T)}{2} - \frac{k}{(2 \cdot q)} \cdot a0 \quad Et\left[TT_{start}\right] = 0.794 \quad Et\left[TT_{end}\right] = 0.791$$

A4.3.4 Verify the Fermi Level Dependence on the other Side :

$x := 2 \quad T := 273, 275 .. 373T3 := 273, 275 .. 320$

Graph of Normalized Noise versus Reciprocal Temperature

To Verify the Fermi-Level Dependence on the Rising Slope

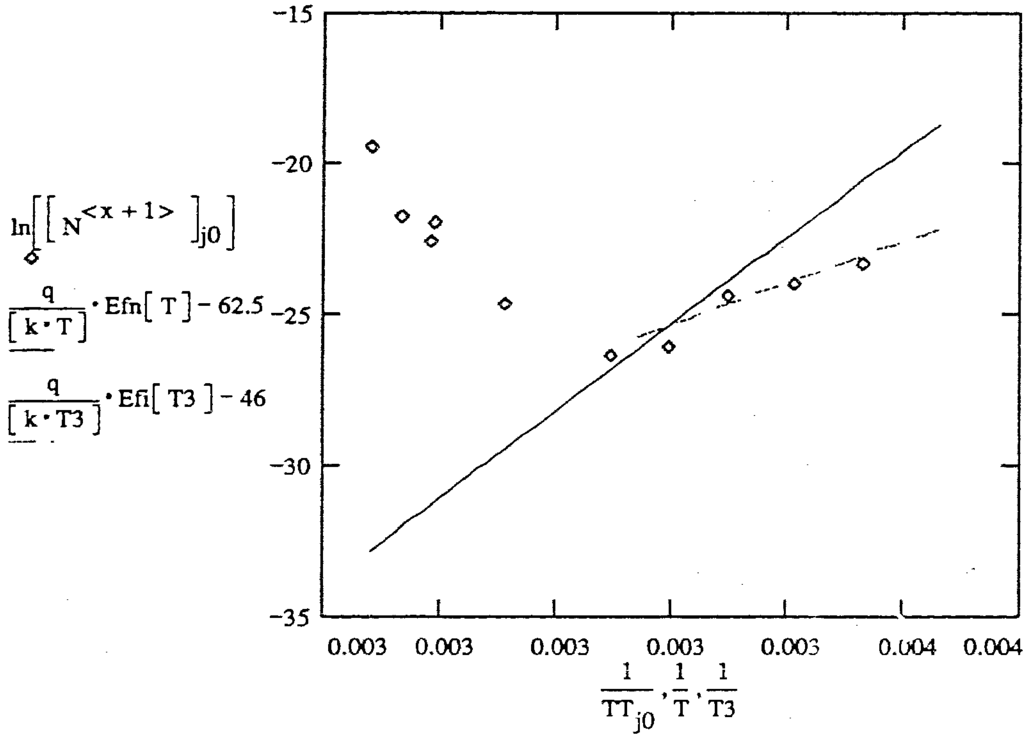

A4.3.5 Determin from experimental data, A's power in the graph of log normalized Ib versus area ln (Si/Ic^2) = ln c tau0 - m ln A

$jT := 6 \qquad TT_{jT} - 273 = 85 \qquad Size := (.5 \quad 1 \quad 2 \quad 4 \quad 15 \quad 30 \quad 45)^T$

$start := 0 \quad end := 6 \quad x := 0, 1 .. (end - start) \qquad x0 := 0, 1 .. 6$

$S(x, jT) := \left[N^{<x+1>}\right]_{jT}$

$x2_x := \log\left[Size_{x+start}\right] \; z2_x := \log(S(x + start, jT))$

$a0 := slope(x2, z2) \quad b0 := intercept(x2, z2) \quad c0 := corr(x2, z2) \quad start := 0$

$a0 = -2.238 \qquad b0 = -8.435 \qquad c0 = -0.968$

Graph of Normalized Noise Power measured for Experiments vs. Temperature

Slope = $a0 = -2.238$

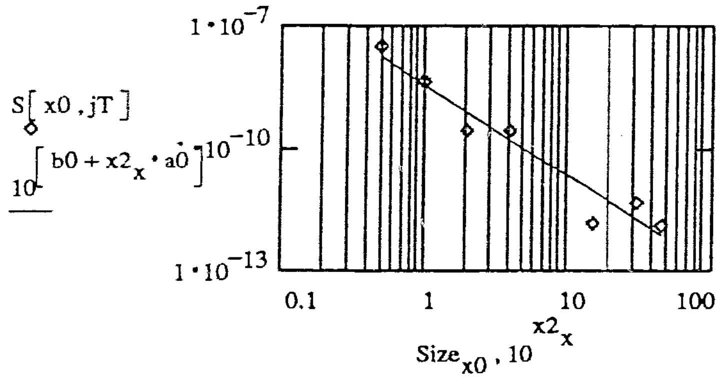

A4.3.6 Determine how the Number Fluctuation $\overline{\Delta N^2}$ varies with the Emitter Area (Pasted directly from file Sf_Snf6.mcd)

Calculate the Quasi-electron Fermi Level

$m0 := 9.1091 \cdot 10^{-31}$ $me\_eff := 1.38 \cdot m0$ for electron in Si $mh\_eff := 0.946 \cdot m0$ $p := 1.2 \cdot 10^{16}$

$$Nc(T) := 2 \cdot \frac{\left[\frac{[2 \cdot \pi \cdot me\_eff \cdot k \cdot T]}{h^2}\right]^{1.5}}{10^6} \qquad Eg(T) := 1.16 - \frac{[7.02 \cdot 10^{-4} \cdot T^2]}{(T + 1108)}$$

$$Ei(T) := \frac{Eg(T)}{2} + \frac{3 \cdot k \cdot T}{4} \cdot \ln\left[\frac{mh\_eff}{me\_eff}\right] \qquad ni(T) := Nc(T) \cdot \exp\left[\frac{\left[\frac{-Eg(T)}{2}\right] \cdot q}{k \cdot T}\right]$$

$$Ef(T) := Ei(T) - \frac{k \cdot T}{q} \cdot \ln\left[\frac{p}{ni(T)}\right]$$

Read in raw results $i := 0, 1 .. 9$ $N := READPRN(SI\_T_i) := \left[N^{\langle 0 \rangle}\right]_i + 273$

****

GR Noise Model for BJT

Goal : Find Cnf and m in A^m
Define R as Cnf / A^m, which can be determined by fitting the model to the experimental data. Then by plotting R vs.A, both Cnf and m can be determined.

$$\tau[\tau 0, Ea, T] := \tau 0 \cdot \exp\left[\frac{(q \cdot Ea)}{k \cdot T}\right]$$

$$\Delta E1(Et, T) := Eg(T) - Et$$

$$ft(Et, T) := \frac{1}{\left[1 + \left[\exp\left[\frac{(q \cdot ((Et - Ef(T))))}{k \cdot T}\right]\right]\right]}$$

$$SGR1[R, \tau 0, Et, T, f, Ic] := R \cdot Ic^2 \cdot \frac{\tau[\tau 0, \Delta E1(Et, T), T]}{\left[1 + [[2 \cdot \pi \cdot f] \cdot \tau[\tau 0, \Delta E1(Et, T), T]]^2\right]} \cdot ft(Et, T) \cdot (1 - ft(Et, T))$$

$$SGR2[R, \tau 0, Et, T, f, Ic] := R \cdot Ic^2 \cdot \frac{\tau[\tau 0, Et, T]}{\left[1 + [[2 \cdot \pi \cdot f] \cdot \tau[\tau 0, Et, T]]^2\right]} \cdot ft(Et, T) \cdot (1 - ft(Et, T))$$

****

$Ic(T) := 1 \cdot \beta(T)$ Since noise data were normalized to Ib = 1A

$$\tau 0 := \begin{bmatrix} 1.1 \cdot 10^{-5} \\ 5 \cdot 10^{-7} \end{bmatrix} \quad Ea := \begin{bmatrix} 0.11 \\ 0.82 \end{bmatrix}$$

$$R := \begin{bmatrix} 1. \cdot 10^{-3} & 4 \cdot 10^{-4} & 8 \cdot 10^{-5} & 2 \cdot 10^{-6} & 1 \cdot 10^{-6} & 1.2 \cdot 10^{-7} & 9.99 \cdot 10^{-8} \\ 2 \cdot 10^{4} & 4 \cdot 10^{3} & 3 \cdot 10^{2} & 2 \cdot 10^{2} & 1 \cdot 10^{1} & 7 \cdot 10^{0} & 1 \cdot 10^{0} \end{bmatrix} \cdot \frac{4}{\beta(300)^2}$$

Define two g-r noise $x := 3$

$$Sgr0(x, T, f) := SGR2\left[R_{[0, x]}, \tau 0_0, Ea_0, T, f, Ic(T)\right] \cdot \frac{1}{f}$$

$$Sgr1(x, T, f) := SGR1\left[R_{[1, x]}, \tau 0_1, Ea_1, T, f, Ic(T)\right] \cdot \frac{1}{f}$$

$tt := 273, 278 .. 373 \quad tt := 100, 105 .. 600 \quad tt := 250, 255 .. 400$

$$ili := 1, 2 .. 20 \quad tlt_{ili} := 10^{\left[\frac{[\log[1300] - \log[100]]}{20} \cdot ili + \log[100]\right]}$$

Graphs of Noise Data and Noise Model vs. Temperature

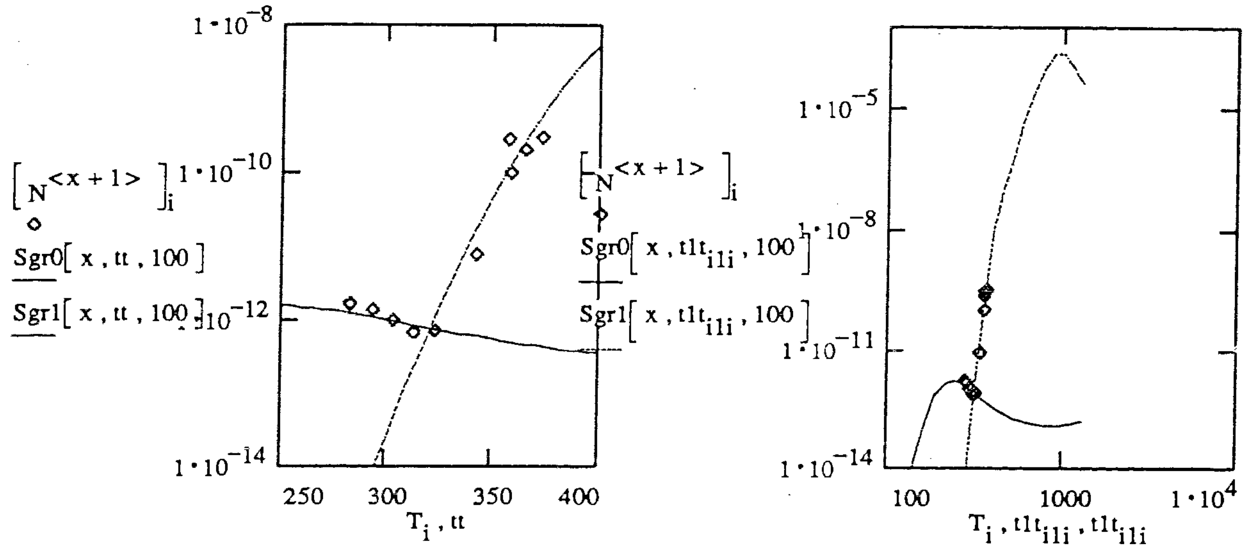

Determine Cnf and m in A^m by plotting R = Cnf / A^m versus emitter area in a log-log graph

$j := 0, 1 .. 6 \qquad Size := (.5 \;\; 1 \;\; 2 \;\; 4 \;\; 15 \;\; 30 \;\; 45)^T \cdot 3.2 \cdot \left[10^{-6}\right]^2$

$x9_j := \log\left[Size_j\right] \qquad y9_j := \log\left[\left[R^{<j>}\right]_0\right] \qquad fit91_j := 10^{\left[slope[x9, y9] \cdot x9_j + intercept[x9, y9]\right]}$

$x8_j := \log\left[Size_j\right] \qquad y8_j := \log\left[\left[R^{<j>}\right]_1\right] \qquad fit81_j := 10^{\left[slope[x8, y8] \cdot x8_j + intercept[x8, y8]\right]}$

Graphs of Cnf (=$\overline{\Delta N^2}$) versus Emitter Area

Semi-Log Graph *Log-Log Graph*

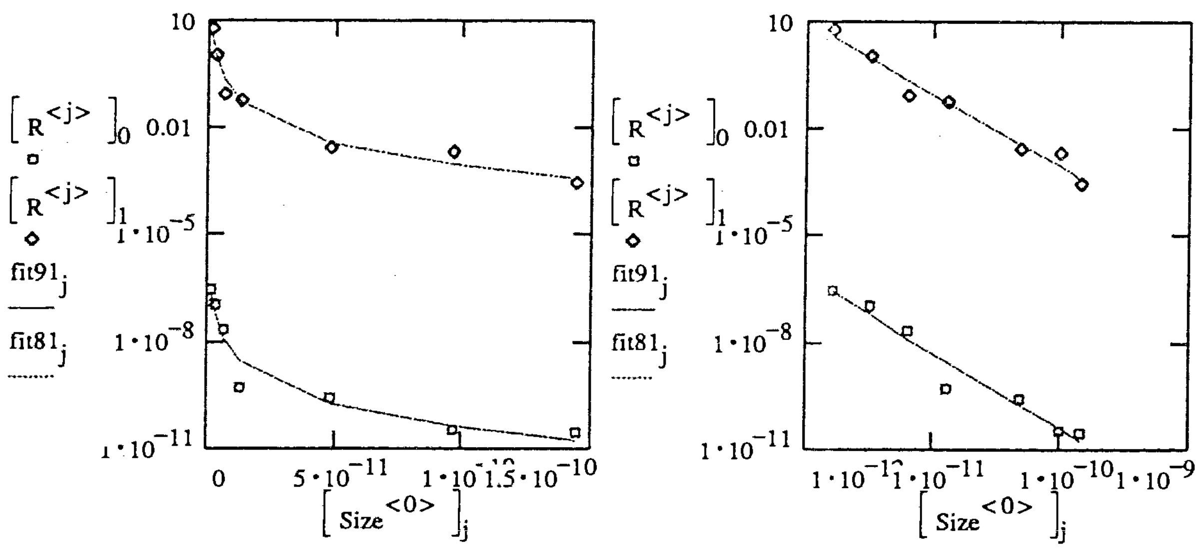

m $\quad slope(x9, y9) = -2.144$

$\quad slope(x8, y8) = -2.037$

Cnf $\quad 10^{intercept[x9, y9]} = 1.389 \cdot 10^{-32}$

$\quad 10^{intercept[x8, y8]} = 3.418 \cdot 10^{-24}$

**************************A4.4 FLICKER NOISE MODELLING ********************************

Lacttice Constant $\quad a := 5.43\cdot 10^{-10}\,\mathrm{m}$

Speed of light in vac $\quad c := 3\cdot 10^{8}\,\mathrm{m/s}$

$m := 1.00\cdot 9.1\cdot 10^{-31}\,\mathrm{Kg}$

α for Umklapp Process: m $\quad \alpha 1 := \dfrac{[4\cdot\alpha 0]}{[3\cdot\pi]}\cdot\left[\dfrac{h}{(m\cdot a\cdot c)}\right]^2 \qquad \alpha 1 = 6.201\cdot 10^{-8}$

a for Normal Collision Process: $\quad \alpha 2(T) := \dfrac{[4\cdot\alpha 0]}{[3\cdot\pi]}\cdot\left[\dfrac{(6\cdot k\cdot T)}{[m\cdot c^2]}\right]$

Debyte Temperature for Si: $\quad \theta := 645\ \mathrm{K}$

Probability factors: $\quad P1(T) := \exp\left[\dfrac{-\theta}{(2\cdot T)}\right] \quad P2(T) := \left[1-\exp\left[\dfrac{-\theta}{(2\cdot T)}\right]\right]$

Composite Hooge's parameter: $\quad \alpha H(T) := \alpha 1\cdot P1(T)+\alpha 2(T)\cdot P2(T)$

Convert x to actual area x={0,1,2,3,4,5,6} Area=0.32*10^-32*{0.5,1,2,15,30,45}

$E(x) := A_x$

****

Fundamental Flicker Noise Model

$$\alpha H(CH, Ae, T) := [\alpha 1\cdot P1(T)+\alpha 2(T)\cdot P2(T)]\cdot\frac{CH}{Ae^2}$$

$$G(T, IEp, WE) := \pi\cdot fT[T, IEp\cdot\beta(T)]\cdot q\cdot\ln(p\_ratio(T, WE))$$

$$Sf(CH, Ae, IEp, T, f) := \frac{G(T, IEp, We)\cdot\alpha H(CH, Ae, T)}{f}\cdot IEp$$

****

Plot of both noise vs frequency $max\_j := 20 \quad j := 0, 1 .. max\_j \quad f_j := 10^{\left[j\cdot\frac{[\log[10^5]-\log[10^0]]}{max\_j}+\log[1]\right]}$

$T0 := 300\ f0 := 100 \quad Total(CH, x, T, f) := Sf(CH, E(x), Ib1A, T, f)+Sgr0(x, T, f)+Sgr1(x, T, f)$

$CH := 3\cdot 10^{-18} \qquad x := 3 \quad f1Hz := 1$

Graph of Total Noise, GR Noise #1, GR Noise #2 and Flicker Noise Dervied from Model versus Frequency

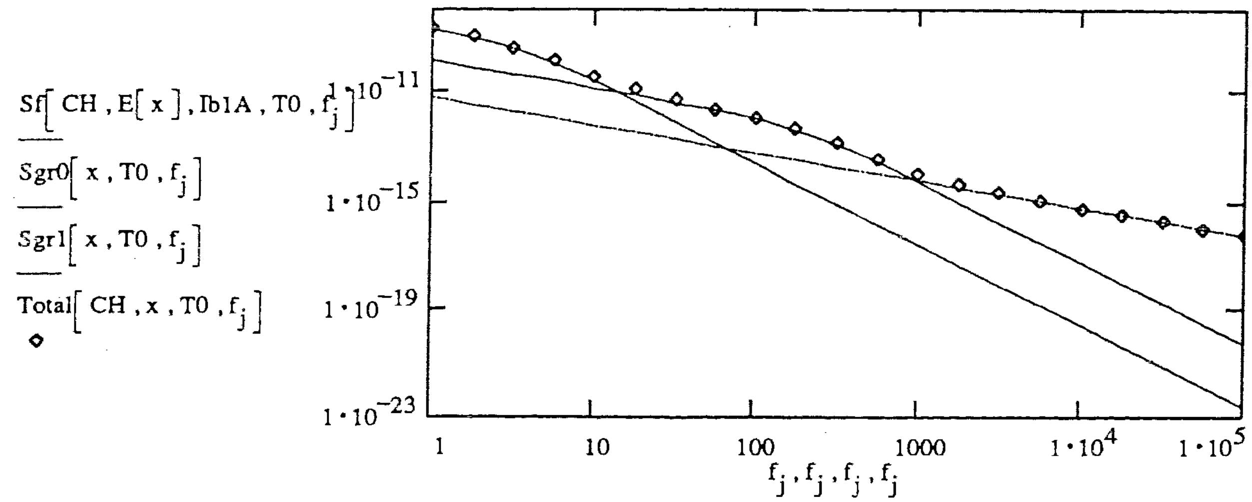

Graph of Total Noise, GR Noise #1, GR Noise #2, Flicker Noise and Experimental Data vs Temperature

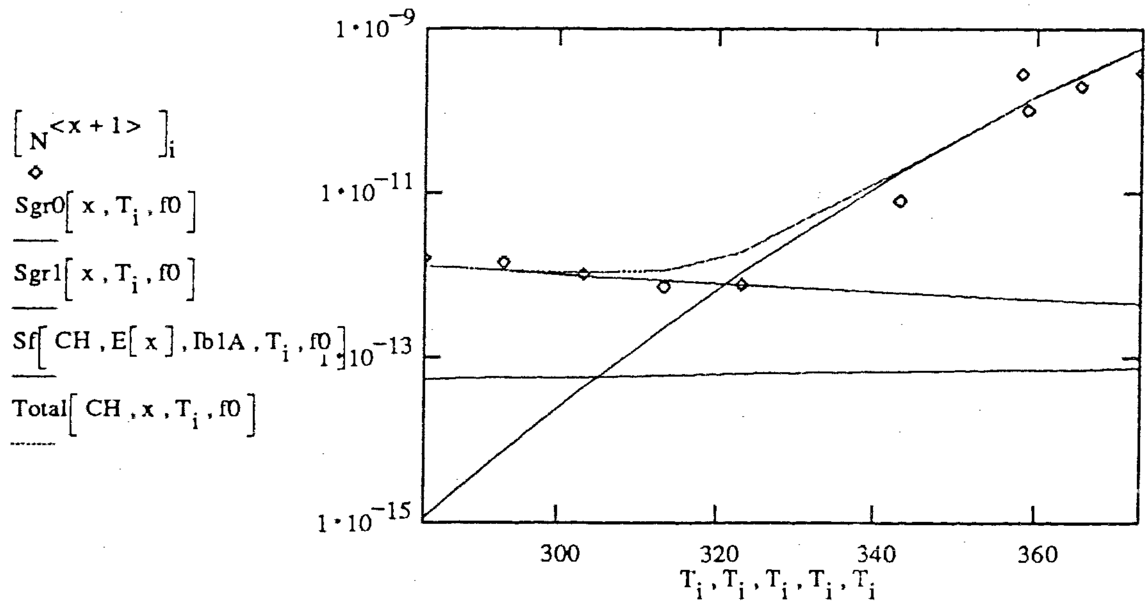

$$i2i := 1, 2 .. 20 \quad t2t_{i2i} := 10^{\left[\frac{[\log[1200] - \log[100]]}{20} \cdot i2i + \log[100]\right]}$$

Graph Identical to the Previous One except with a Wider Temperature Range

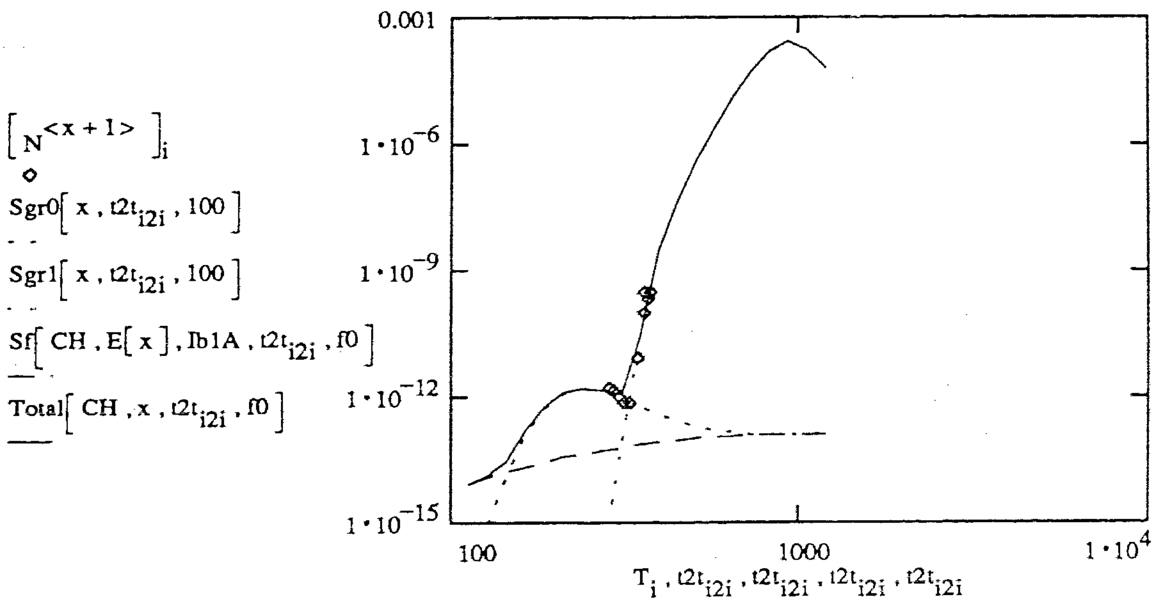

$i2i := 1, 2 .. 20 \qquad t2t_{i2i} := 10^{\left[\frac{[\log[9000]-\log[60]]}{20}\cdot i2i+\log[60]\right]}$

================= A4.5 OTHER EXPERIMENTAL DATA =====================

A4.5.1 Modelling J.Kilmer et al, "Mobility Fluctuation 1/f Noise in Silicon p+-n-p Transistor ," Solid State Electronics, Vol-28, (3), pp 287-288 (1985)

Read in actual results $max\_i := 19 \quad i := 1, 2 .. max\_i \quad M2 := READPRN(KILMER)$

****

GR Noise Model (for BJT., ft is temperature dependent)

$$\tau[\tau 0, Ea, T] := \tau 0\cdot\exp\left[\frac{(q\cdot Ea)}{k\cdot T}\right]$$

$$\Delta E(Et, T) := Eg(T) - Et$$

$$ft(Et, T) := \frac{1}{\left[1+\left[\exp\left[\frac{(q\cdot((Et-Ef(T))))}{k\cdot T}\right]\right]\right]}$$

$$SGR[Cnf, \tau 0, Et, T, f, Ib, m, A] := \frac{[Ib\cdot\beta(T)]^m\cdot Cnf}{A^2}\cdot\frac{\tau[\tau 0, \Delta E(Et, T), T]}{1+[2\cdot\pi\cdot f\cdot\tau[\tau 0, \Delta E(Et, T), T]]^2}\cdot ft(Et, T)\cdot(1-ft(Et, T))$$

****

$T0 := 300 \qquad f_i := \left[M2^{<0>} \right]_i \qquad Ib := \left[6 \cdot 10^{-6} \quad 3 \cdot 10^{-6} \quad 1 \cdot 10^{-6} \right]^T \qquad m0 := 0.85$

$\tau 0 := 2 \cdot 10^{-14} \qquad Ea0 := .570 \qquad \tau\left[\tau 0 , Ea0 , 300 \right] = 7.532 \cdot 10^{-5} \quad Cnf0 := 2.833 \cdot 10^{-33} \quad Cf := 2.2 \cdot \left[10^{-23} \right]$

$S\_total(k , T , f , Ib) := SGR\left[Cnf0 , \tau 0 , Ea0 , T , f , Ib , m0 , 10 \cdot \left[10^{-6} \right]^2 \right] + Sf(Cf , E(3) , Ib , T , f)$

$Snf(k , f) := SGR\left[Cnf0 , \tau 0 , Ea0 , T0 , f , Ib_k , m0 , 10 \cdot \left[10^{-6} \right]^2 \right]$

$Sfl(k , f) := Sf\left[Cf , E(3) , Ib_k , T0 , f \right]$

$max\_j8 := 20 \quad j8 := 0 , 1 .. max\_j8 \quad f8_{j8} := 10^{\left[j8 \cdot \frac{\left[\log\left[10^5 \right] - \log\left[10^1 \right] \right]}{max\_j8} + \log\left[10^1 \right] \right]} \qquad m := 0$

GRAPH OF CURRENT NOISE VS. FREQUENCY

Y axis : ln (Si) [A^2/Hz] X axis : Frequency [Hz]

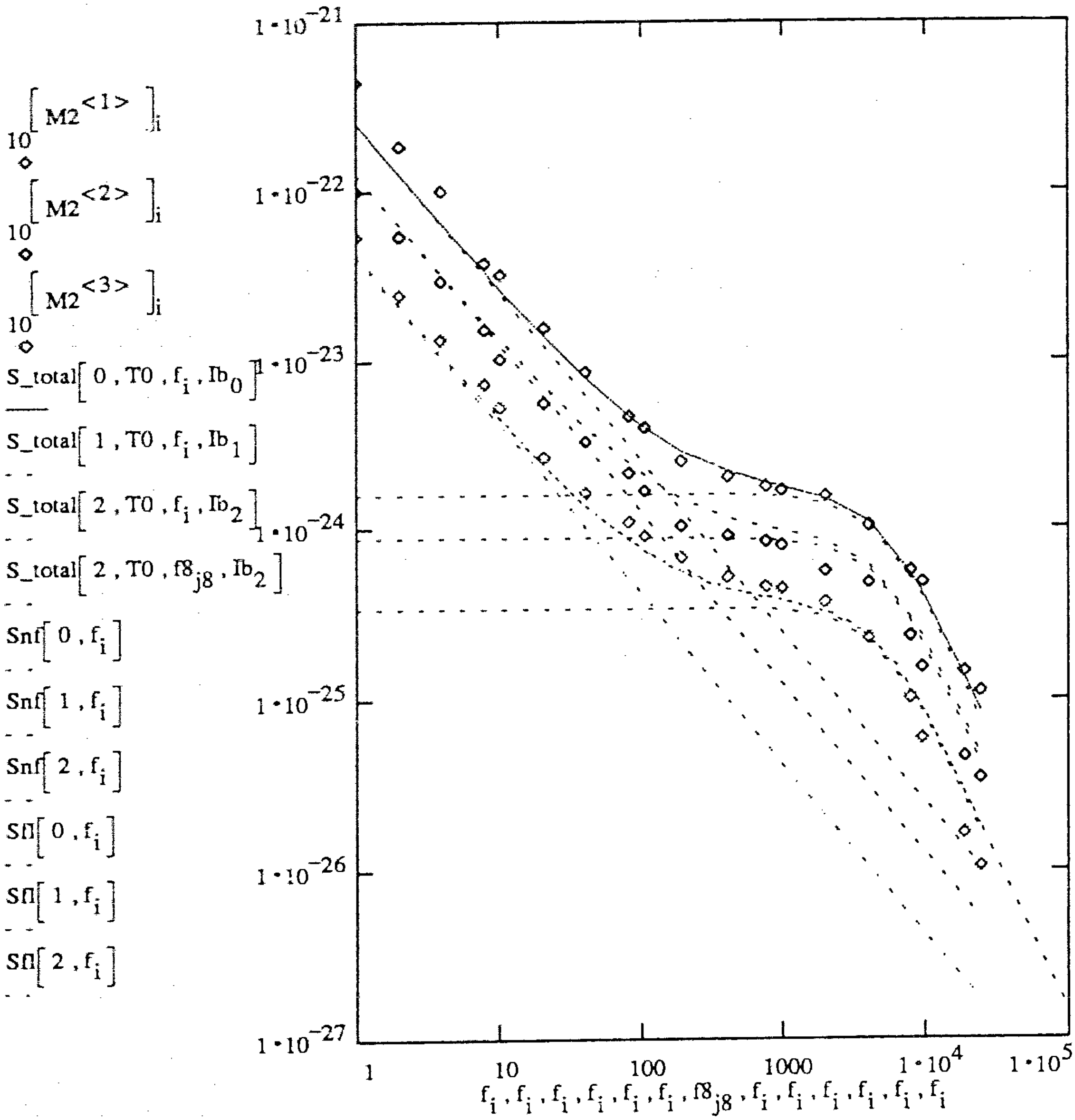

GR Noise Definitions (for JFET, ft is treated as temperature independent)

$$\tau[\tau 0, Ea, T] := \tau 0 \cdot \exp\left[\frac{(q \cdot Ea)}{k \cdot T}\right]$$

$$SGR[Cnf, \tau 0, Ea, T, f, \eta, A, Id] := Cnf \cdot \frac{Id^2}{A^2} \cdot \frac{\tau[\tau 0, Ea, T]}{1 + [[2 \cdot \pi \cdot f] \cdot \tau[\tau 0, Ea, T]]^{\eta}}$$

A4.5.2 Modelling K.K.Wang, A. Van der Ziel, and E.R.Chenette's Experimental Result [K.K. Wang,"Fundmental of Semiconductor Theory and Device Physics", Prentice Hall, New Jersey, pp 215, (1989)

$max\_i := 28 \quad i := 0, 1 .. ma\!:\!M2 := READPRN(KKWANG) \qquad T_i := [M2^{<0>}]_i$

$K\_Ea := (0.17 \quad 0.23 \quad 0.42 \quad 0.6 \quad 1.04)^T \; f0 := 100 \; Hz$

$Cnf := [3.84 \cdot 10^{-32} \quad 8.08 \cdot 10^{-32} \quad 8.08 \cdot 10^{-32} \quad 1.28 \cdot 10^{-32} \quad 4 \cdot 10^{-??}]^T \; Cf := 6 \cdot 10^1$

$K\_\tau 0 := [2. \cdot 10^{-13} \quad 7.5 \cdot 10^{-13} \quad 5.5 \cdot 10^{-13} \quad 9 \cdot 10^{-14} \quad 2 \cdot 10^{-18}]^T$

$S(j, T, f) := SGR\left[Cnf_j, K\_\tau 0_j, K\_Ea_j, T, f, 1.6, 10 \cdot [10^{-6}]^2, 0.050\right] + 10^{-25}$

$S\_total(T, f) := S(0, T, f) + S(1, T, f) + S(2, T, f) + S(3, T, f) + S(4, T, f) + Sf(Cf, 1, 1, T, f)$

$S\_total0(T, f) := S(0, T, f) + S(1, T, f) + S(2, T, f) + S(3, T, f) + S(4, tt, f) \; 50, 55 .. 350$

Graph of K. K. Wang's Noise Data and Our Noise Model vs. Temperature

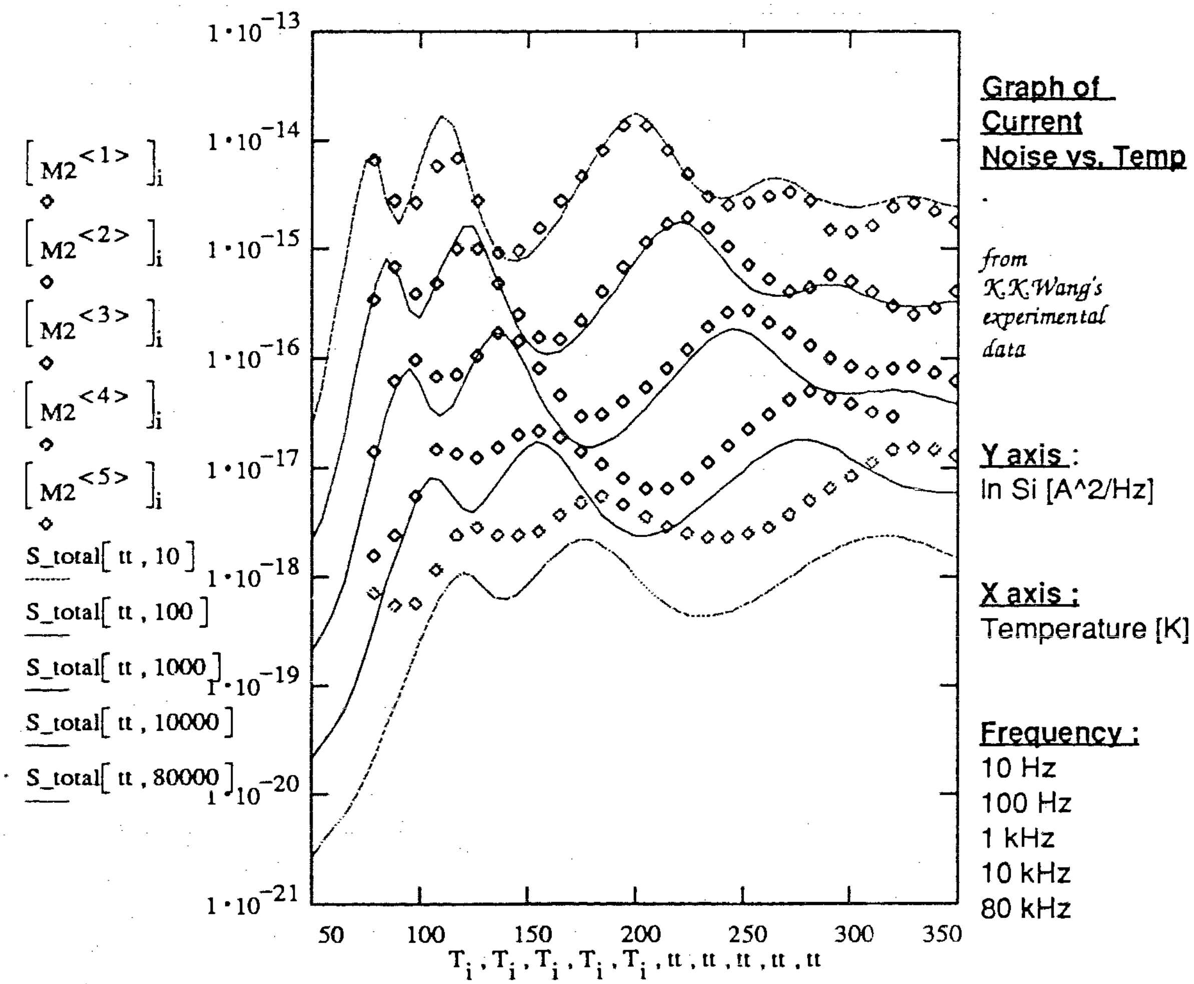

fover_3(x) := if(x = 10000 , 4 , 5)

fover_2(x) := if(x = 1000 , 3 , fover_3(x))   fover_1(x) := if(x = 100 , 2 , fover_2(f0))

Get_f(x) := if(x = 10 , 1 , fover_1(x))   f_2_i(x) := Get_f(x)   f_2_i(f0) = 2

$m := 10^{-18}$

Graph of K. K. Wang's Experimental Data, Total Noise from Noise Model, Total Noise less flicker Noise, the Five GR Noises and the Flicker Noise vs. Temperature